Theory of Sonoluminescence

by

Ljubinko Kondić

A dissertation submitted to the Graduate Faculty in Physics in partial fulfillment of the requirements for the degree of Doctor of Philosophy, The City University of New York.

1995

This manuscript has been read and accepted for the Graduate Faculty in Physics in satisfaction of the dissertation requirement for the degree of Doctor of Philosophy.

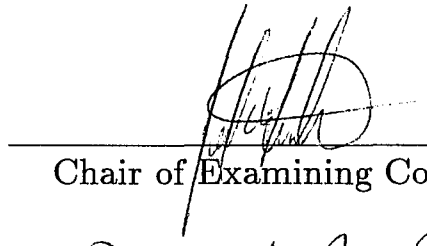

3/15/95

Chair of Examining Committee — Date

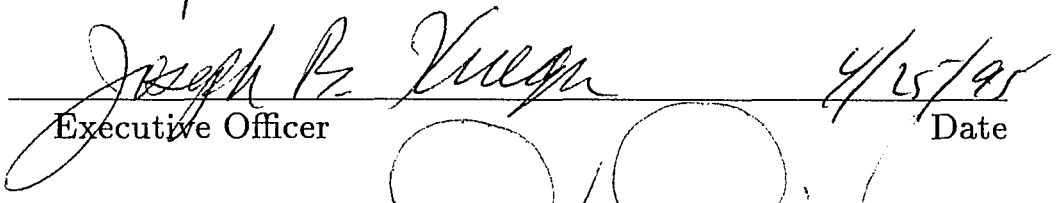

4/25/95

Executive Officer — Date

Professor A. Acrivos

Professor A. Genack

Professor J. Koplik

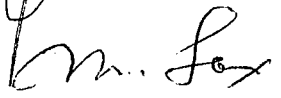

Professor M. Lax

Supervisory Committee

THE CITY UNIVERSITY OF NEW YORK

Abstract

THEORY OF SONOLUMINESCENCE

by

Ljubinko Kondić

Adviser: Professor Joel. I. Gersten

The subject of this work is a theoretical explanation of Sonoluminescence: optical radiation from strongly modulated bubbles in liquids. The observed radiation is characterized by a high energy concentration and a spectrum which is black-body like and of very short duration, on the picosecond time scale. Different theoretical approaches to the problem have been explored. It is found that for most of the time the adiabatic approach (i.e., the assumption of spatial uniformity of the thermodynamic variables) is a very good approximation. But, shortly before the bubble reaches its minimum radius, the motion of the bubble wall becomes supersonic and shock wave(s) are produced. In this region a full solution of the gas-dynamic equations inside a modulated gaseous bubble coupled with the bubble wall dynamics is required in order to correctly understand the physical properties of the gas in the bubble.

The propagation of the shock waves is followed and its consequences are compared with those of a self-similar behavior. The energy loss and change of equation of state of the gas resulting from the high temperatures and pressures in the collapsing bubble are incorporated. The effects of dissociation, ionization and radiation energy loss are included self-consistently in the treatment of the gas-dynamics equations. The radiation energy loss results in a sonoluminescent pulse whose properties are fully explored. We find that the inclusion of loss terms, especially due to radiation, is necessary to correctly describe the bubble dynamics and the resulting sonoluminescent pulse. A theoretical explanation of the pulse length and its spectral properties are presented and compared with experimental results. It is found that, for a variety of experimental conditions, the results of our theory are in very good agreement with experiment, although there remain aspects of the experiments that are not addressed by our theory.

I would like to express my gratitude to my adviser, Professor Joel I. Gersten for his guidance and patience during our research. I am also thankful to the members of my Committee and especially Professor Chi Yuan whose invaluable contribution increased the quality of my research.

The Mina Rees Fellowship of Graduate School of The City University of New York provided partial funding for the last year of my study, which is greatly appreciated.

Contents

List of Tables

List of Figures

Chapter 1

Introduction

Sonoluminescence - Light from Sound

Sonoluminescence (SL) is the emission of light which is sometimes observed when ultrasound is passed through a liquid containing dissolved gases. The effect represents a remarkable degree of energy concentration (as high as 12 orders of magnitude) and consists of easily observable, extremely short (less than 50 ps) bursts of visible light extending into the ultraviolet. These pulses are emitted from strongly modulated gaseous bubbles in liquids with clock-like precision, synchronized to a few parts in 10^{11}. The bubble(s) oscillate with the period of the sound field and for the experimental parameters for which SL pulses are observed, exhibit strongly nonlinear oscillations.

The major breakthrough in research of SL happened a few years ago when it became possible to achieve single bubble sonoluminescence (SBSL), compared to multiple bubble sonoluminescence (MBSL) which was known for about 60 years. The SBSL (on which most of this work will be concentrated), allowed for obtaining precise experimental results and a better theoretical understanding of the effect. It was found in SBSL experiments

that the intensity and spectral distribution of the emitted optical radiation are strongly dependent on experimental conditions - the nature of the liquid, the gas content of the light-emitting bubble, the applied acoustic pressure amplitude and the initial bubble size.

1.1 The Purpose and Organization of this Work

The main goal of this work is to explain the effect of SL and also to give qualitative, and, if possible, quantitative explanations of the intriguing dependence of the SL emission on the experimental conditions mentioned above. We also discuss possible new experiments which should be performed as well as the importance and the possible applications of sonoluminescence.

This work is organized as follows.

- Chapter I: *Introduction.* Here we give an historical overview of SL, summarize the existing theories about SL and explain the experimental techniques used for achieving and observing SL. The experimental data regarding SL are given as well. At the end of this chapter we present arguments for the importance of SL and summarize some current and possible future applications of SL.

- Chapter II: *Cavitation and Theoretical Overview.* In this chapter we explain the phenomenon of cavitation. We concentrate mainly on acoustic cavitation, which occurs in ultrasonically excited liquids, and represents the most common way of achieving cavitation in liquids. We also give an overview of the experimental techniques and present a simple theory which governs the strongly nonlinear bubble oscillations. In the second

part of this chapter we present an overview of a few of our theoretical approaches to the problem of sonoluminescence. These hypotheses are based on the results for the bubble dynamics following from the first part of this chapter. We will see that it is not possible to understand SL based on these results and that a better theory for the bubble dynamics and the values of the thermodynamic parameters of the gas in the bubble are needed in order to explain all the experimental SL data.

- Chapter III: *Bubble Dynamics.* A more complete theory of the bubble dynamics is given in this chapter. We will see that one of the assumptions made in the previous discussion of bubble dynamics, namely the spatial uniformity of the bubble content, has to be relaxed in order to properly understand the bubble dynamics and SL. A shock wave is produced in the collapsing gaseous bubble in a liquid, resulting in high values of the temperature, pressure and density of the gas in the bubble. In this chapter we go even beyond the usual formulation of gas dynamics and self-consistently include the possibility of the dissociation and ionization of the gas, as well as the possibility of radiation effects. All the necessary theory needed for an understanding of SL is presented in this chapter, which we consider to be the most important in this work.

- Chapter IV: *Sonoluminescence.* In this chapter we give an explanation of Sonoluminescence. The approach developed in the previous chapter is used in order to explain most of the important facts about SL: periodicity, the short duration of the pulse and the spectral characteristics. The discussion of the strong dependence of the SL radiation on some of the experimental parameters is given as well. We will see that, using

our theory, we are able to explain most of the known facts concerning sonoluminescent radiation.

- Chapter V: *Conclusion.* Our results are summarized here. We also give some suggestions for future experimental and theoretical research in this exciting field.

1.2 Historical Perspective and the Existing Theories

SL was first observed almost 60 years ago when it was discovered that a photographic plate could be fogged by immersing it in a water bath subjected to a high ultrasonic field. Chambers [1], one of the first researches in the field, investigated the optical emission from 36 different liquids of aqueous and nonaqueos solutions. His approach, as well as many others, was concerned with the SL emission from "bubble clouds", or multiple bubble SL (MBSL). The single bubble SL (SBSL) was first observed just a few years ago [2, 3] and we will say more about it later. Some of the MBSL results for different liquids and dissolved gases, as well as some of the gas and liquid parameters which might be important for understanding the effect, are summarized in Tables 1.1 and 1.2. The existing theories for MBSL, in chronological order, are:

- *The Triboluminescent Theory (1936);* Established by Chambers [1], who suggested that SL had a similar origin to the light produced when crystals are crushed. (At that time, it was thought that liquids had a quasi-crystalline structure.)

Gas	*SL Intensity*	*Solubility*	*I.P.* (eV)	$\kappa\,[10^{-2}\,W/(m\,K^2)]$
He	0.5	8.7	24.6	14.30
Ne	1.3	19.0	21.6	4.72
Ar	12.5	31.8	15.8	1.73
Kr	21.0	54.0	14.0	0.94
Xe	52.0	103.8	12.1	0.55
H_2	0.4	18.1	15.4	18.40
N_2	0.5	14.6	15.6	2.52
O_2	1.0	27.7	12.1	1.64
Air	1.0	17.1		2.52
CO_2	0.4	n/a	13.7	1.56

Table 1.1: *SL intensity for different gases in water. Solubility and thermal conductivity* κ *are measured at* $20°C$ *and SL intensity (relative units) at* $25°C$*. The data are taken from [4, 5, 6].*

- *The Balloelectric Theory (1939);* Suggested by Harvey [7, 8] and based on the idea that charged bubbles exist in liquids. According to this theory, the decrease of the bubble size leads to an increase in the electric field around the bubble and dielectric breakdown in the liquid results in SL.

- *The Electrical Microdischarge Theory (1940);* This theory postulates the creation of non-spherical cavities as the liquid pressure decreases. Statistical fluctuations are then supposed to create regions of opposite

charges on the cavity walls and lead to a microdischarge inside the bubble and thus to radiation.

- *The Mechanochemical Theory (1949);* It was suggested that the light emission occurred by the photochemical recombination of the free ions produced by the mechanical dissociation of molecules at the nascent surfaces of growing cavities.

- *The Thermal (Hot-spot) Theory (1950);* Initially formulated by Noltingk and Neppiras [9], this theory is based on the adiabatic heating of the bubble content during the rapid bubble collapse. The temperatures which may be achieved in the collapsing bubbles are of the order of a few thousand degrees. As a result of this theory, SL is black-body radiation emitted from a hot gas in the bubble.

- *The Chemiluminescent Theory (1950);* According to this approach, the high temperatures in the collapsing bubbles may lead to a variety of chemical reactions, some of which may be of radiative character. A lot of research following this approach was done in the last two decades [10]-[16].

- *The Anion-discharge Theory (1974);* Degrois and Baldo [17] formulated a variation of an electrical theory. According to their hypothesis, the charges on gaseous bubbles arise from the neutralization of anions on the bubble surface by gas molecules adsorbed at the gas-liquid interface. This theory was later criticized [10], when it was shown that the predictions of this theory do not correspond to experimental observations. Another variation of the electrical approach was presented more recently by Margulis [18]-[21].

Liquid	*SL Intensity*	ϵ	$\kappa\,(cal/(cm\,s\,°C^2))$	$\mu\,[10^2\,g\,cm\,s)]$
Glycerine	4.6	42.5	7.03	1.49
Ethyl Glycol	3.7	37.0	6.24	1.99
Water (tap)	1.0	78.5	14.56	1.00
Toluene	0.5	2.4	3.22	0.59
Ethyl alcohol	0.3	3.7	3.99	1.20
Chlorobenzene	0.2	5.6	3.46	0.80
Acetone	0.2	n/a	4.54	0.32
Benzene	0.06	2.27	3.78	0.65
Liquid nitrogen	0.005	n/a	n/a	n/a

Table 1.2: *SL intensity for different aerated liquids. The SL intensity (relative units) is measured at* $25°C$ *and the data for the dielectric constant* ϵ*, thermal conductivity* κ*, and viscosity* μ*, are at* $20°C$*, (except for* κ *for acetone at* $16°C$*, for benzene at* $22.5°C$ *and* μ *for benzene at* $25°C$*). The data are taken from [4, 5, 6].*

For the time being there is no conclusive evidence supporting any of the above mentioned theories. Still, the experimental results allow us to rule out some of them. Today we know that the SL pulse is emitted during the collapse part of the bubble cycle, eliminating Triboluminescence, Microdischarge and Mechanochemical Theories, which suggest that the SL emission happens during the expansion part of the bubble cycle. Furthermore, the SL intensity is not sensitive to the changes in the electrical conductivity of the liquid, as follows from the Balloelectric approach (viz. Table 1.2). Anion-

discharge Theory suggests that a homonuclear gases should give a stronger emission than the corresponding rare gases, opposite to experimental results. This leaves us with two theories: Thermal and Chemoluminescence.

Both of these theories get some experimental support. One of the consequences of the Thermal approach is the increase of the SL emission with increase of γ of the gas in the bubble, since higher γ leads to higher temperatures (through the adiabatic collapse). Thus, the emission from rare gases should be stronger, in correspondence with the results in Table 1.1. On the other hand, gases with the same γ should lead to the same SL emission, in contradiction to different SL intensities for different rare gases (viz. Table 1.1). This discrepancy could be explained, at least in a qualitative manner, by noticing [22] that the rare gases with the higher thermal conductivities lead to lower SL intensities. This is because gases with higher thermal conductivities transfer more energy to the liquid, leading to lower temperatures in the bubble and correspondingly lower SL intensities. The results are in reasonable agreement with experiments.

The observation of molecular and/or atomic bands in the SL spectrum [4, 23, 24], suggests that some chemical processes must occur in the collapsing, high-temperature bubble interior. The observed spectrum is largely explained on the basis of different, sometimes fairly complicated, chemical transitions involving excited water vapor or hydroxyl radicals.

Some other interesting observations about SL emitted from bubble fields (MBSL), not yet mentioned are:

- SL intensity increases with the increase of acoustic pressure;
- SL intensity from different liquids correlate with σ^2/p_v, where σ is the surface tension and p_v is the vapor pressure of the liquid [25]. (The

log-log graph of the SL intensity versus σ^2/p_v is roughly linear);

- SL intensity depends strongly on the liquid temperature, and the proportionality is of the form $\ln I \sim 1/T$, where I is the SL intensity and T is the liquid temperature. This dependence was attributed to the Helmholtz free energy associated with the cavity growth [13]. More about the dependence of the SL pulse on the liquid temperature in the case of SBSL is given later.

Still, a complete up-to-date theory which would explain all the details of the SL emission is missing. The main problem in explaining MBSL is that the experimental conditions are not precisely known and, also, the behavior of a bubble cloud is too complicated to be understood in any precise manner. The spatial scale of an individual SL event is on the order of a micron, and the temporal scale is on the order of nanosecond. Thus, studies of MBSL involve some kind of time averaging over a bubble field, which consists of bubbles which are of various sizes and at different stages of collapse. Later, in chapter 2, we will see that the oscillations of the bubbles might be stable (repeating themselves with the period of the applied sound field), or transient (the bubble collapses after a few acoustic periods). These two possibilities might lead to very different physical conditions in the collapsing bubbles and different mechanisms for the production of light. In the experiments performed with the bubble fields, it is not clear which one of these two modes of the bubble response to the applied acoustic pressure is taking place, increasing the complexity of the problem.

Single bubble experiments, performed only recently [2, 3] removed this major obstacle to obtaining a better understanding of SL, and were expected to lead to a much more precise explanation of the effect. But, the new data

resulting from these experiments made the understanding of the effect even more complicated. The peak power of the pulse of 30 mW (lower limit), the duration of the pulse of less than 50 ps and a spectrum which could be successfully fit to a black-body of temperature between $15,000$ and $30,000$ K, are definitely surprising. It is also observed that the SL pulse is emitted just shortly before the bubble reaches its minimum radius (for a typical response of a sonoluminiscenting bubble to a sound field, see Fig. 2.2 on page 30). The bubble oscillations in these single bubble experiments turn out to be extremely stable - a single bubble could be made to oscillate (and produce SL pulses) for hours. Furthermore, it is found that the SL intensity strongly depends on the liquid temperature - a tenfold increase of the SL emission is observed if the water temperature is decreased to a few degrees centigrade. (For the time being, SBSL experiments are done only with water [3] and a water-glycerin mixture [2].)

These results, especially the extremely short duration of the SL pulse, represent a serious challenge to a possible theoretical explanation. The time which the bubble spends close to the minimum radius is fairly short, but still much longer than the duration of the SL pulse. The Thermal Theory, based on the high temperatures resulting from the adiabatic compression of the bubble, cannot explain why this high temperature should exist only for less than 50 ps. Also, the temperatures of more than $15,000$ K cannot be explained by this approach. On the other hand, the SBSL spectrum does not appear to contain any spectral bands or emission lines which would indicate the importance of molecular or atomic transitions. The conclusion is that neither of the previously mentioned theories is able to reproduce even the main observable facts of single bubble sonoluminescence. Actually, quite recently it was suggested [26] that SBSL is intrinsically different from MBSL

and that completely different physical processes might be responsible for these two effects.

Correspondingly, new theories have to be developed in order to explain SBSL. There are a few recently developed theoretical approaches to the problem.

- An interesting interpretation was proposed by Schwinger [27] and is based on the dynamical Casimir effect. For the time being, the model exists only in mathematical form, and has not been tested against experimental results.

- Quite recently, a new model was proposed by Atchley and Frommhold [28], based on collision-induced emission. The basic assumption of the model is that the temperature in the bubble is rather low (less than $10,000\ K$). This assumption does not seem to correspond to the experimental results [3, 29]. Also, the question is how one could expect to get visible photons of energy about 6 eV as a result of collisions of the molecules at a much lower temperature.

- In the more complete approach by Wu and Roberts [30], the gas-dynamic equations for the gas in the bubble are solved and it was shown that a spherically collapsing shock wave is produced in the bubble. They explain SL as bremsstrahlung radiation from the hot bubble center. It is not easy to understand how the bremsstrahlung spectrum could be related with the experimental one, which is black body-like.

- Finally, our approach is based on the evident production of a shock wave in the collapsing bubble. Gas-dynamic equations for a gas which is allowed to dissociate, ionize and radiate are solved self-consistently.

Correspondingly, our approach is a natural extension of the work of Wu and Roberts where dissociation, ionization and radiation of the gas in a bubble were not included in gas-dynamic equations. The conclusion is that SBSL is most probably based on thermal radiation which is emitted from the high temperature gas in the bubble.

1.3 Experimental Techniques and Results

Here we are going to concentrate on the recent experiments [2, 3], which lead to SBSL. Cavitation itself and the methods of achieving stable, single bubble oscillations are explained in chapter 2.

The simplified schematic diagram of the experimental apparatus used is given in Fig. 1.1, based on [2]. The experiment consists of two different parts. In both of them an acoustic resonator (levitation cell) was used to excite a standing-wave sound field in the liquid, which was water or a water-glycerin mixture. A single gaseous bubble in the liquid is stabilized at a pressure antinode. Acoustic pressure amplitudes are typically in the range of $1.0 - 1.5\ atm$ and frequencies are $15 - 25\ KHz$. In the first part of the experiment, the light from an Ar-ion laser was scattered from the bubble (typical size of a few microns) and detected with a photodiode. The amplitude of the scattered light, modulated by the radial bubble pulsations, was converted to a radius of the bubble using a previously determined experimental transfer function. The result of this part of the experiment is the bubble radius versus time curve. In the second part of the experiment, SL from the bubble is detected using a photomultiplier tube. The SL emission was correlated in time with the bubble radius, thus obtaining the phase of SL emission relative to the bubble pulsations. For future reference, let us mention here that the

uncertainty of the experimental parameters (the acoustic pressure amplitude and the equilibrium bubble radius) is about $10 - 20$ percent.

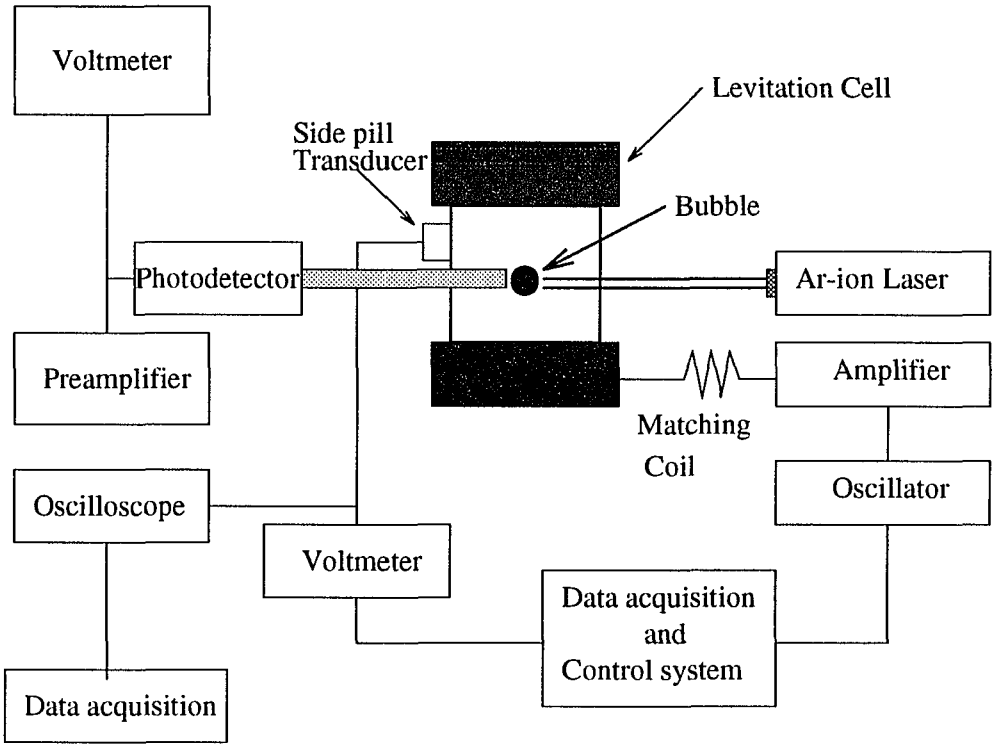

Figure 1.1: *Schematic diagram of experimental apparatus [2].*

Measuring the parameters of the emitted SL radiation turned out not to be easy. Even the world's fastest microchanel-plate photomultiplier is not fast enough to determine the SL pulse duration. When the impulse response of the SBSL emission is compared with that of 34 *ps* pulsed laser, it is found that the SL flash is extinguished faster than that of the laser [31]. Also, the attempts to measure the pulse duration using streak cameras and other high speed devices have been unsuccessful [32]. The conservative upper limit on the pulse duration was put at 50 *ps*. A further remarkable characteristic of

SBSL is the degree of synchonicity of the flashes, which are emitted with the period of the sound field. The relative phase angle between the acoustic pressure and the SL emission is found to be stable within a degree for a periods of several minutes. (There are about 25,000 periods in a second!) The peak power output of the SL pulse is strongly dependent of the liquid temperature and acoustic pressure amplitude. It varies between 30 mW and 0.15 W, as given in [33]. The spectrum of the emitted radiation is successfully fit to the black body one with a corresponding temperature of 20,000 K for an air bubble in water at $25°C$, and to 30,000 K for the same bubble in water at $1°C$.

Recently, it was reported [33] that the spectrum and the peak power of the SL pulse strongly depend on the nature of the gas in the bubble. For example, the emission from a nitrogen bubble is much smaller than one from an air bubble (similar to MBSL experiments, viz. Table 1.1). The addition of 1 percent of Ar brought the emission back to the one from an air bubble. At present there is no explanation of this effect and it is not clear how the stability of the bubbles is affected by the nature of the gas.

Experimental as well as theoretical research are still in progress and new results appear very frequently.

1.4 Importance of the Research

Research on SL is strongly connected with cavitation, which has a lot of practical importance in engineering, fluid mechanics and biological systems. Correspondingly, SL, which often occurs during cavitation, might be used as a probe of cavitation. Anyway, until the recent progress in SL research, it was mainly of academic interest, as an example of a strongly nonlinear phe-

nomenon. But, the recent results make SL a "hot" subject. A lot of research has been done in a last few years [2, 3, 4, 21, 24] [26]-[42] and articles about sonoluminescence appear in general science journals [3, 4, 32, 33] [43]-[46] or even the daily press [47]. The fact that SL results from an imploding shock wave is especially important. Since the bubble is far from boundaries, is exposed to relatively low acoustic pressures and is relatively small, so it remains spherical, the imploding shock wave very likely remains spherical until the final stages of its collapse [32]. The calculations suggest that temperatures as high as $10^7 - 10^8\ K$ and pressures of $10^9 Mbar$ are to be expected. Therefore, there is a potential for creating some exotic physical and chemical processes. The possibility of the emission of X-rays [42], neutron emission [35] and inertial confinement fusion with a deuterium-tritium mixture have been suggested.

For the time being, research on the consequences of the imploding shock wave have been performed only for the case of SBSL, since this simple system is much easier to analyze. Still, the production of shock waves might be expected in the MBSL experiments as well, which could be of even stronger intensity, since transient cavities could be driven with higher acoustic pressure amplitudes (viz. Fig. 2.1 on page 21). Research in the connected field of sonochemistry suggests that many chemical reactions could be influenced by ultrasound, with many of them having practical significance [32].

Future research, both experimental and theoretical, is going to be performed, and, for the time being, one cannot see what the limits of SL radiation and energy concentration are. Let us just mention that, if the scaling of the SL intensity with σ^2/p_v [5, 25] works also for SBSL (as established for MBSL), one could expect an SBSL intensity from mercury to be 10^4 times stronger than that for water!

Chapter 2

Cavitation and Theoretical Overview

2.1 Introduction; About Cavitation

2.1.1 Historical Perspective

> In 1894., the destroyer *H. M. S. Daring* failed to meet specifications: its speed and efficiency were inexplicably low. Sir John Thornycroft and Sidney Barnaby observed severe vibrations and excessive slippage of the ship's screw propeller. After four sets of blades had been replaced, a solution to the problem was found by simply increasing the surface area of the propeller and decreasing its angular velocity.

Their description of the associated bubble formation was the first report of the phenomenon known as cavitation, which occurs during turbulent liquid flow and also under ultrasonic radiation of a liquid. The above mentioned problem was so serious that in the year 1915, Lord Rayleigh was asked to join a special committee investigating this phenomenon. His work [48] still

represents a basis for the current studies of cavitation.

At the same time as Lord Rayleigh's work, the first trials to measure the tensile strength (cavitation threshold) of water were performed. For many decades there was a serious discrepancy between experimental ($1 - 25\ atm$) and theoretical (more than $1,000\ atm$) results. It was not clear why bubbles form in the water exposed to an acoustic pressure of the amplitude of the order of $1\ atm$. Many different theoretical models were formulated in order to explain this effect. The most successful one was initially formulated by Harvey [7, 8] who suggested that gas pockets trapped in a crevice in a solid inhomogeneity present in liquid were responsible for the effect. His approach was one of the first of those which tried to explain cavitation based on the presence of foreign bodies in liquids - or heterogeneous cavitation. The other approaches are based on a homogeneous model - explaining the effect on the basis of pressure, temperature and density fluctuations in a given liquid. Today we know that most cavitation events really have to do with the presence of impurities in a liquid. Different theoretical explanations exist, based on the presence of organic molecules, cosmic rays, etc.

2.1.2 Methods of Achieving Cavitation and Experimental Techniques

There are many possible ways of achieving cavitation experimentally. One of the first ones was so called hydrodynamic cavitation caused by flowing a liquid through a Venturi tube [25]. Other techniques include optical cavitation - the use of a pulsed laser beam, spark-induced cavitation, etc. Here we are going to concentrate on the most widely used technique for inducing cavitation, and that is to pass a sound wave through a liquid. This acoustic cavitation usually functions via the growth of pre-existing entrapped bubbles

rather than by causing true cavitation of the liquid. In this part, we first explain the basis of general cavitation experiments. Secondly, we concentrate on the single bubble experiments, which are of main interest to us.

Experimentally, the system consists of a spherical or cylindrical flask filled with liquid and having one or more transducers affixed to its side. When the transducers are driven, the entire flask vibrates and if the transducer-flask system is driven at one of its resonant frequencies, the amplitude of the oscillations are fairly large. The acoustic frequencies used are ultrasonic (typically $20 - 300\ KHz$). As the flask oscillates radially the acoustic field is focused at the center of the flask. At this point, if the acoustic field is strong enough, cavitation occurs. The other way to produce acoustic cavitation is to have a uniform sound field propagating through the liquid. The disadvantage of this method is that the cavitation could be produced anywhere in the liquid and, also, usually one achieves a production of "bubble clouds" - many bubbles are produced, leading to complicated bubble-bubble interactions. This is an interesting field of research in itself, but for the purpose of exploring bubble dynamics, the previous approach, based on the use of a focused sound field, is giving much better results.

There are a few factors which are very important for serious research on bubble dynamics. Apfel [49] formulated them in the following way: *"(1) know thy sound field, (2) know thy liquid, (3) know when something happens"*. The amplitude of the sound field is important in order to be able to compare experimental results with theoretical ones, as will be explained in the following sections. The properties of liquid, for example the purity of the water, determine the onset of cavitation and also have a big influence on the consequent bubble dynamics. Finally, one should somehow observe that the cavitation really happens. This can be done in a few ways: Chemically -

through a variety of reactions that often involve free-radical production and are enhanced by the presence of bubble clouds; Acoustically - since the bubbles are a good absorber of ultrasound, the onset of absorption often signals the onset of cavitation; Optically - the recent techniques include Mie scattering of a bubble (usually useful for a single bubble detection), or, finally, by observing sonoluminescence, which often follows cavitation events.

The single bubble cavitation events turned out to be very difficult to achieve. The procedure which finally led to to the result was to introduce a single bubble by hand into degassed water or a water-glycerin mixture [2, 3]. The experimental procedure consists of introducing a gaseous bubble in the liquid and slowly increasing the sound field amplitude which produces a standing wave pattern in the liquid, until a single bubble is stabilized at the pressure antinode. It seems that the major obstacle to achieving this result is that the parameter space (the acoustic pressure amplitude and the concentration of the gas in the liquid), allowing for stable bubble oscillations is fairly small. The flow of mass between the bubble and the liquid, which is important in stabilizing the bubble oscillations, will be explained in more details in 2.2.2. The different regimes of bubble oscillations will now be considered.

2.1.3 Transient and Stable Cavitation

Here we concentrate on acoustic cavitation. As already mentioned, the behavior of the bubbles in a sound field is very sensitive to many parameters, primarily on the initial bubble radius, R_0, the acoustic pressure amplitude, P_a, and the nature of the liquid and the gas in the bubble. Such effects as mass and heat flow between the bubble and the liquid are essential in studies involving the stability of bubbles. Still, the most important factor which de-

termines the nature of the bubble oscillations in the sound field is the acoustic pressure. In Fig. 2.1 we show the general pattern which governs the behavior of oscillating bubbles. This pattern was observed for many different liquids and different bubble contents. The values of the acoustic pressure shown in Fig. 2.1 are characteristic for air bubbles in water of the typical size of a few microns. If the acoustic pressure amplitude is relatively small (less than about 0.9 atm) bubbles oscillate with rather small amplitudes. Increasing P_a leads to surface instabilities and non-spherical pulsations. If P_a is further increased, the lower stability threshold is reached (about 1.1 atm). The bubble exposed to P_a larger than this value is going to oscillate periodically with the period of the sound field, for long periods of time (measured in minutes or even hours). An hysteresis effect was observed [2], meaning that once the stability threshold is reached (see Fig. 2.1), the pressure could be decreased below the stability threshold and stability is maintained. Further increase of the acoustic pressure leads to stronger bubble oscillations, until the upper stability threshold is reached. For P_a above this value the bubble becomes transient. It means that bubble will grow very large during the expansion part of the cycle and then violently collapse and disintegrate into many smaller bubbles.

In the rest of this work we will be interested in stable cavitation. Sonoluminescence was also observed with transient cavitation, but the irregularity of the SL events and inability to precisely reconstruct the terminal stages of bubble collapse represent the major obstacle for studies of transient sonoluminescence. The major effects responsible for the remarkable stability of the bubble oscillations (in the stable region), and the theoretical formulation of bubble dynamics, are presented in the following sections. Before that, let us say something about the practical importance of cavitation.

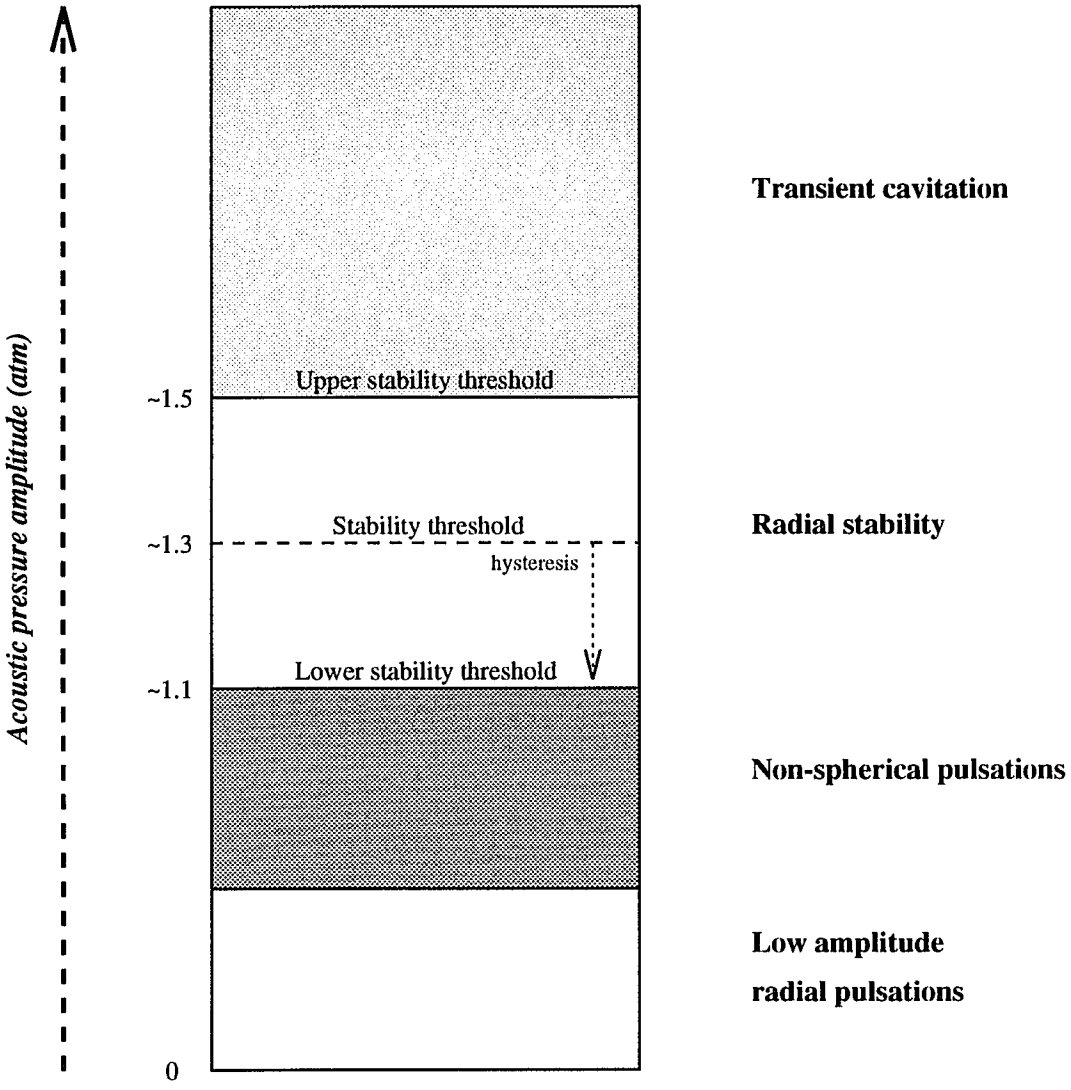

Figure 2.1: *Diagram of observed radial stability thresholds for air bubbles in water.*

2.1.4 Importance and Applications of Cavitation

The influence which bubble fields might have in turbulent liquid flows was already mentioned. Cavitation combined with ultrasound has many important industrial applications, like cleaning, erosion testing, dispersion of solids, degassing etc. Aside from the industrial aspect, there are many other important fields where cavitation has an influence. One of them is cavitation in biological tissues, which has been explored to some extent [4, 50]. There, the characteristics of the ultrasound used for medical purposes are similar to those used in the acoustic cavitation experiments. It is not clear if stable cavitation could be expected to produce high temperatures and free radicals in biological tissues. Also, there is the possibility of the production of shock waves, high-velocity jets, uncontrollable growth of bubbles, etc. All these effects have not yet been carefully explored.

2.2 Bubble Dynamics

Theoretical investigation of the bubble dynamics is an extremely complicated subject. The coupling between a bubble and a liquid is extensive and manifests itself in mass and heat flow, acoustic and optical radiation, etc. Also, the motion of the bubble surface ("bubble wall" in what follows) can become comparable to the speed of sound even in the case of stable cavitation, which we are going to concentrate on here. In the first part of this section we formulate the "bubble equation", which, under certain assumptions, determines the motion of the bubble wall. In the following parts we give a brief analysis of the different coupling mechanisms between the bubble and the liquid.

2.2.1 Bubble Equation

We make the following approximations in order to formulate an equation which determines the bubble wall motion:

1. The bubble remains spherical. The necessary condition for this assumption to hold is to have the long wavelength limit for the acoustic field satisfied ($kR << 1$). Here k is the wave number of the sound field and R is the bubble radius;

2. The internal pressure, temperature and density must stay uniform throughout the bubble oscillations. Furthermore, these variables are assumed to obey the van der Waals equation;

3. No mass or heat flow between the bubble and liquid takes place;

4. The liquid is incompressible.

These assumptions place severe limitations on the model which we use, especially when the pulsations are large and the bubble wall velocity gets to be comparable to the speed of sound. Still, as we going to see, in many circumstances we are able to obtain solutions which compare favorably with experimental data. In the simplest approximation, the motion of the bubble wall follows from the Euler equations [51]

$$\frac{\partial \vec{v}}{\partial t} + \vec{v} \cdot \nabla \vec{v} = -\frac{\nabla P}{\rho_l} \tag{2.1}$$

where ρ_l and P are the density and the pressure in the liquid and $\vec{v}$ is the local mean velocity of a particle in the liquid. For simplicity, the viscosity of the liquid is neglected at this point. Assumption 4 in the above list implies that

$$\nabla \cdot \vec{v} = 0 \tag{2.2}$$

Assuming spherical symmetry ($\vec{v} = \hat{r}v$) we see that the radial velocity is given by $v = A(t)/r^2$, where the function $A(t)$ is unknown for the time being. The next step is to integrate Eq. (2.1) from r to "infinity" (container wall). That gives the following solution for the pressure in the liquid at a distance r from the origin (the bubble center), where $r > R$

$$P(r) = P_\infty + \rho_l \left[\frac{\dot{A}(t)}{r} - \frac{A(t)^2}{2r^4} \right] \tag{2.3}$$

If we put $r = R(t)$ (bubble wall radius), and use the boundary condition that the speed of the liquid just next to the bubble wall is equal to the speed of the wall, i.e. $v(R^+(t)) = \dot{R}(t)$ we get the following equation for R

$$R\ddot{R} + \frac{3}{2}\dot{R}^2 = \frac{1}{\rho_l} \left[P(R^+) - P_\infty \right] \tag{2.4}$$

which determines the motion of the bubble wall, assuming that we know the pressure in the liquid just next to the bubble wall $P(R^+)$ and the pressure at infinity P_∞. This latter pressure is simply the hydrostatic pressure P_0 modulated by the applied sinusoidal acoustic pressure amplitude, $P_\infty = P_0 - P_a \sin(\omega_a t)$, where ω_a is the acoustic angular frequency. The next step is to connect the pressure in the liquid just next to the bubble wall with the pressure inside the bubble. At equilibrium (i.e. $R = R_0$, $\dot{R} = 0$), the result is simple since the pressures inside and outside have to be in equilibrium. By including the surface tension σ in the consideration, the connection is $P_g(R_0^-) = P(R_0^+) + 2\sigma/R_0$, since the pressure in the gas P_g has to equalize the outside pressure and the surface tension[1]. Now, following assumption 2

[1]In what follows we are going to use expression for $P_g(R_0^-)$ also for nonequilibrium conditions. The role which surface tension plays in the bubble dynamics is not very clear, especially recalling the small bubble size (of the order of few microns). The effect of surface tension is mainly going to be neglected in chapter 3, where we are going to correct one of the most problematic assumptions, about the spatial uniformity of the bubble interior.

from above, the pressure in the gas is given by adiabatic equation

$$P_g = P_0 \frac{(R_0^3 - a^3)^\gamma}{(R^3 - a^3)^\gamma} \tag{2.5}$$

where R_0 is the equilibrium radius of the bubble, a is the assumed hard core radius and γ is the ratio of specific heats. If one also includes viscosity ν_l of the liquid and the possibility of acoustic radiation [52, 53], the following equation is obtained

$$R\ddot{R} + \frac{3}{2}\dot{R}^2 = \frac{1}{\rho_l}\left[P_g(R) - P_a(t) - P_0 - \frac{2\sigma}{R}\right] + \frac{R}{\rho_l c_l}\frac{d}{dt}[P_g(R) - P_a(t)] - 4\nu_l\frac{\dot{R}}{R} \tag{2.6}$$

This equation is known as the Rayleigh - Plesset (R.P.) equation, or, sometimes, the R.P.N.N.P. equation [5], following the main contributors toward its formulation by Rayleigh [48], Plesset [54, 55], Nolting and Neppiras [56] and Poritsky [57]. We should mention here that the above equation represents just one of the possible models for the bubble dynamics (for other approaches to the problem, see [58]-[64]). More sophisticated models developed recently are summarized in [2]. In these models one or a few of the assumptions mentioned above are relaxed. We will discuss the importance of these side effects in the rest of this section.

2.2.2 Diffusion and Rectified Diffusion

A flow of mass via mass diffusion between a bubble and liquid is known to take place. So the question which naturally arises is, how a bubble in a liquid could be expected to maintain stability and not dissolve away. The answer is that there are two competing effects taking place. One is mass diffusion from the bubble to the liquid. This is a relatively slow process, but it could make bubble dissolve in a few seconds [56]. The other effect is the so-called

rectified diffusion, and is connected with a bubble oscillating nonlinearly in a sound field [59, 65]. Hence, when the bubble contracts below its equilibrium radius, the concentration of the gas in the interior of the bubble increases, and the gas diffuses from the bubble. On the other hand, when the bubble expands past the equilibrium radius, the concentration of the gas decreases, leading to a back flow of gas from the liquid to the bubble. Because the time spent at these large radii exceeds the time spent at small radii and the diffusion rate is proportional to the surface area, more gas enters the bubble during the expanded phase than leaves during the contracted phase, leading to a net increase in the amount of the gas in the bubble. The reason why the mass flow can be neglected in our approach is that we are interested in the bubble dynamics after it reaches its steady state regime. Thus, it is known experimentally [2] that the bubble needs some time (a few seconds) to reach the state where the equilibrium radius does not change in time. In this regime, the effects of diffusion and rectified diffusion are in equilibrium. This is the reason why we can neglect this effect in our approximate treatment of the bubble dynamics.

2.2.3 Thermal Coupling

The question of the importance of the heat flow between the bubble and the liquid is still open. The estimate by Neppiras [56] shows that, for most of the experimentally important choices of parameters (mainly bubble radius and acoustic frequency), under the assumption of small oscillations of the bubble radius about its equilibrium value, it can be assumed that heat conduction is not important. That implies that the bubble interior can be assumed to follow the adiabatic law. (In this part, we limit our discussion to the case of an air bubble in water.) More precise models, formulated mainly by Crum

and Prospereti [38, 52, 53] [66]-[69], tend to formulate the behavior of the gas in the bubble in terms of so called "polytropic exponent". The idea is that one can include the effect of heat conduction by assuming a polytropic law for the gas in the bubble. In this formulation, the relation between the pressure and the volume of ideal gas is given by $P\,V^{\kappa} = const$, where κ is the polytropic exponent. Its value is equal to the ratio of specific heats for the gas, γ, if the gas behaves adiabatically, and it is equal to 1, if the gas behaves isothermally. In general, it could assume any value between these limiting cases. In this formulation the conclusion is again that, for the most important choices of the experimental parameters, the bubble may be assumed to follow the adiabatic law. So, in the rest of this work we are going to neglect the heat flow between the gas and the liquid. More discussion about the importance of the heat flow during the short time the bubble spends close to its minimum radius is given in Appendix E.1.

2.2.4 Assumption of the Spatial Uniformity of the Gas in the Bubble

The common point of all of the theoretical models for the bubble dynamics mentioned until now is the assumption of the spatial uniformity of the bubble interior. Also, most of the analytical results are derived assuming small oscillations of the bubble about its equilibrium radius. The reason for these assumptions is that they considerably simplify the problem, without clear experimental evidence that they are correct. Still, in the next section we will see that we are able to reproduce most of the experimental observations concerning the motion of the bubble wall assuming uniformity of the gas. This is true as long as the motion of the bubble wall is not too fast and the bubble is not driven too strongly. The case of a strongly driven bubble is

going to be discussed in some more detail in chapter 3 where we will see that, for the conditions where the motion of the bubble wall reaches the (local) speed of sound of the gas in the bubble, this assumption has to be relaxed in order to properly understand the bubble dynamics.

2.3 Rayleigh - Plesset Equation

The Rayleigh - Plesset equation, Eq. (2.6) is a relatively simple ordinary differential equation, but it still shows a very rich structure and a variety of solutions for different input parameters. A typical solution for a strongly driven bubble ($P_a = 1.325\ atm$) is presented in Fig. 2.2 on page 30.

The first attempts toward solving the equation which determines the motion of the bubble go back to Rayleigh [48], who was considering the collapse of an empty cavity. Actually, it is worth noticing that during the beginning of the collapse part of the bubble cycle, when all the terms on the right hand side of Eq. (2.6) are very small, (compared to the terms on the left hand side), the motion of the bubble wall basically follows Rayleigh's solution [48] for the collapse of an empty cavity. This solution is given by $R(t) = R_0\,(1 - t/t_0)^{2/5}$, where R_0 is the initial bubble radius and t_0 would be the collapse time if the gas in the bubble did not inhibit the motion of the bubble wall. As the bubble collapses, however, the influence of the bubble interior becomes more important and it cannot be neglected anymore. It enters into Eq. (2.6) through the $P_g(t)$ terms.

Before we proceed to the full solution of R.P. equation, let us make a comment about the natural frequency of the bubble. By writing $R = R_0 + r$ in Eq. (2.6), where R_0 is the equilibrium radius, and assuming small oscillations,

i.e. $r/R_0 << 1$, we obtain the following equation for r

$$\ddot{r} + \omega_r^2 r = \frac{P_a}{\rho_l R_0} \sin(\omega_a t) \tag{2.7}$$

where only first order terms are retained and the viscosity and the acoustic radiation term are neglected. The resonance frequency ω_r is given by

$$\omega_r^2 = \frac{1}{\rho_l R_0^2} \left[3\gamma \left(P_0 + \frac{2\sigma}{R_0} \right) - \frac{2\sigma}{R_0} \right] \tag{2.8}$$

(The ideal gas law is assumed here.) For the typical choice of equilibrium bubble radius of $R_0 \sim 4\ \mu m$, the value of the resonant frequency is about $300-400\ KHz$. This is usually much higher than typical acoustic frequencies used in single bubble experiments ($20-30\ KHz$), but for the initially large bubbles one could expect interference between forced and natural bubble oscillations. We will discuss the influence this coupling has on the bubble dynamics later.

2.3.1 Solution of the Rayleigh - Plesset Equation

We solve Eq. (2.6) numerically, with the pressure in the gas given by Eq. (2.5). The numerical algorithm used was based on the Runge - Kutta method with repeated Richardson extrapolation. The result for the choice of parameters used in the experiments [34] is presented in Fig. 2.2. This result represents the typical nonlinear response, where the maximum bubble radius is many times larger than the equilibrium one. The expansion phase is followed by a fast contraction. The motion of the bubble wall is periodic with the period of the sound field. One should also note the small oscillations after the first minimum. The period of these oscillations is equal to the inverse of the resonant bubble frequency.

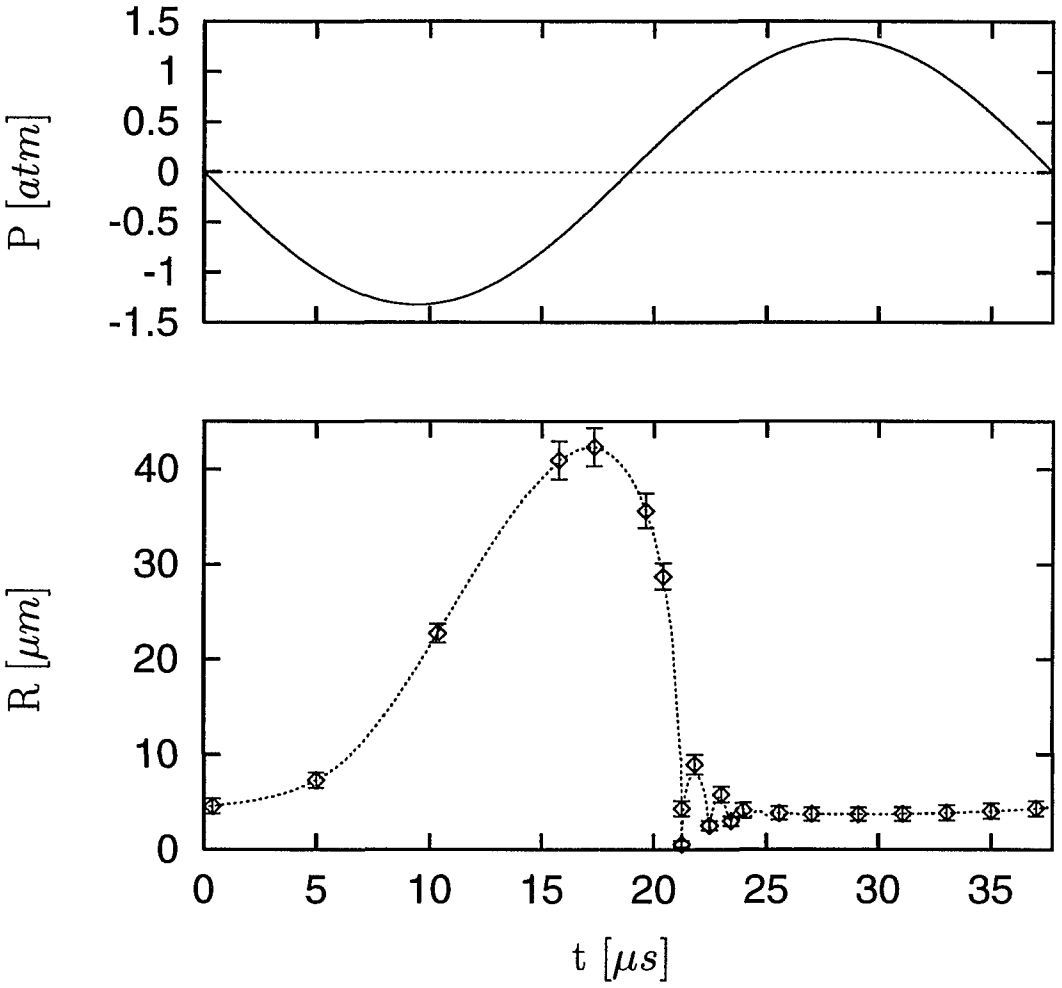

Figure 2.2: *Bubble radius versus time for one full period for a strongly driven bubble, as a result of the R.P. equation. Points with errorbars are experimental results. The acoustic pressure amplitude (presented in the upper part of the figure) is* 1.325 *atm and the initial bubble radius is* 4.5 μm. *The other parameters entering are: acoustic frequency* $f_a = 26.5\ KHz$, $\gamma = 1.4$, $1/b = 0.794\ g/cm^3$, $\rho_l = 1.0\ g/cm^3$, $c_l = 1.481\ km/s$, $\nu_l = 0.01\ cm^2/s$ *(for water at* $20°C$*). A surface tension* $\sigma = 72.5\ dyn/cm$ *was included.*

The numerical results which we obtain are in very good agreement with experimental data [2, 3, 29, 34], as shown on the above figure. For the comparism, we also show the solution obtained with a lower acoustic pressure amplitude in Fig. 2.3. We see that in this case, the response of the bubble is much weaker. This response is typical for the linear regime of the bubble oscillations. Note that the oscillations occurring for $t > 21\,\mu s$ correspond to the resonant frequency of the bubble.

2.3.2 Sensitivity to Input Parameters

Since a more complete treatment of the bubble dynamics is going to be given later in chapter 3, we will not go here into the details of the bubble response to the change of the input parameters. Let us just mention that the motion of the bubble wall is extremely sensitive to the change of the acoustic pressure amplitude, P_a. The results for some important quantities determining the bubble motion for a few pressure amplitudes and different initial bubble radii can be seen in the first few columns of Table 4.1, on page 100. These results follow from the more complete treatment of bubble dynamics, given in chapter 3, but the results for the maximum bubble radius are almost the same as those following from the approach given here.

An interesting observation can be made by integrating the R.P. equation for many periods and for increasing initial bubble radius. The steady-state results are presented in Fig. 2.4. We see that for an initially small bubble, the maximum bubble radius R_{max} grows as the initial radius R_0 increases. The oscillations which start to develop for the initial radius of about $6\,\mu m$ are due to the nonlinear resonances of the radial motion (interference between forced and natural frequency). As the initial radius is increased further, we observe period doubling, also known as pitchfork bifurcation. Here, the values of

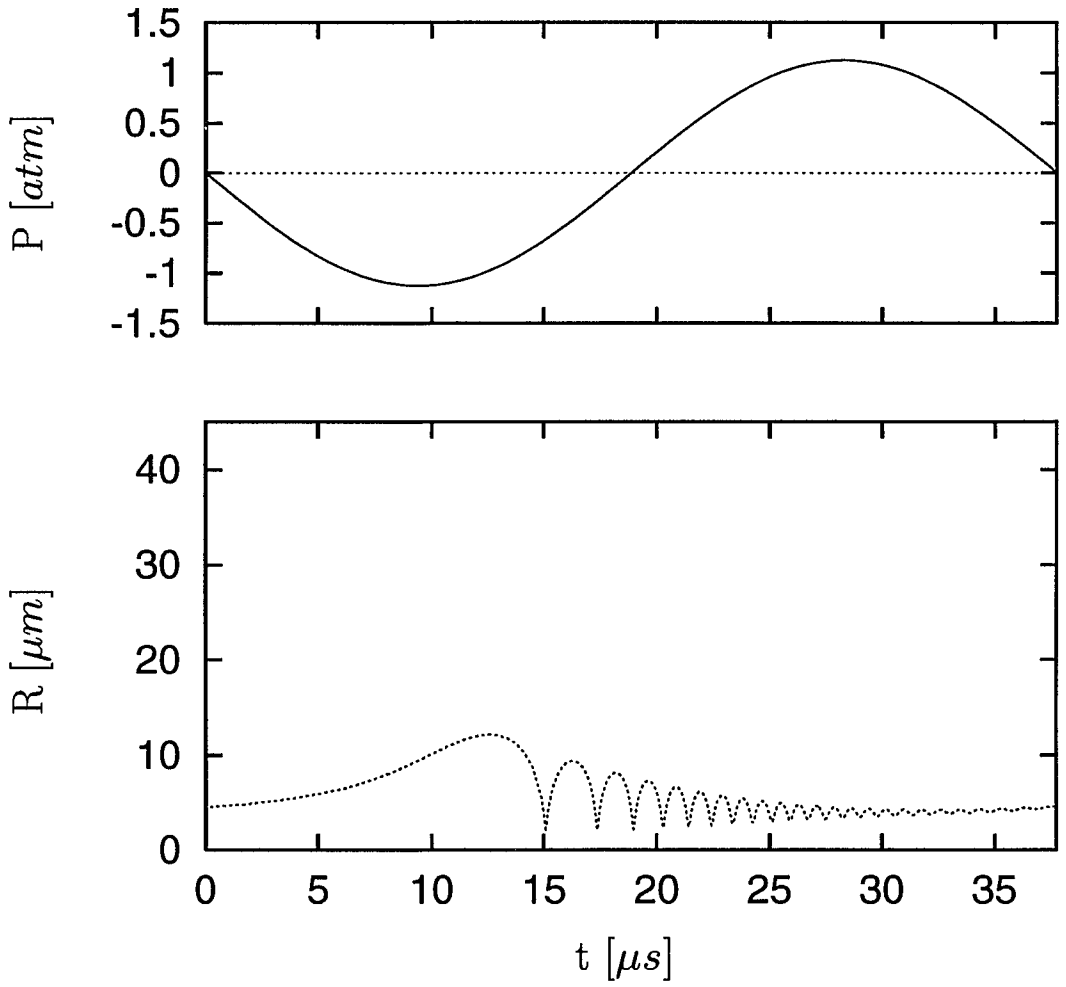

Figure 2.3: *Bubble radius versus time for a weakly driven bubble (acoustic pressure amplitude* 1.125 *atm), as a result of the R.P. equation. Other parameters are the same as in the previous figure.*

R_{max} alternate between two different values from one acoustic period to the next. This transition typically occurs for the values of R_0 about $0.1 \times R_{res}$, where R_{res} is defined as a value of the equilibrium bubble radius which would make the resonant bubble frequency, given by Eq. (2.8), equal to the acoustic frequency. As the initial bubble radius R_0 is further increased, a period four transition is observed as well, (not in Fig. 2.4), as the bubble advances on its route to chaos.

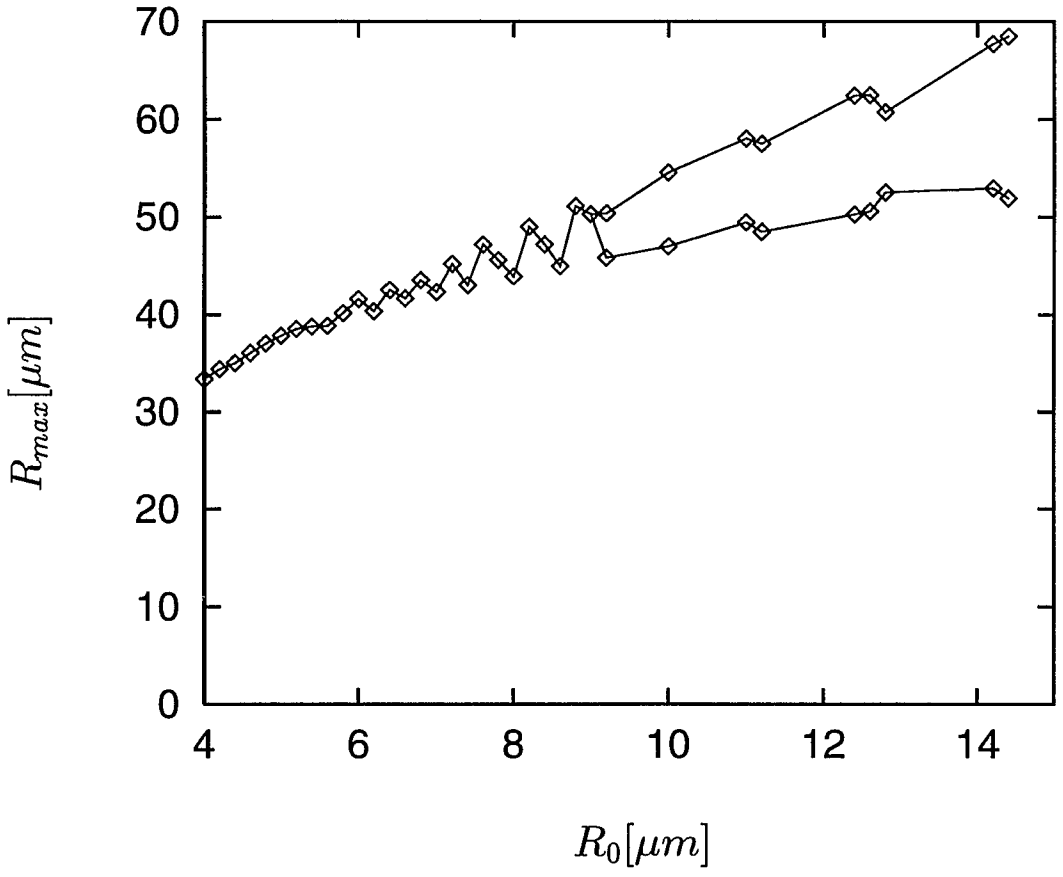

Figure 2.4: *Bubble response to an applied acoustic pressure of* 1.325 *atm as a function of equilibrium bubble radius* R_0.

2.4 Preliminary Theoretical Overview

In this section we will present a few of our early theoretical attempts to explain the effect of sonoluminescence. These are based on the results for the thermodynamic properties of the gas in the bubble following from the solution of Rayleigh - Plesset equation, presented in the first part of this chapter. Here we give just an overview of the different methods we used. More details are given in Appendices A-D. Based on our analysis of these effects we were able to reject them as being viable explanations. In later chapters we will present what we believe to be the correct theory.

Collective Effects

The short duration of the SL pulse was our motivation to explore the possibility that some collective effect, like superradiance or superflourescence, could take place.

The cooperative emission from a system of $N >> 1$ atoms is a typical many body effect consisting of an emission proportional to N^2 and a duration proportional to N^{-1}. Superradiance is a cooperative emission from a system excited by a coherent pulse into a "correlated" state which has a macroscopic dipole moment. If we start from the initially uncorrelated excited atoms and the system spontaneously creates correlation, we are talking about the phenomenon of superflourescence. A third "kind" of radiation, also proportional to N^2 is free induction decay, which has to do with the strong inhomogeneous broadening - loss of the coherence through dephasing among atoms with different natural frequencies. For a short time the radiation is enhanced by the coherence, but the energy released is just a small fraction of the total energy. "Short" here refers to the dephasing time - the time needed to destroy the

coherence.

Our theoretical model is presented in Appendix A. We find that some of our results do not seem to be compatible with the experimental ones, e.g. the spectral distribution of the emitted radiation.

Trapping of Light

Here we explore the optical properties of the gas in the bubble. The basic idea is that the extreme conditions in the bubble might be expected to lead to high values of the dielectric constant of the gas and eventual trapping of radiation in the bubble. The details are presented in Appendix B, where we also explore the possibility that shock waves might be produced in the bubble during its final stages of collapse.

"Electrical" Models

We formulated a few models where we explored the consequences of the high temperatures in the bubble on its electrical properties. These models, presented in Appendix C, examine the possibility of charge separation in the bubble, or in the bubble-liquid system. Although we cannot rule out that some of these effects are taking place, we could not find conclusive evidence that they are important for the emission of sonoluminescent radiation.

Plasma radiation

The high temperatures which develop in the bubble naturally lead to the idea that a plasma could form in the bubble close to its minimum radius. Relatively high temperatures are required, so this assumption is based on the formation of shock waves in the bubble or the adiabatic collapse of the bubble

with a large compression ratio. The details are presented in Appendix D. We find that the observed SL radiation cannot be explained on the basis of simple radiation from a plasma and that a more elaborate approach is required in order to fully understand the effect.

Conclusion

In this chapter we presented the fundamental mechanisms which lead to cavitation, and explained the basic model which is able to reproduce most of the experimental observations in the field of cavitation. The maximum temperature which is achieved in the bubble, following from this approach, is of the order of a few thousand degrees. This stems from the use of the adiabatic equation of state for the gas, Eq. (2.5). It is not clear if the motion of the bubble wall becomes supersonic or not relative to the speed of sound in the gas. The answer to this questions is going to be given in chapter 3, where we will present the solution of the R.P. equation and where the assumption of the spatial uniformity of the gas inside the bubble is relaxed. This will turn out to be the most important factor in obtaining a correct understanding of the dynamics of a strongly driven gaseous bubble in a liquid. We also presented a few theoretical models with the goal of trying to understand SL. It is found that a better understanding of the thermodynamic properties of the gas is required in order to fully understand the effect of sonoluminescence.

Chapter 3

Bubble Dynamics

Introduction

The detailed measurement of the radius of the bubble as a function of time [34] offers the possibility that the wall of the bubble achieves supersonic speeds prior to the onset of luminescence. It has been proposed that SL is associated with the production of shock waves in the air in the bubble [34], as previously noted. Of course, if the conditions for launching the shock waves in the bubble are really satisfied, the adiabatic approximation used in chapter 2, as well as the assumption that the thermodynamic variables (pressure, density, temperature) are independent of the position, are not valid anymore.

We develop a few approaches with which we can address these issues. In section 3.1 we simulate the gas molecules in the bubble as hard spheres. This approach does not give us a definitive answer to our question about the production of shock waves, but it still provides interesting side-results about random close packing and helps justify our use of the gas-dynamic equations. Section 3.2 represents our first trial to solve the R.P. equation,

Eq. (2.6), coupled with the gas-dynamic equations for the gas in the bubble. This method confirmed that the bubble wall achieves supersonic speeds with respect to the speed of sound in the bubble. The complete solution of the gas-dynamic equations coupled with the R.P. equation, Eq. (2.6), is presented in section 3.3. The results without inclusion of corrections due to vibrational degrees of freedom, dissociation, ionization and radiation, as well as the comparison of our results with the self-similar solution, are presented in section 3.4. Finally, inclusion of the correction terms and consequent changes in the results are the subject of the last two sections 3.5-3.6.

3.1 Simulation

We model our bubble as follows: a certain number of spheres are randomly distributed inside a pulsating spherical cavity. These spheres (simulating atoms/molecules) were given random velocities according to the Maxwellian distribution and were allowed to specularly collide with each other and with the bubble wall. Between the collisions, free flight was assumed. The rotational degrees of freedom were not included, so we were able to simulate a monoatomic gas. The collisions were assumed to be elastic and no correction for the loss of the kinetic energy due to ionization was included. The parameters for the simulation were chosen in such a way that the internal energy, the mean free path for the collisions and the mass density inside the bubble were the same as in experiment [34]. The temperature in the bubble was obtained by examining the local velocity fluctuations away from the mean flow velocity and extracting the kinetic energy fluctuations. The pressure was obtained as the ratio of the average force (which acts on the bubble wall because of the collision with the spheres) to the area of the bubble. We

started the evolution of the system from the maximum radius, assuming that all terms on the right hand side of R.P. equation, Eq. (2.6), can be safely neglected. (The effect of these terms grow with time, but the time scale for the collapse of the bubble from the maximum radius to the minimum is much shorter than the acoustic period.) At the point where the pressure developed in the bubble was high enough to influence the motion of the wall, the term $P_g(R)/\rho$ was included[1]. In order to keep the computing time at a reasonable level, the number of spheres was limited to 1,000.

The results of our simulation and the van der Walls fit are in very good agreement. By fitting the average temperature in the bubble to the form

$$T(R^3 - a^3)^{\gamma-1} = C \tag{3.1}$$

where R is the bubble radius, we obtained the values for the fitting parameters $\gamma = 1.678$, $a = 4.413 \times 10^{-5}\, cm$ and $C = 4.77 \times 10^{-5}$. These results are consistent with those obtained from the analogous pressure fit. The fitting value of γ is very close to the value for monoatomic gases (5/3), as might be expected. The excluded radius a gives the result that the ratio of the excluded volume to the volume actually occupied by the spheres is equal to 5.3 ± 0.7, close to the value of 4 which is given, for example, in [70]. The excluded volume is of crucial importance, giving a high temperature close to the point of the maximum contraction. We also noted a well defined spatial dependence of the gas density in the bubble. During the compression part of the cycle, the density is higher close to the wall, and during expansion it is higher close to the bubble center.

However, this spatial dependence, for a variety of initial conditions, could

[1]The other terms on the right hand side of Eq. (2.6) should not be very important compared to the pressure in the gas, which gets to be very high.

not be connected with the Hugoniot jump conditions for strong shock waves. Since our spheres have to be fairly large (in order to keep the mean free path the same as in a real gas), it seems that this kind of simulation is not the best way to give a definite answer concerning the existence of sharp gradients of the thermodynamic variables. So, our goal in the next sections of this chapter is going to be a direct integration of the gas-dynamic equations.

Before that, let us mention the interesting result of our simulation in a slightly different context.

3.1.1 Random Close Packing

Let us consider the following experiment: a large number of hard spheres is quickly introduced into a container and are compacted. The resulting structure is called random close packing (rcp) and is characterized by a filling factor (percentage of total volume occupied) of 0.637 [71]. This means that random close packing is about 86 % as dense as is crystalline close packing (filling factor 0.7405). Theoretical investigations have confirmed that this structure represents a local energy minimum. Although it corresponds to a metastable configuration, there is no possible continuous transition to a lower energy state (e.g. fcc structure). Random close packing has been observed in nature and currently it represents one of the best models for the structure of amorphous metals.

We tried to reproduce these experimental results using our simulation approach. In order to achieve this goal we assumed that our bubble was contracting in a rigid manner, so the bubble wall moved inwards, irrespective of the huge pressure which developed inside the bubble. The goal was to verify that the maximum achievable density is comparable to the value for random close packing. Our numerical results are presented in Fig. 3.1. Since

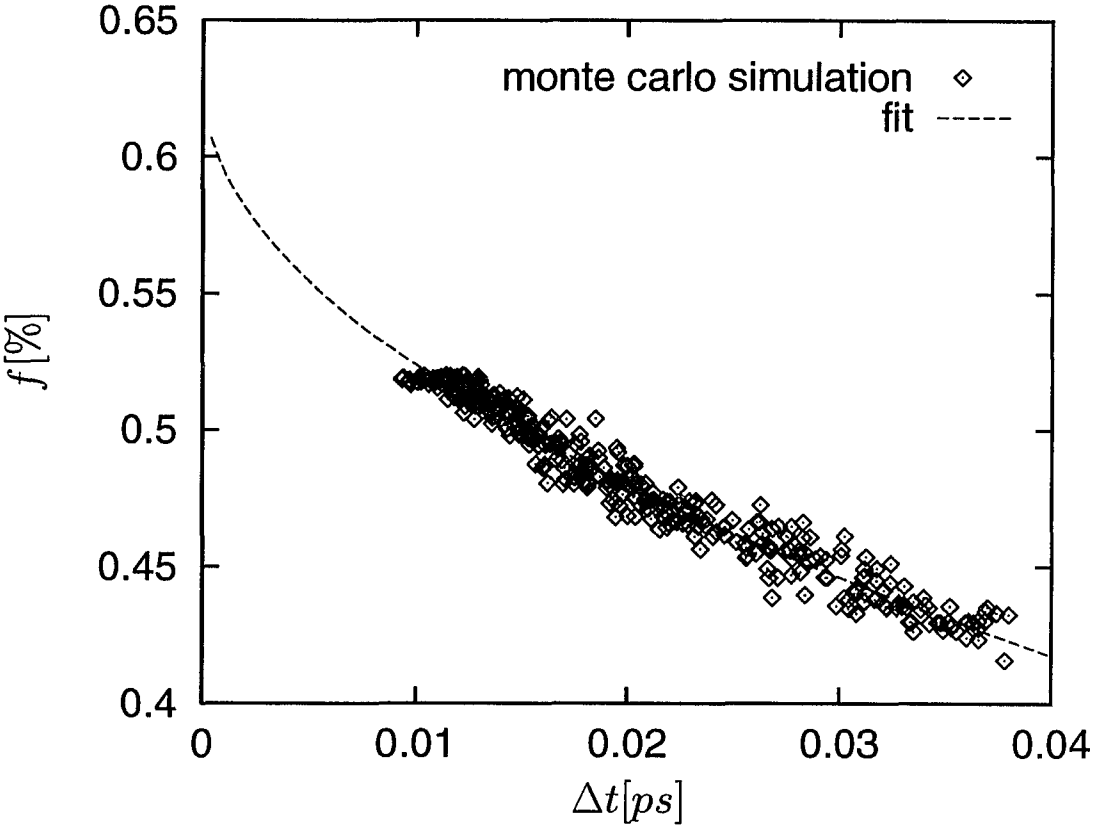

Figure 3.1: *Theoretical calculation of the volume occupied by spheres f(in percent of total volume) as a function of the time between collisions. Each point represents the time for* 100 *collisions. The analytical fit is of the form* $f(\Delta t) = a + b(\Delta t)^{\alpha}$, *with the values of the coefficients* $a = 0.627$, $b = 1.082$ *and* $\alpha = 0.51$.

the average time between the collisions goes to zero, (the distance between the spheres gets to be very small), the computing time goes to infinity in this limit. Correspondingly, we employ our model until the average time between the collisions reaches the fairly small value of about $10^{-16}\,s$ (in Fig. 3.1 each point corresponds to the time needed for 100 collisions). The fit which is presented in this figure gives the value for the filling factor of 0.627, fairly close to the value for random close packing. However, our result differs slightly for different forms of the fitting function, and since we are not able to approach the origin ($\Delta t = 0$) more closely, it has a rather large uncertainty.

3.2 Integration of the Gas Dynamics Equations: POST Package

Assuming spherical symmetry and neglecting viscosity and heat conduction of the gas in the bubble, the gas-dynamic equations are

$$\frac{\partial \rho}{\partial t} + \frac{1}{r^2}\frac{\partial}{\partial r}(r^2 \rho v) = 0 \tag{3.2}$$

$$\frac{\partial}{\partial t}(\rho v) + \frac{1}{r^2}\frac{\partial}{\partial r}(r^2 \rho v^2) + \frac{\partial P}{\partial r} = 0 \tag{3.3}$$

$$\frac{\partial}{\partial t}[\rho \frac{v^2}{2} + \frac{1-b\rho}{\gamma - 1}P] + \frac{1}{r^2}\frac{\partial}{\partial r}[r^2 v(\rho \frac{v^2}{2} + \frac{1-b\rho}{\gamma - 1}P)] = 0 \tag{3.4}$$

where r is distance from the center of the bubble, ρ is the gas density, P is the gas pressure, v is the radial gas velocity and b is the excluded volume $(1/\rho_m)$, where ρ_m is the maximum possible density. For practical purposes, we changed independent variables to $x = r/R(t)$, $t = \tau$, where $R(t)$ is the bubble radius, so the problem is always confined to the region $0 < x < 1$, independent of the actual bubble size. We also choose to use the velocity,

pressure and entropy as the primary dependent variables. The equation of state is

$$P = \frac{k_B}{m}\frac{\rho T}{1-b\rho} \tag{3.5}$$

where m is the molecular mass and k_B Boltzmann's constant. Using the local adiabatic assumption, the entropy per particle s can be simply expressed in terms of the pressure and density

$$s = \frac{k_B}{\gamma - 1}\left[ln\left(\frac{P}{P_0}\right) + \gamma\ ln\left(\frac{1/\rho - b}{1/\rho_0 - b}\right)\right] \tag{3.6}$$

where ρ_0, P_0 are the initial values of the pressure and density. The entropy s is defined with respect to the initial entropy s_0. We also define the auxiliary quantity D and the speed of sound c

$$D = \frac{\dot{R}(\tau)}{R(\tau)}x - \frac{v}{R(\tau)}$$

$$c^2 = \frac{\gamma P}{\rho(1-b\rho)}$$

Thus, the final form of the equations we want to solve are

$$\frac{\partial v}{\partial \tau} = D\frac{\partial v}{\partial x} - \frac{1}{\rho R}\frac{\partial P}{\partial x} \tag{3.7}$$

$$\frac{\partial P}{\partial \tau} = D\frac{\partial P}{\partial x} - \frac{\rho c^2}{R}\frac{\partial v}{\partial x} - \frac{2\rho v c^2}{Rx} \tag{3.8}$$

$$\frac{\partial s}{\partial \tau} = D\frac{\partial s}{\partial x} \tag{3.9}$$

We started integrating Eqs. (3.7 - 3.9) coupled with Eq. (2.6) from the point where the bubble radius is at a maximum. The initial conditions for Eqs. (3.7 - 3.9) are

$$v(x, \tau = 0) = 0 \tag{3.10}$$

$$P(x, \tau = 0) = P_0 \tag{3.11}$$

$$s(x, \tau = 0) = 0 \tag{3.12}$$

where P_0 is assumed to follow from the globally adiabatic expansion of the bubble from its equilibrium radius. The boundary conditions are

$$v(x = 1, \tau) = \dot{R} \tag{3.13}$$

$$v(x = 0, \tau) = 0 \tag{3.14}$$

$$s(x = 1, \tau) = 0 \tag{3.15}$$

The condition, Eq. (3.13) connects the bubble wall velocity $\dot{R}$ with the velocity of the gas just next to the wall and Eq. (3.14) results from the spherical symmetry of the problem. The last boundary condition, Eq. (3.15) follows from the assumption of constant entropy and is satisfied as long as dissipative mechanisms (like shock production) are not present. For integration of our equations we use the POST package [72], nonlinear partial differential equation solver, available as a part of the PORT library. This software uses the very stable Backwards-Euler time discretization connected with a B-spline fit to the space profile of the solution at any point in time. The results which we present were obtained with 100 points in the space grid and the time step was varied from 10^{-9} s (at the beginning of the integration) to 10^{-15} s (close to the minimum bubble radius). From Fig. 3.2 we can see that the motion of the bubble wall gets to be supersonic with respect to the local speed of sound just inside the bubble at the point where the bubble radius is about 2.8 microns. This conclusion could not have been made on the basis of the solution of Eq. (2.6) which assumes adiabatic conditions in the bubble (Fig. 2.2). The supersonic motion of the bubble wall with respect to the gas implies that the production of shock waves inside the bubble can

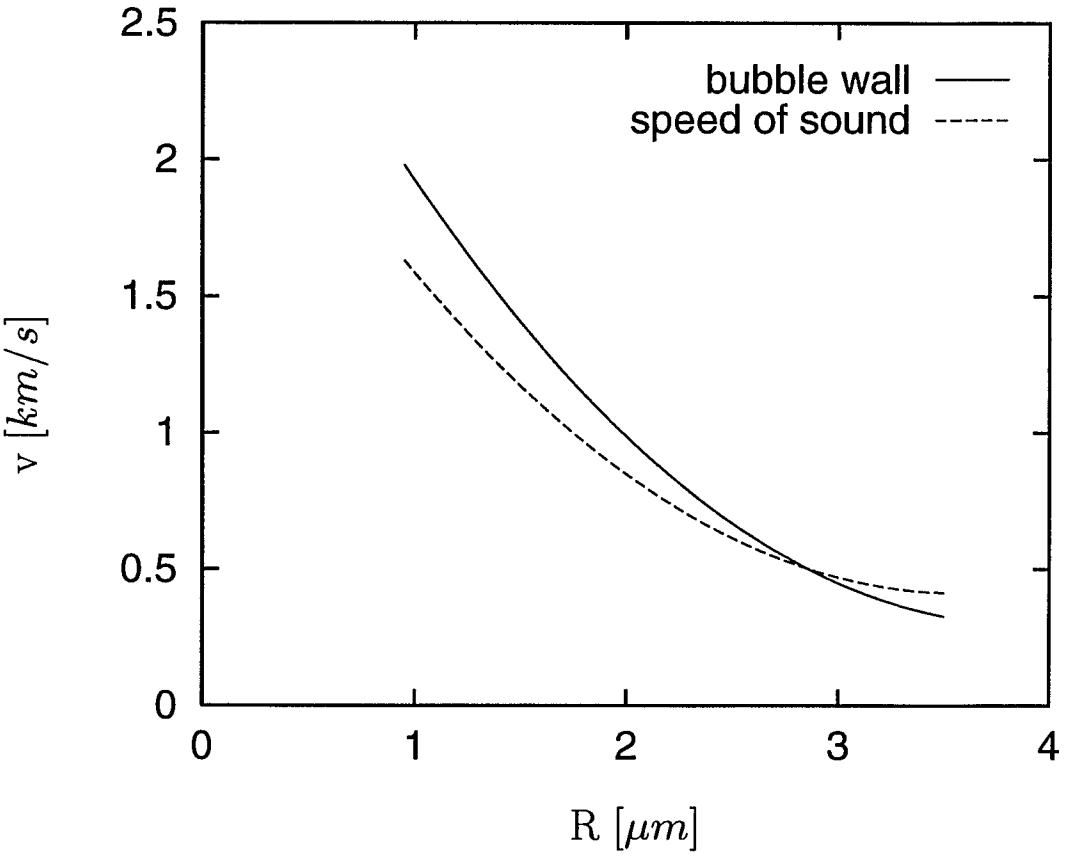

Figure 3.2: *The speed of sound in the bubble just next to the wall and the speed of bubble wall close to the minimum radius. This is the result of the POST program. The motion of the bubble wall becomes supersonic at about 2.8 μm. The parameters entering are the same as in Fig. 2.2.*

be expected. Because of numerical difficulties[2] the POST package was not the optimum tool to integrate all the way through the collapse of the bubble. For this purpose we used a different algorithm which is explained in the following section.

3.3 Integration of the Gas Dynamics Equation: Godunov Method

In this section we use the Godunov method for integration of the gas-dynamic equations. This method is a modification of the Method of Characteristics and is known to work well [73, 74] for problems where the production of shock waves is expected.

3.3.1 Formulation of the Problem

Our problem consists of the gas-dynamic equations coupled with R.P. equation, Eq. (2.6). Following the same assumptions as in section 3.2, the gas-dynamic equations in a Lagrangian formulation are

$$\frac{\partial V}{\partial t} - \frac{\partial}{\partial \xi}(r^{\alpha} u) = V^2 \, \mathcal{L} \tag{3.16}$$

$$\frac{\partial u}{\partial t} + r^{\alpha} \frac{\partial p}{\partial \xi} = \mathcal{F} \tag{3.17}$$

$$\frac{\partial E}{\partial t} + \frac{\partial}{\partial \xi}(r^{\alpha} u p) = -\Lambda + u\mathcal{F} - p\mathcal{L}V^2 \tag{3.18}$$

[2]These numerical difficulties result from the shock production. The production of a shock leads to singularities in Eqs. (3.7 - 3.9). Through certain remappings of the coordinates, in principle it is possible to use the POST package for this situation. The transition from a non-shock to a shock region, however, proved to be extremely sensitive in the numerical sense.

coupled with

$$\frac{\partial r}{\partial t} = u \tag{3.19}$$

which specifies the radial motion of the gas particle. In Eqs. (3.16 - 3.18) $V = 1/\rho$ is the specific volume, $E = \epsilon(p,\rho) + u^2/2$ is the energy per unit mass and $\epsilon(p,\rho)$ determines the equation of state. The variables p, ρ, u are the pressure, density and velocity of the gas, respectively. Here α specifies the geometry of the problem, being $0, 1, 2$ for the planar, cylindrical and spherical cases, respectively. We are going to use $\alpha = 2$ in the calculations. The Lagrangian coordinate ξ and r are related by

$$d\xi = (r^\alpha/V)\ dr = \rho r^\alpha dr \tag{3.20}$$

or, equivalently, in terms of the initial particle position r_0

$$\rho_0 r_0^\alpha dr_0 = \rho r^\alpha dr \tag{3.21}$$

The additional terms which appear in Eqs. (3.16 - 3.18) are $\mathcal{L}$, $\mathcal{F}$ and Λ which represent mass loss, body force (momentum loss) and energy loss, respectively. If the possibility of the gas being dissociated or ionized is excluded (the approximation which is going to be corrected in section 3.5), the equation for the internal energy per unit mass as a function of temperature T is

$$\epsilon(T) = \frac{N}{\gamma - 1} k_B T \tag{3.22}$$

which, together with van der Waals equation

$$P\frac{(1 - b\rho)}{\rho} = N k_B T \tag{3.23}$$

gives $\epsilon(p,\rho)$, which enters the energy equation, Eq. (3.18). Here b is the inverse of the maximum allowed density, N is the number of particles per unit mass, k_B is the Boltzmann constant and γ is the ratio of specific heats.

If there is no energy loss, Eq. (3.18) can be rewritten in the simple form[3] $\partial S/\partial t = 0$, where S is the entropy. Using this form of the energy equation, Eqs. (3.16) and (3.17) can be written in the characteristic form

$$\left(\frac{\partial u}{\partial t} + a\frac{\partial u}{\partial r}\right) + \frac{1}{\rho a}\left(\frac{\partial p}{\partial t} + a\frac{\partial p}{\partial r}\right) = \mathcal{F} - \frac{\alpha a u}{r} - \frac{\mathcal{L}a}{\rho} \tag{3.24}$$

$$\left(\frac{\partial u}{\partial t} - a\frac{\partial u}{\partial r}\right) + \frac{1}{\rho a}\left(\frac{\partial p}{\partial t} - a\frac{\partial p}{\partial r}\right) = \mathcal{F} + \frac{\alpha a u}{r} + \frac{\mathcal{L}a}{\rho} \tag{3.25}$$

where a is the speed of sound defined by $a^2 = (\partial p/\partial \rho)_S$. So, along the characteristics, Eqs. (3.16 - 3.18) are

$$du + \frac{1}{\rho a}dp = \left(-\frac{\alpha a u}{r} - \frac{\mathcal{L}a}{\rho} + \mathcal{F}\right)dt \quad \text{along } C_+ : \ \frac{dr_0}{dt} = a\frac{\rho r^\alpha}{\rho_0 r_0^\alpha} \tag{3.26}$$

$$du - \frac{1}{\rho a}dp = \left(\frac{\alpha a u}{r} + \frac{\mathcal{L}a}{\rho} + \mathcal{F}\right)dt \quad \text{along } C_- : \ \frac{dr_0}{dt} = -a\frac{\rho r^\alpha}{\rho_0 r_0^\alpha} \tag{3.27}$$

$$dS = 0 \qquad \text{along } C_0 : \ \frac{dr_0}{dt} = 0 \tag{3.28}$$

The last set of equations, Eqs. (3.26 - 3.28), is going to be used in the following section where we will explain the application of Godunov algorithm to our problem.

3.3.2 Godunov Method

This method was originally formulated with the goal of establishing a method which will retain the simplicity of the Method of Characteristics. At the same time it should include the possibility of surfaces of discontinuity such as shock waves and fluid interfaces. The essence of the method lies in dividing the

[3]Note that the partial derivative with respect to time in Lagrangian coordinates (keeping ξ constant) corresponds to the total time derivative in Eulerian coordinates.

region of interest into a number of cells and averaging the values of the thermodynamic variables in each cell. The values at the boundaries are calculated using the gas-dynamic equations in characteristic form. These boundary values are consequently used to determine the average values at a later time. The algorithm effectively introduces an artificial viscosity which converts discontinuities common in shock problems into sharp gradients which allow numerical treatment. The basic cell (zone) which is used in the algorithm is shown in Fig 3.3. Integer values of the index i correspond to the zone boundary, and half-integer values to the zone average. Averaged values are usually overlined. Subscripts (e.g. r_i) refer to the current time t and superscripts (e.g. r^i) to the following time $t + \Delta t$. The values at the zone boundaries are capitalized.

Interfacial Quantities

The first step in the algorithm is to follow the characteristics forward in time and determine values of U_i and P_i at the intermediate time $t + \Delta t'$, where $\Delta t' < \Delta t$. Using Eqs. (3.26) and (3.27), the following expressions are obtained for U_i and P_i (see Fig. 3.3)

$$U_i - u_{i-1/2} + \frac{P_i - p_{i-1/2}}{(\overline{\rho a})_{i-1/2}} = \left[-\alpha \left(\frac{\overline{ua}}{\overline{r}} \right)_{i-1/2} - \left(\frac{\overline{\mathcal{L}a}}{\overline{\rho}} \right)_{i-1/2} + \overline{\mathcal{F}}_{i-1/2} \right] \Delta t' \tag{3.29}$$

along C_+, and

$$U_i - u_{i+1/2} + \frac{P_i - p_{i+1/2}}{(\overline{\rho a})_{i+1/2}} = \left[\alpha \left(\frac{\overline{ua}}{\overline{r}} \right)_{i+1/2} - \left(\frac{\overline{\mathcal{L}a}}{\overline{\rho}} \right)_{i+1/2} + \overline{\mathcal{F}}_{i+1/2} \right] \Delta t' \tag{3.30}$$

along C_-. The intermediate time step is given by $\Delta t' = \Delta t / f$, where $f > 1$. The choice of Δt is going to be explained later (see page 53). For all practical

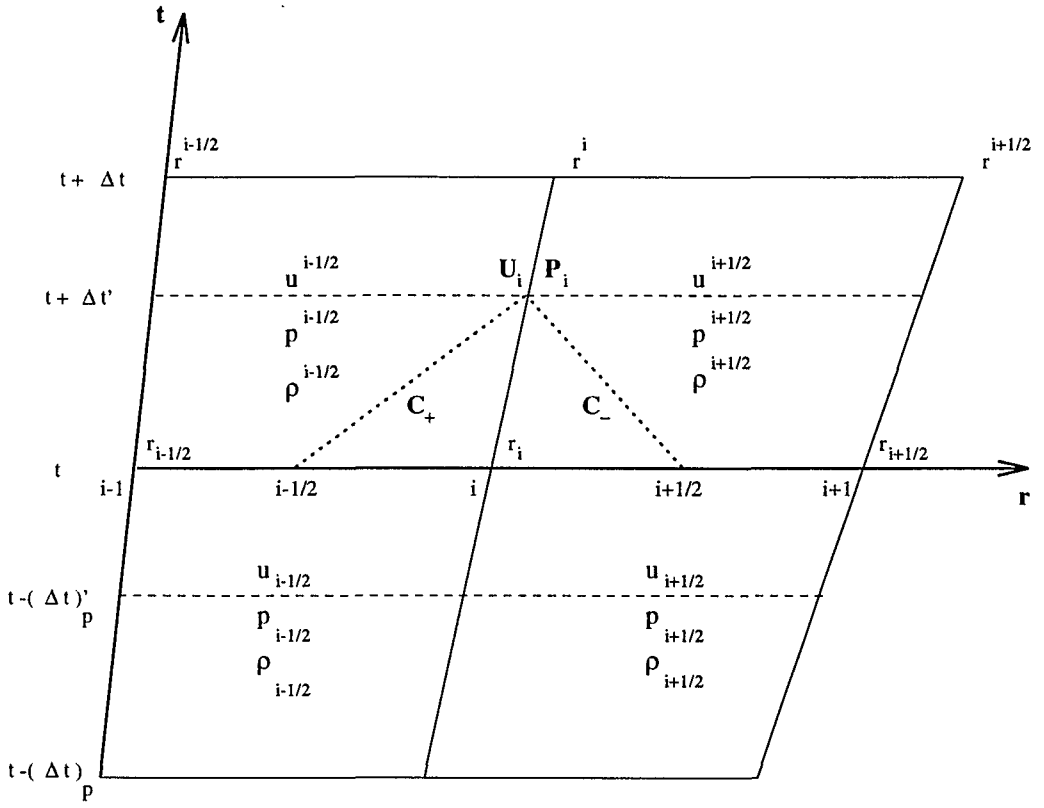

Figure 3.3: *Basic zone scheme as used in Godunov method.*

purposes, we may use

$$\Delta t' = \frac{1}{2}\left(\frac{\Delta r}{\overline{a}}\right)_{i\pm 1/2} \tag{3.31}$$

where[4]

$$(\Delta r)_{i\pm 1/2} \equiv |r_{i\pm 1} - r_i| \tag{3.32}$$

Equations (3.29 - 3.31) could be combined and written in terms of the Riemann Invariants form (the upper sign corresponds to a C_+ characteristic and the lower one to a C_- characteristic)

$$U_i - u_{i\mp} \pm \frac{P_i - p_{i\mp}}{(\overline{\rho a})_{i\mp 1/2}} = 0 \tag{3.33}$$

where

$$p_{i\mp} \equiv \overline{p}_{i\mp 1/2} \pm \frac{1}{2}(\overline{\rho\mathcal{F}})_{i\mp 1/2}\ \Delta r_{i\mp 1/2} \tag{3.34}$$

$$u_{i\mp} \equiv \overline{u}_{i\mp 1/2} \mp \frac{\alpha}{2}\left(\frac{\overline{u}}{\overline{r}}\right)_{i\mp 1/2} \Delta r_{i\mp 1/2} \mp \frac{1}{2}\left(\frac{\overline{\mathcal{L}}}{\overline{\rho}}\right)_{i\mp 1/2} \Delta r_{i\mp 1/2} \tag{3.35}$$

Eqs. (3.33), together with the definitions (3.34) and (3.35), represent a system of two equations with two unknowns (U_i, P_i) which can be solved.

Numerical Procedure

We now calculate quantities for the next time step. The Godunov method uses the following relations for the quantities r^i and $u^{i+1/2}$

$$\left(\frac{r^{\alpha+1}}{\alpha+1}\right)^i = \left(\frac{r^{\alpha+1}}{\alpha+1}\right)_i + r_i^\alpha\ U_i\ \Delta t \tag{3.36}$$

and

$$u^{i+1/2} = u_{i+1/2} - \overline{r}^\alpha_{i+1/2}\ \frac{P_{i+1} - P_i}{(\overline{\rho r^\alpha})_{i+1/2}\ \Delta r_{i+1/2}}\Delta t + \mathcal{F}_{i+1/2}\ \Delta t \tag{3.37}$$

[4]Practically, we calculate $(\Delta t)_i$ for each point i in the spatial grid and choose the shortest one for the next time step.

Equation (3.37) follows directly from Eq. (3.17). It is important to note that the interfacial quantities, calculated at the intermediate time $t + \Delta t'$, are used for the time evolution of the system. The motivation for Eq. (3.36) is as follows. If the density at time t is given by

$$\rho_{i+1/2} \left[\left(\frac{r^{\alpha+1}}{\alpha+1} \right)_{i+1} - \left(\frac{r^{\alpha+1}}{\alpha+1} \right)_{i} \right] = (\Delta\xi)_{i+1/2} \tag{3.38}$$

($(\Delta\xi)_{i+1/2}$ is a mass in the zone), Eq. (3.36) combined with the continuity equation, Eq. (3.16), guarantees that the same relation is going to be valid at later time, $t + \Delta t$

$$\rho^{i+1/2} \left[\left(\frac{r^{\alpha+1}}{\alpha+1} \right)^{i+1} - \left(\frac{r^{\alpha+1}}{\alpha+1} \right)^{i} \right] = (\Delta\xi)^{i+1/2} \tag{3.39}$$

The mass in the zone is either conserved or lost at a rate $\mathcal{L}$

$$(\Delta\xi)^{i+1/2} = (\Delta\xi)_{i+1/2} \ \exp\left[-(\mathcal{L}/\rho)_{i+1/2} \, \Delta t \right] \tag{3.40}$$

so[5] the density at time $t + \Delta t$ can be calculated from Eq. (3.39).

The pressure in the zone may be obtained using the energy equation, Eq. (3.18), which is rewritten as

$$\frac{\partial E}{\partial t} = -\frac{\partial}{\partial t}(r^{\alpha} u p) + \mathcal{G} \tag{3.41}$$

where

$$\mathcal{G} = -\mathcal{L} + u\mathcal{F} - p\mathcal{L}V^2 \tag{3.42}$$

As before, we use a forward difference for the time derivative and the interfacial quantities for the derivative with respect to ξ. The energy at the

[5]The exponential factor in Eq. (3.40) makes sure that the mass cannot become negative in the zone.

following time is given by

$$E^{i+1/2} = E_{i+1/2} - \frac{r_{i+1}^{\alpha}\, U_{i+1}\, P_{i+1} - r_i^{\alpha}\, U_i\, P_i}{\left(\overline{r^{\alpha}\rho\Delta r}\right)_{i+1/2}}\Delta t + \mathcal{G}_{i+1/2}\,\Delta t \qquad (3.43)$$

Now, the pressure at the following time can be calculated using Eqs. (3.22) and (3.23)

$$p^{i+1/2} = \frac{(\gamma-1)\rho}{1-b\rho}\left[E^{i+1/2} - \frac{1}{2}\left(u^{i+1/2}\right)^2\right] \qquad (3.44)$$

In principle, the algorithm is now fully defined. In the rest of this section we are going to discuss the stability criterion and initial and boundary conditions.

Stability Criterion

A proper choice of time step is of crucial importance. In order for the algorithm to be stable, the Courant-Friedrichs-Lewy condition must be respected

$$\frac{(\Delta r)_{i+1/2}}{\Delta t} > \overline{a}_{i+1/2}\ ,\ \forall i \qquad (3.45)$$

i.e. the computational speed should be faster than the speed of sound for every i, so information can be carried across a zone before the sound wave reaches there[6].

The second condition which must be satisfied is the "non-crossing" condition. Namely, it is required that two adjacent boundaries do not cross each other. Thus,

$$\Delta\left(\frac{r^{\alpha+1}}{\alpha+1}\right)^{i+1/2} > 0\ ,\ \forall i \qquad (3.46)$$

[6]In practical calculations we used $\Delta t = 3/4\,\Delta r/\overline{a}$. We have to make sure that the intermediate time step $\Delta t'$ given by Eq. (3.31) is always shorter than the complete time step.

For practical purposes, we use the condition

$$(\Delta r)^{i+1/2} > \frac{1}{2}(\Delta r)_{i+1/2} \ , \ \forall i \tag{3.47}$$

The factor 1/2 in Eq. (3.47) is arbitrary. It may be any value less than 1.

Finally, non-negative density and energy conditions have to be satisfied. In our problem we neglect flow of mass between the bubble and the liquid, so mass is conserved. Consequently we cannot have the problem of a negative density. If loss of mechanical energy is present (see section 3.5), an expression similar to Eq. (3.40) should be used for the energy in a zone.

Initial and Boundary Conditions

The initial conditions are basically the same as in chapter 2. We start the evolution of the bubble from its equilibrium radius (typically 4.5 μm, as in [34]), and assume spatial uniformity of all the variables.

The boundary conditions are more complicated. Assuming that we have N points in our spatial grid, the outer boundary conditions in this formulation reduce to one, i.e. $U_N = \dot{R}$. The bubble wall speed $\dot{R}$ follows from the R.P. equation, Eq. (2.6). The characteristic equation applicable at this point is the one along the C_+ characteristic (see Eq. (3.33))

$$U_N - u_{N-} + \frac{P_N - p_{N-}}{(\overline{\rho a})_{N-1/2}} = 0 \tag{3.48}$$

where u_{N-} and p_{N-} are defined by Eqs. (3.34) and (3.35). Since from Eq. (3.36) it follows that (for $\alpha = 2$)

$$r^N = r_N \left(1 + 3\frac{U_N}{r_N}\Delta t\right)^{1/3} \simeq r_N + U_N \Delta t \tag{3.49}$$

or

$$R(t + \Delta t) = R(t) + \dot{R}(t)\Delta t \tag{3.50}$$

and it is consistent with the original Rayleigh's formulation. Certain freedom exists here in the formulation of this boundary condition, since the quantity U_N is calculated at the time $t+\Delta t'$. We choose to integrate the R.P. equation from time $t-(\Delta t-\Delta t')_{previous}$ to $t+\Delta t'$. This time interval is almost the same as Δt[7]. Another complication arises from the fact that the pressure in the bubble, next to the wall, enters the R.P. equation. In order to be consistent we used the value $P_N[t-(\Delta t-\Delta t')_{previous}]$ for this purpose. As a result of this procedure, we get the value of $\dot{R}(t+\Delta t')$, which gives U_N. Equation (3.48) can now be solved for P_N and we are able to proceed on to the other quantities of the problem.

Because of the singular nature of the gas-dynamic equations at the origin, a small sphere around $r = 0$ has to be excluded from the treatment. In practical terms, the inner boundary was taken to be at $i = I$ ($i = 0$ would represent the origin)[8]. The boundary condition which we choose is that $U_I = 0$, so the inner boundary is stationary. The characteristic equation which is applicable here is along C_- (see Eq. (3.33))

$$U_I - u_{I+} - \frac{P_I - p_{I+}}{(\overline{\rho a})_{I+1/2}} = 0 \tag{3.51}$$

where u_{I-} and p_{I-} are defined by Eqs. (3.34) and (3.35). Using our boundary condition, Eq. (3.51) can be solved for P_I.

The last equation completes the description of the algorithm. At this point we are able to calculate all the quantities in the zones bounded by times t and $t+\Delta t$. Thus, we can proceed to the next step and march forward in time.

[7]The time steps need not be the same, but the two consecutive time steps do not differ by very much.

[8]In the calculations I was typically given the value of $3-4$. The total number of points in the space grid is $500-1,000$, so the excluded radius is of the order of 10^{-6} *cm*.

3.4 Results without Inclusion of Loss Terms and Comparison with Self-Similar Solution

The method explained in the previous part was applied to our problem of a bubble oscillating in sound field. We start the time evolution of the system from its equilibrium radius and follow all the way through an acoustic period. The time step varied from 10^{-8} s at the point where the bubble radius is maximum to 10^{-18} s close to the minimum radius. The stability criterion discussed in 3.3.2 ensures the stability of the algorithm. We checked the results with different numbers of points in the space grid. For a number of points between 500 and 2,000 the results are almost independent of the number of points. The results presented in the rest of this section are obtained with 1,000 points.

The results are extremely sensitive to even small changes of the input parameters, as might be expected for driven nonlinear oscillators. As our first goal is to compare the results with experiment [34], we tried to follow the experimental conditions as closely as possible. The parameters entering the problem are $P_a \sim 1.3\ atm$, $\omega_a/2\pi = 26.5\ kHz$, $\nu = 0.01\ cm^2/s$, $\gamma = 1.4$, $R_0 = 4.5\ \mu m$, and $1/b = 0.794\ g/cm^3$. The gas in the bubble is assumed to be air (approximated as a nitrogen-oxygen mixture). The discussion of the influence of the change of some of these parameters on the results will be presented in the following chapter. The results for the bubble radius versus time for one acoustical period and for the choice of parameters mentioned above are presented in Fig. 3.4. The results of direct integration of the R.P. equation, Eq. (2.6), for the same parameters, are presented as well. The maximum radius the bubble reaches is about 42.5 μm at approximately

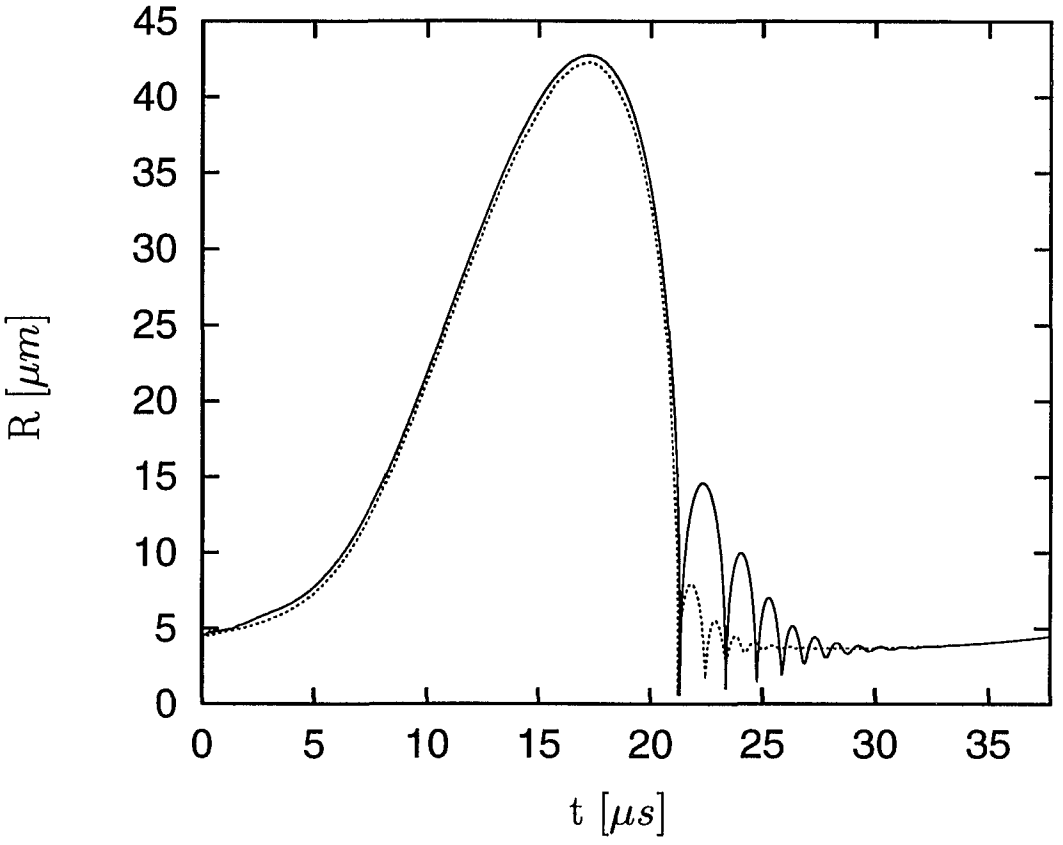

Figure 3.4: *Bubble radius versus time for one acoustic period. The solid line is the complete solution of Eqs. (3.16 - 3.18) combined with Eq. (2.6). The dotted line is the solution of Eq. (2.6) assuming adiabatic conditions in the bubble. These are the results for an acoustic pressure of* 1.325 *atm and an initial bubble radius of* 4.5 μm. *The other parameters entering are: acoustic frequency* $f_a = 26.5\ KHz$, $1/b = 0.794\ g/cm^3$, $\rho_l = 1.0\ g/cm^3$, $c_l = 1.481\ km/s$, $\nu_l = 0.01\ cm^2/s$ *(for water at* $20°C$*). The value of* γ *in the adiabatic solution is* 1.4. *A surface tension* $\sigma = 72.5\ dyn/cm$ *was included.*

17.2 μs after the start of the cycle and the minimum is 0.55 μm at about 21.3 μs. For the first part of the cycle, it is easy to see that there is almost no difference in the results between the "adiabatic" solution and the full solution of the system of equations, Eqs. (3.16 - 3.18). After the collapse of the bubble starts, however, the motion of the bubble wall becomes faster and when the bubble radius reaches values of a few microns it becomes supersonic with respect to the speed of sound in the gas. The bubble wall speed and speed of sound in the gas just next to the wall are presented in Fig. 3.19b on page 89, for the above choice of parameters[9]. These results are similar to those we already presented in section 3.2. After this point the shock wave starts to develop in the bubble and the adiabatic approach from chapter 2 is no longer applicable.

Let us now follow the time development of the thermodynamic variables in the bubble close to its minimum radius. The shock wave itself can be readily followed from Fig. 3.5, which shows the spatial profile of the velocity of the gas in the bubble close to the minimum for a period of about 80 ps around the time t_c, which is defined as the time when the bubble wall velocity changes sign ($t_c = 21.3132347\ \mu s$). A strong shock starts to develop at about $t_c - 50\ ps$ when the bubble radius is 0.68 μm. It propagates inward and hits the origin 8.1 ps before t_c. After the collapse the shock bounces back and propagates outwards (velocity of the gas is positive). It hits the bubble wall approximately 4 ps before t_c (the bubble is still collapsing). The shock wave partially reflects from the bubble wall and starts propagating inward again. At time t_c the bubble wall velocity changes sign and the gas close to the wall

[9]The results in this figure are obtained using the more complete treatment where energy loss terms were included. However, the result for the bubble wall speed and the speed of sound in the bubble are almost identical at the point of bubble collapse, with or without loss terms.

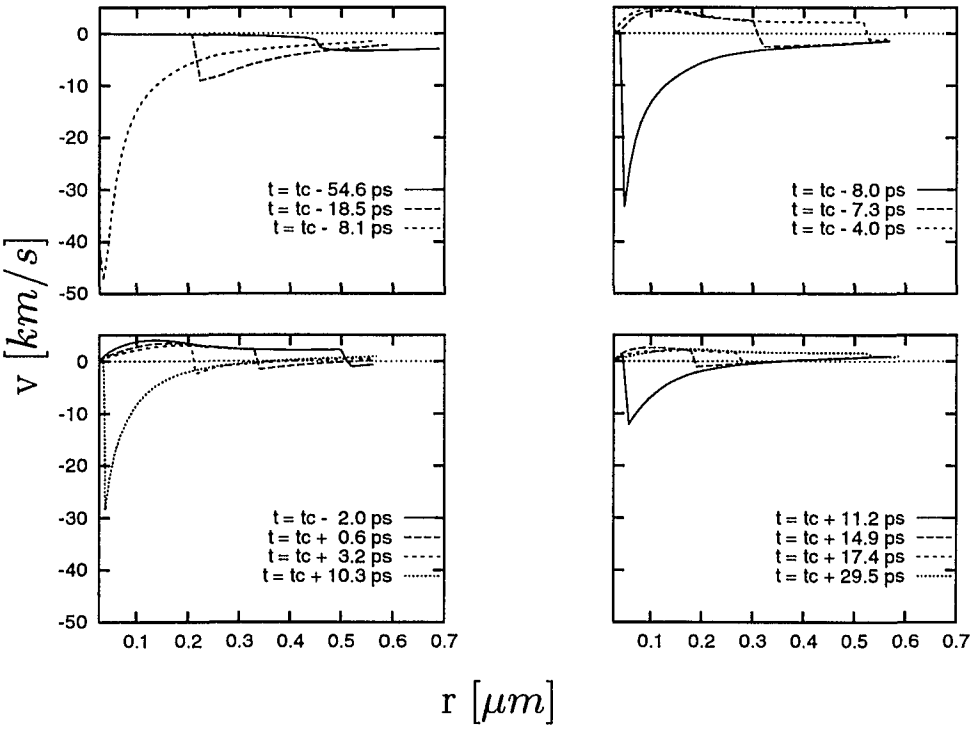

Figure 3.5: *Velocity of the gas in the bubble close to its minimum radius. The quantity t_c is defined as the time when the bubble wall velocity changes sign. In the first part of the figure the shock is moving inward. The complete collapse happens about 8.1 ps before t_c. The shock rebounds (second part), propagates outwards and hits the wall at about 3 ps before t_c. It reflects from the wall and collapses again (third part). After the second collapse, at about 10.5 ps after t_c, it rebounds and propagates outwards (fourth part).*

starts propagating outwards, while the second shock is still moving toward the center. This wave reaches the origin at about 10.5 ps after t_c, rebounds and propagates outwards as a weaker disturbance. It should be noted that all of this happens in less than 100 ps. The pressure profile is presented in Fig. 3.6. We see that the pressure reaches values on the order of 10^{14} dyn/cm^2

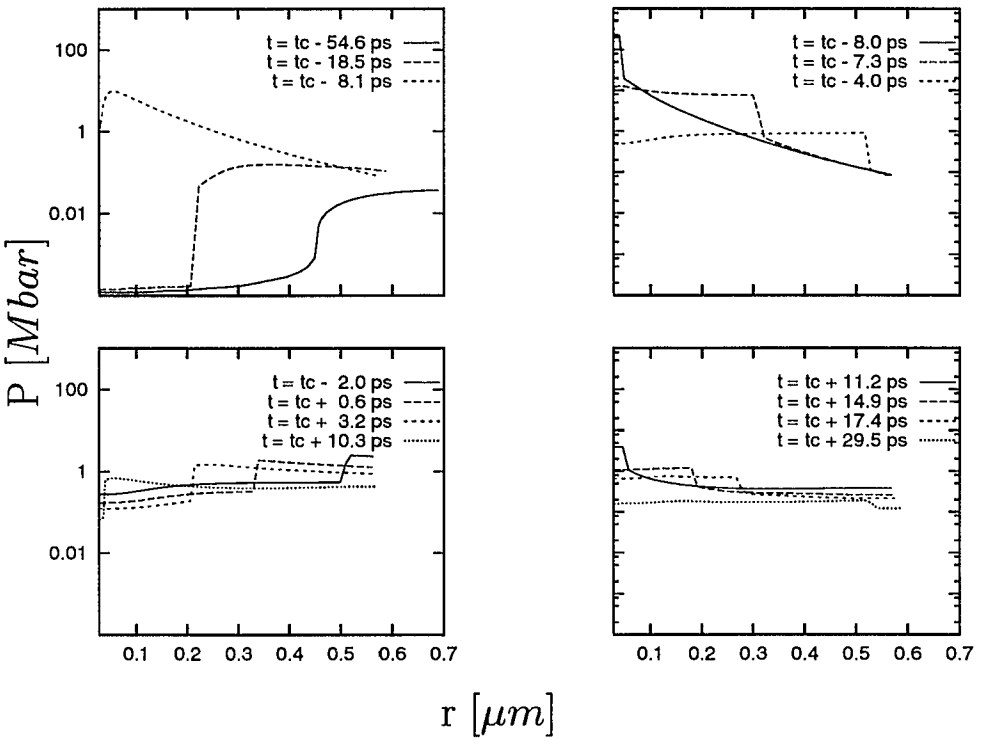

Figure 3.6: *Pressure of the gas in the bubble close to its minimum radius. The quantity t_c is defined as the time when the bubble wall velocity changes sign.*

at the center of the bubble. The temperature profile is given in Fig. 3.7. The enormous temperatures, reaching values of more than ten million degrees,

develop close to the origin[10]. The propagation of the shock wave can also be traced in this figure, with a high temperature following the shock front.

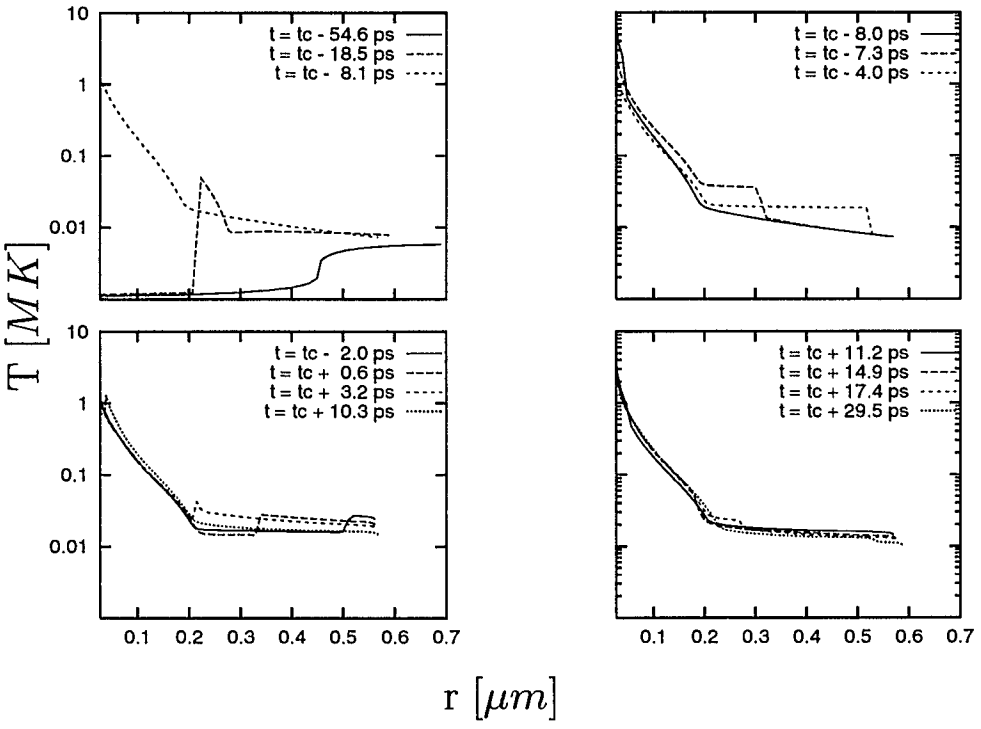

Figure 3.7: *Temperature of the gas in the bubble close to its minimum radius. Again t_c is defined as the time when the bubble wall velocity changes sign. Note the huge temperatures developing close to the bubble center.*

Finally, the complete space-time dependence of the thermodynamic variables during this most exciting part of the bubble collapse is presented in Fig. 3.8. It can be seen that the first collapse of the shock wave is stronger than the second one. The results which are presented in this section give a definitive answer as to the existence and the production of shock waves in

[10]Even higher temperatures develop for higher acoustic pressure amplitudes.

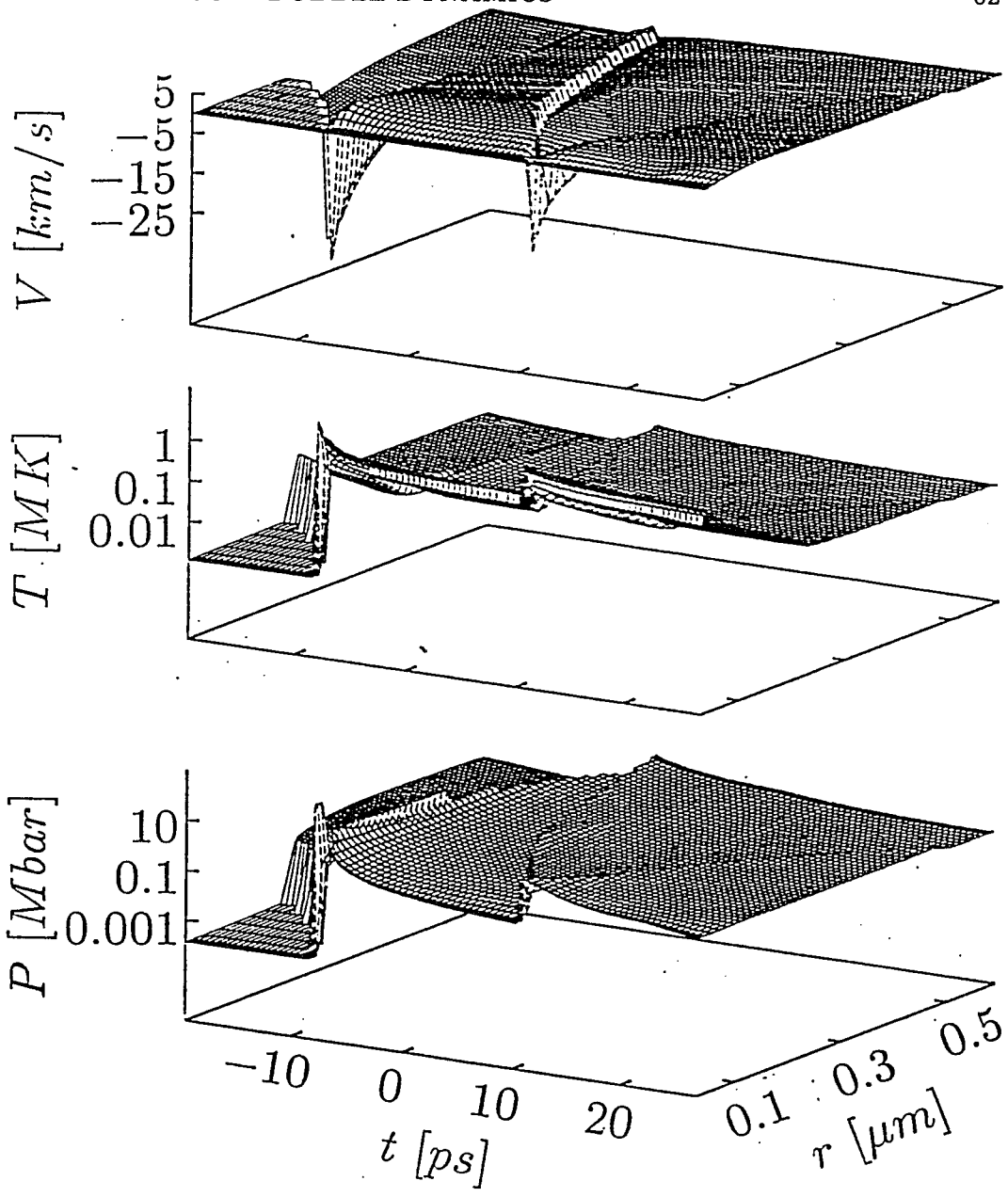

Figure 3.8: *Space-time profile of the velocity, temperature and pressure of the gas. The propagation of the shock waves can easily be followed.*

strongly modulated gaseous bubbles in liquids, at least for the parameters we specified. We should note here that the results are very sensitive to the input parameters. For example, if the acoustic amplitude is taken to be 1.2 *atm* (instead of 1.3 *atm*), the collapse of the bubble is much more peaceful and the motion of the bubble wall is never going to become supersonic. The shock wave is not produced and the adiabatic approach from chapter 2 is applicable. More discussion of the influence of the changes of some of the physical parameters will be presented in the following chapter, where we are going to discuss the important role played by the radiation coming out of the bubble in the form of sonoluminescence. Before we come to that point, let us compare our results with the well known self-similar solution for the spherically symmetric collapse of shock waves.

Comparison with the Self-Similar Solution

Self-similarity is a well known property of the gas-dynamic equations, resulting from their ability to admit scaling transformations. That means that there is a possibility for different flows to be derivable from each other by changing the basic scales of length, time and density. Without going into details[11], the net result is that the system of partial differential equations, Eqs. (3.2 - 3.4), or, equally well, Eqs. (3.16 - 3.18) (with loss terms neglected) can be rewritten as a system of ordinary differential equations in terms of a new independent variable ξ (called the similarity variable) which is defined in terms of the radial coordinate r and some typical length scale in the problem $R(t)$, by $\xi = r/R(t)$. In our problem of spherical shock implosion this typical length scale is the shock radius. It turns out that the condition for

[11]Extensive discussion of the self-similar approach is given in [51, 75, 76].

the existence of the solution of the gas-dynamic equations is that $R(t)$ has to satisfy the following relation

$$R(t) = At^{\alpha} \tag{3.52}$$

where α is the so-called self-similarity exponent (this is only one of the possible solutions, see [76]) and A is a constant which has to be determined from the initial conditions. Shock implosion belongs to the second type of self-similar problems, where the similarity exponent α does not follow from the dimensional considerations alone, but it has to be determined from the condition for a single valued solution of the gas-dynamic equations. The value of α for the problem of the shock imploding into vacuum was determined to be approximately equal to 0.717 [75, 76, 77]. It was also determined that the radius of the outward propagating shock (after rebound), is going to follow the same power law, with the same self-similar exponent, but with a different constant A. The bottom line is that the radius of a propagating shock is given by Eq. (3.52). From the same analysis it follows that, for example, the temperature behind the shock front is given by

$$T(t) = Ct^{2(\alpha-1)} \tag{3.53}$$

where C is some other constant, again to be determined from the initial conditions. We should note that this solution is valid only very close to the origin, so the self-similar solution represents the limit which is approached asymptotically by real life problems.

Let us see how our solution corresponds to the self-similar one. In Fig. 3.9 we present the radius of the imploding shock and the self-similar fit. The best fit was obtained with the value of the self-similar exponent $\alpha = 0.53$ (a similar result is given in [30]). The constant A in Eq. (3.52) was determined from

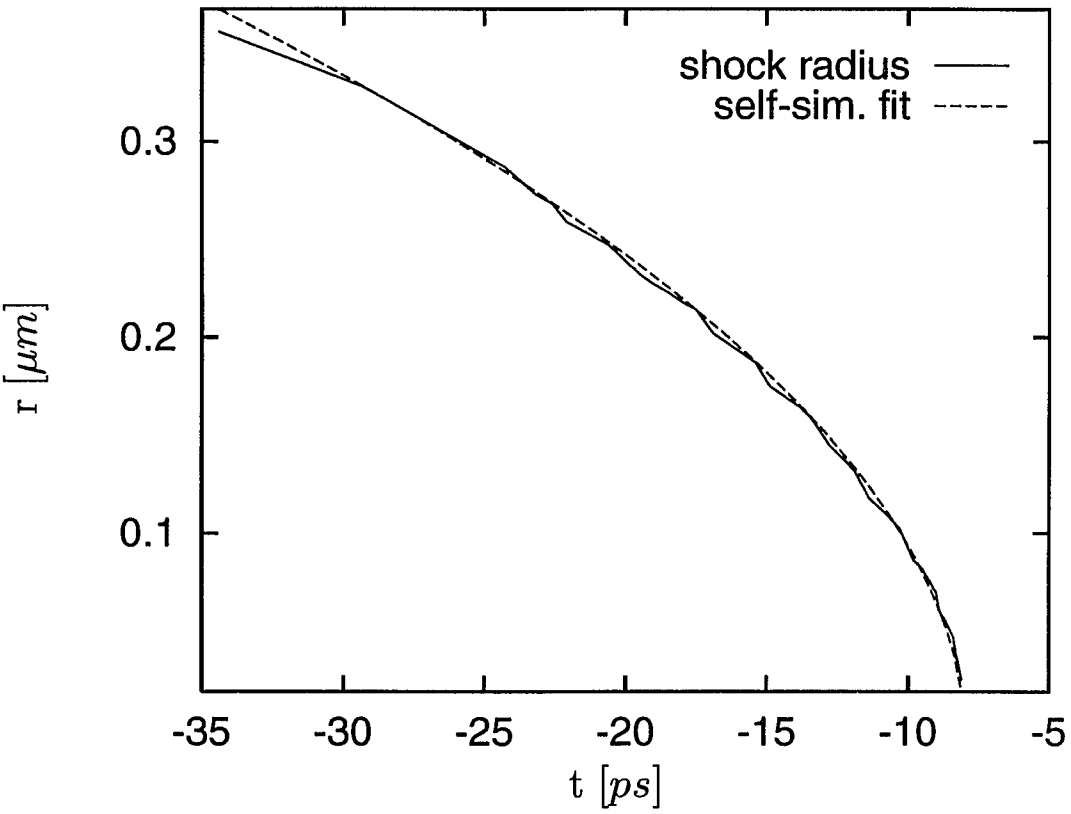

Figure 3.9: *Radius of the collapsing shock. The self-similar exponent is* $\alpha = 0.53$.

the position of the shock wave at a time about 20 *ps* before the complete collapse. Our explanation of the difference in our value of the self-similar exponent α from the previously given one (0.717) is that the self-similar solution was derived under the assumption that the shock is propagating into vacuum, and in our case we have relatively dense gas in front of the shock. Anyway, we see that correspondence with the self-similar solution is very good, especially close to the origin, as it should be. The results for the outgoing shock are presented in Fig. 3.10. We see that the agreement is very good close to the origin. However, the outward propagating shock has to compete with a strong inwards flow of the gas which is still pushed by the motion of the bubble wall. That slows down the expanding shock and the similarity solution is not valid any more. The results for temperature are presented in Figs. 3.11 and 3.12. We again see that the agreement for the imploding shock is fairly good, with big discrepancies for the outgoing shock. The explanation is that, as already mentioned, the outgoing shock has to compete with the inward flow of the gas, leading presumably to higher temperatures in the shock front than one would expect on the basis of the self-similar solution.

3.5 Results including Loss Terms

The results of integrating Eqs. (3.16 - 3.18) without loss terms imply the existence of extreme conditions in the bubble center during the shock collapse. Theoretical temperatures as high as ten million degrees and pressures on a megabar scale have been reported [30, 37, 41]. These results would imply that some very energetic processes, including nuclear fusion might occur in the bubble close to the origin, as pointed out in [35]. These results also

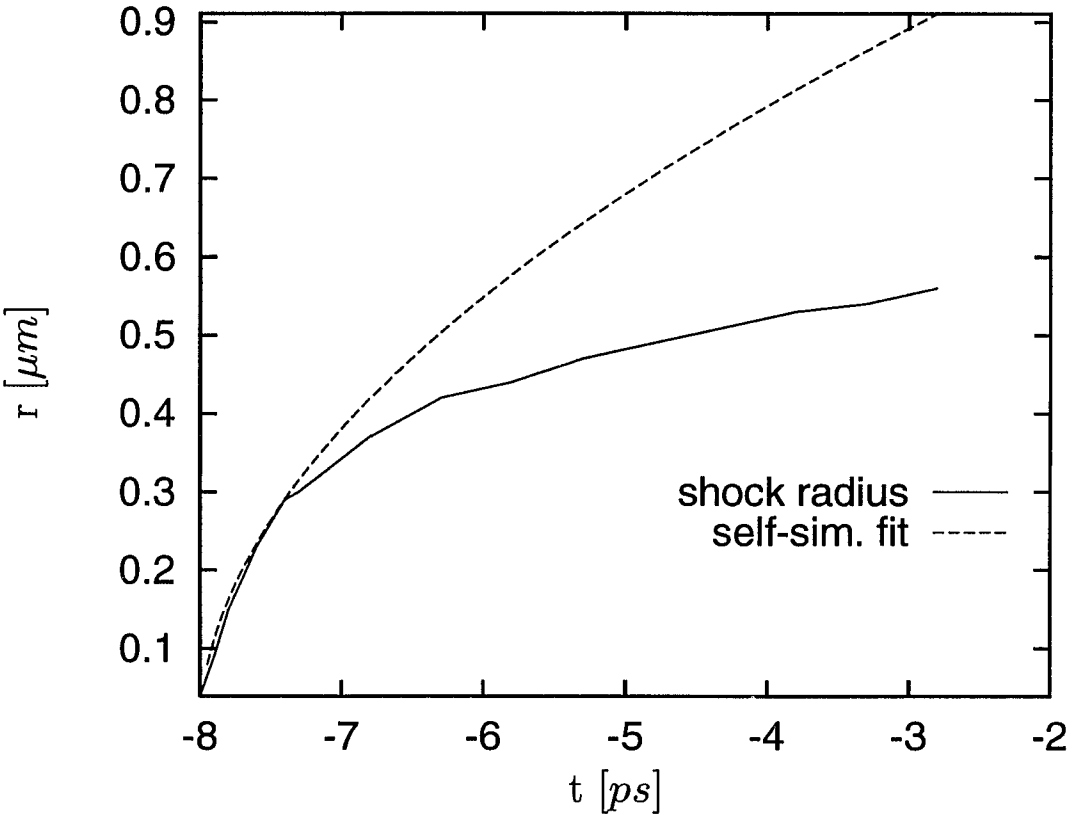

Figure 3.10: *Radius of the rebounded shock (on the way out). The self-similar fit is obtained with the same α as in the previous figure.*

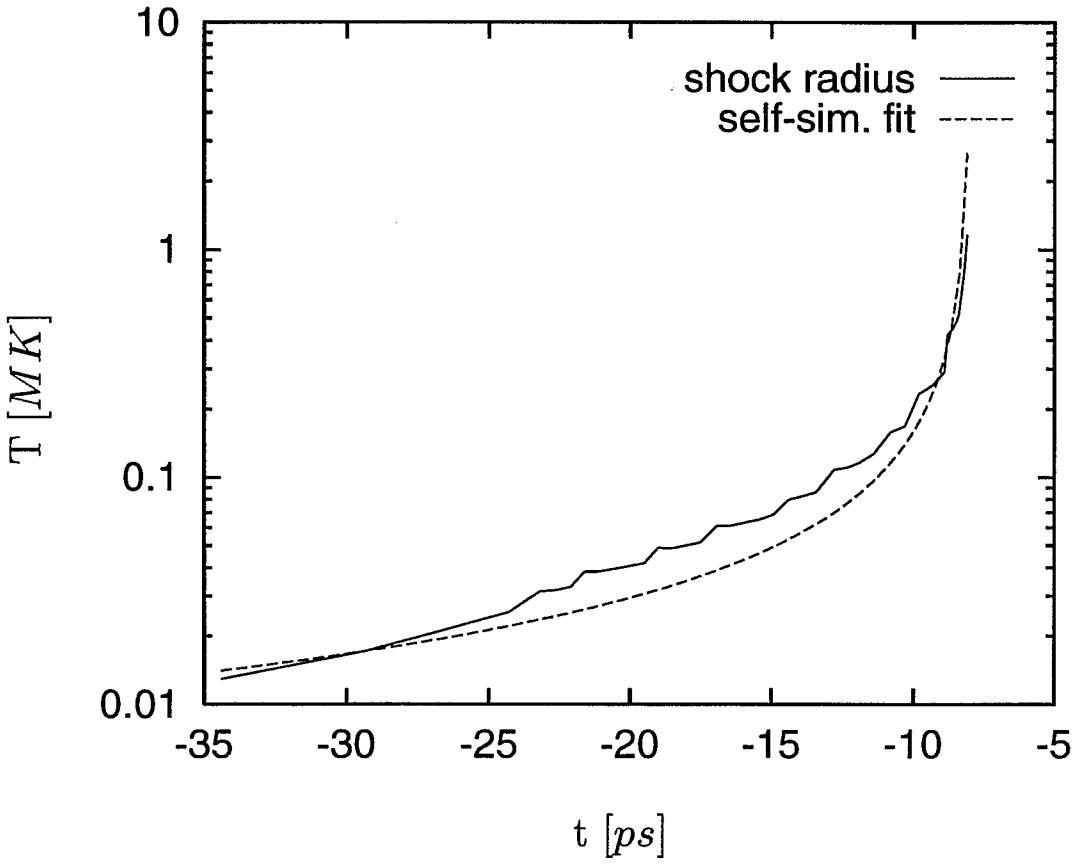

Figure 3.11: *Temperature of the shock on the way in. The self-similar fit is obtained with the same α as before.*

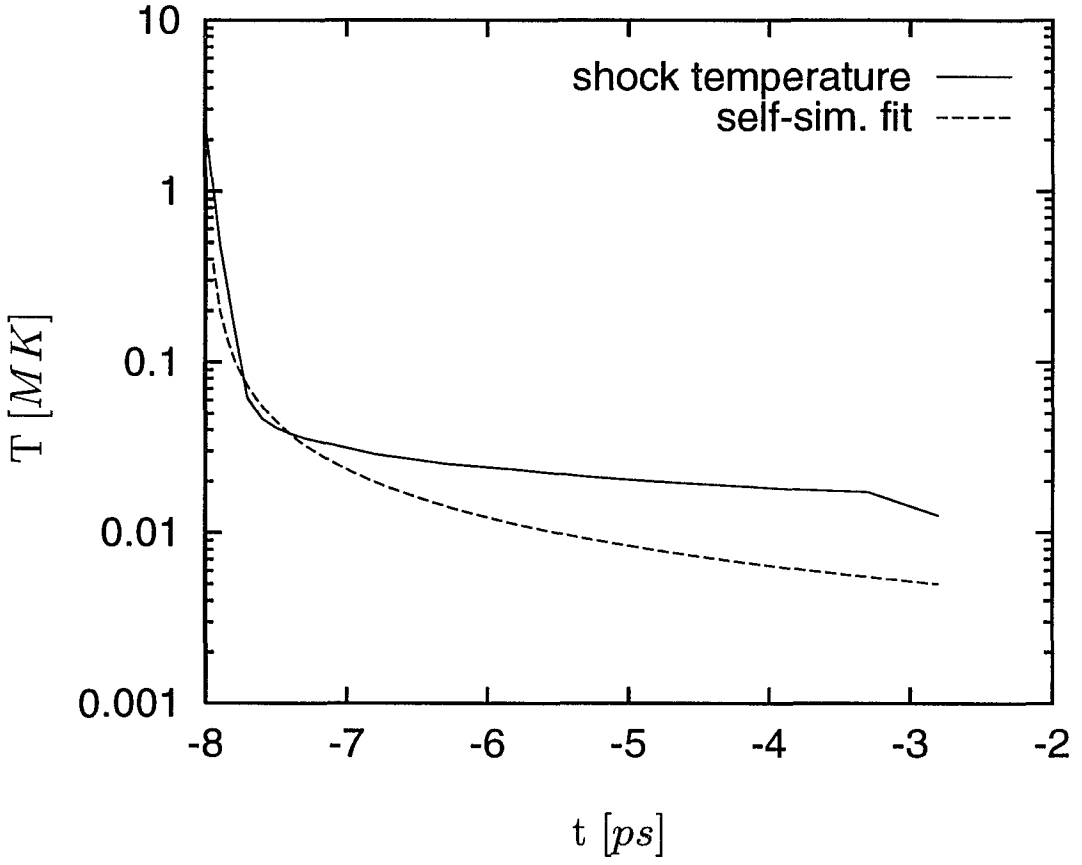

Figure 3.12: *Temperature of the shock on the way out. The self-similar fit is obtained with the same α.*

imply that mechanical energy losses may also be considerable. Inclusion of these terms is important in order to make a self-consistent prediction of the real temperatures which develop in the center of the bubble during the shock collapse(s). Finally, they are responsible for the effect of SL, which we want to explain. These loss terms include the following processes:

- Heat flow between the bubble and liquid;
- Thermal conduction in the gas;
- Inclusion of vibrational degrees of freedom in the equation of state;
- Dissociation of the gas;
- Ionization of the gas;
- Radiation losses which are responsible for the effect of SL.

The first two effects are definitely important in order to completely understand the general bubble dynamics and the remarkable stability of the bubble oscillations, as pointed out in many references [52]-[68]. The discussion of these two effects, based on simple mechanical arguments, is presented in Appendices E.1 and E.2. The conclusion is that these effects do not have an important influence on the gas dynamics on the time scale of interest. This time scale (a few tens of picoseconds) is determined by the time which the bubble spends close to its minimum radius, shock waves are produced, and the SL pulse is emitted.

In the rest of this section we are going to discuss the inclusion of the other physical effects mentioned above in our treatment of the gas-dynamic equations, Eqs. (3.16 - 3.18), and the equation of state, Eq. (3.22).

3.5.1 Vibrational Degrees of Freedom

The temperature at which the vibrational degrees of freedom unfreeze is on the order of a few thousand degrees. As we are mainly interested in much higher temperatures (10^4 K or more), we included this effect simply by changing the ratio of heat capacities from 7/5 to 9/7 for temperatures higher than "critical" ones[12].

3.5.2 Dissociation

The dissociation of air starts at temperatures on the order of 10^4 K [75]. The energies required for dissociation are considerable, 5.11 eV for 0_2 and 9.74 eV for N_2 [6]. The equation of state, Eq. (3.22), becomes

$$\epsilon(T) = \frac{N}{\gamma_m - 1}(1 - \alpha(T))k_B T + 2\frac{N}{\gamma_a - 1}\alpha(T)k_B T + N\alpha(T)U \qquad (3.54)$$

where $\alpha(T)$ measures the degree of dissociation ($N\alpha(T)$ molecules are dissociated) and U is the dissociation energy. Here γ_m is the ratio of molecular heat capacities (9/7 for air if the vibrational degrees of freedom are included), and γ_a is the monoatomic ratio (5/3). The first term on the left hand side of Eq. (3.54) corresponds to the energy of the molecules, the second one to the energy of the atoms and the last one represents the energy required for dissociation. Since our treatment is approximate, we used statistically averaged values for the dissociation energies of O_2 and N_2 mentioned at the beginning of this part. This last term was included in Eq. (3.18) as the mechanical energy loss. Similar to the case of vibrational degrees of freedom, we are not interested in the details of the dissociation process. Hence a simple linear

[12]The critical temperature was taken to be 4×10^3 K. This choice does not have much influence on the final results. The same is true for the choice of temperatures which govern the processes of ionization and dissociation mentioned below.

model was used for $\alpha(T)$:

$$\alpha(T) = \frac{T - T_{D1}}{T_{D2} - T_{D1}} \tag{3.55}$$

where T_{D1}, T_{D2} are temperatures at which dissociation starts and ends, (taken as 5×10^3 K and 10^5 K), respectively. The relaxation time for dissociation for conditions such as ours (high temperature and density) is of the order of 10^{-12} s [75], which is fairly short compared with the time the bubble spends close to the minimum radius. That means that there is enough time for equilibrium to be established.

Finally, the net result of dissociation is that the number of particles per volume increases from N to $[1 + \alpha(T)]\, N$ and there must be a mechanical energy loss which is to be included in our treatment of the gas dynamics.

3.5.3 Ionization

Inclusion of ionization into the gas-dynamic equation is more complicated. Ionization in air starts at temperatures of about 10^4 K, but already at temperatures of a few times this starting temperature there are a considerable number of double and triply ionized atoms. The ionization process (assuming thermal equilibrium), is governed by the Saha equation which becomes complicated to use if there is multiple ionization taking place. To simplify things, we used a continuous approximation which gives the average degree of ionization $\overline{m}$ (number of electrons per initial atom or molecule). Then, the Saha equations gives a system of recurrence relations for the number of ions with degree of ionization m. By replacing finite differences in the Saha equation by differentials and using conservation of the number of particles and of the total charge, the following transcendental equation is obtained

(see Appendix E.3)

$$I(\overline{m}+1/2) = k_B T \; ln\frac{AT^{3/2}}{\overline{m}n} \tag{3.56}$$

where $I(\overline{m}+1/2)$ is given by a continuous curve constructed by joining the points I_m corresponding to ionization potentials for ionization of degree m. In Eq. (3.56) n is the number of atoms (molecules) per unit volume, T is the temperature and A is the constant coming from the Saha equation, $A = 2(2\pi m_e k_B/h^2)^{3/2}$. By solving Eq. (3.56) we get $\overline{m}$ which gives the average degree of ionization and also the energy lost in the ionization process. Results for $\overline{m}$ as a function of temperature are shown in Fig. 3.13.

The equation of state which allows for ionization is as follows

$$\epsilon(T) = \frac{N_a}{\gamma_a - 1}k_b T + \frac{N_m}{\gamma_m - 1}k_b T + \frac{N_a + N_m}{\gamma_e - 1}\overline{m}k_b T + (N_a + N_m)Q(\overline{m}) \tag{3.57}$$

where N_a, N_m are the numbers of atoms and molecules per unit volume, respectively. Here $\gamma_m, \gamma_a, \gamma_e$ are the heat capacity ratios for molecules, atoms and electrons. $Q(\overline{m})$ is the energy required to remove an electron with ionization potential corresponding to $\overline{m}$. The first three terms on the right hand side of Eq. (3.57) are internal energies corresponding to atoms, molecules and electrons, respectively. The electronic excitation energies were neglected in the above equation. The last term in Eq. (3.57) was included in Eq. (3.22) as the mechanical energy loss.

The time scale required to establish thermodynamic equilibrium for the electrons and for the ions is fairly short, about 10^{-14} s. Equalization of electron and ion temperatures, however, takes more time because of the large difference between the electronic and ionic masses. The approximate result for this time is [75]

$$\tau \sim \frac{m}{m_e}\frac{1}{N\overline{v}_e\sigma} \tag{3.58}$$

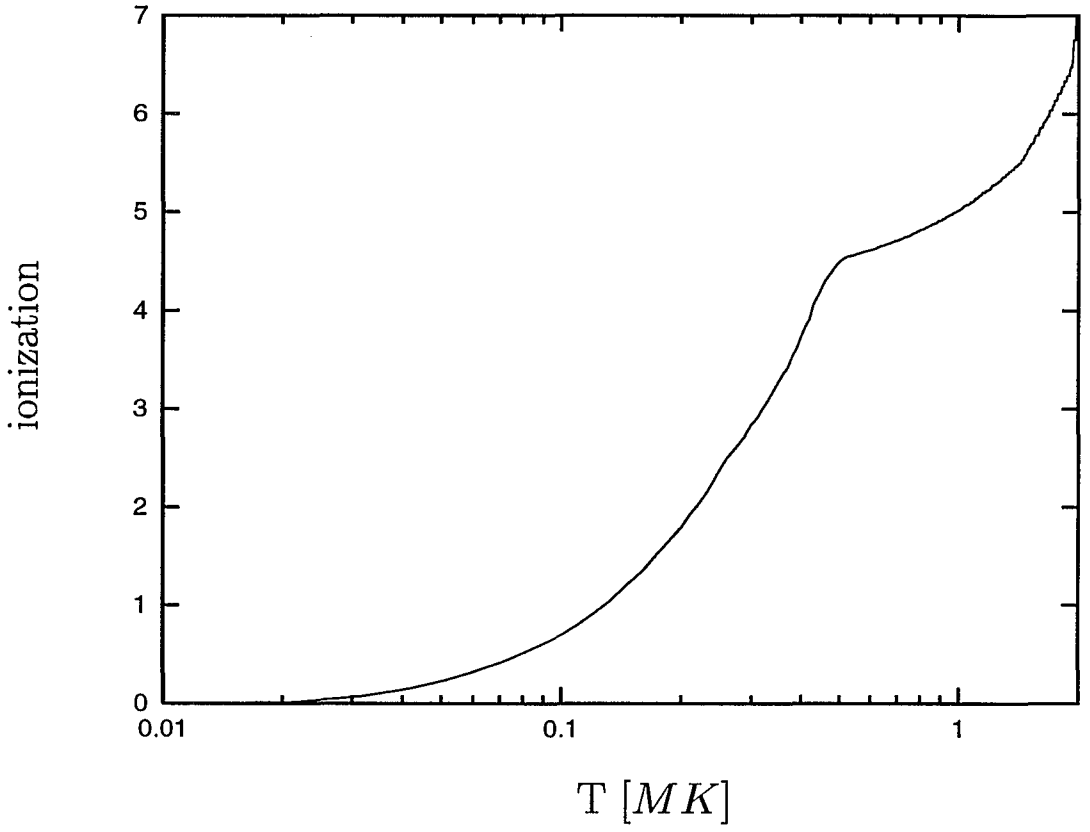

Figure 3.13: *Temperature dependence of the degree of ionization. These results are for a gas density equal to* $0.6\ g/cm^3$. *The "bump" at temperatures of about* $5 \times 10^5\ K$ *is the result of the sharp increase of the ionization potential.*

where m is the ionic mass, m_e is the electron mass, N is the ion number density, $\overline{v}_e$ is the mean electron velocity and σ is the cross section for electron - ion collisions. For typical values of the parameters entering our problem, i.e. $T \sim 10^5\ K$, $N \sim 10^{22}\ cm^{-3}$, the result for τ is of the order of $10^{-12} - 10^{-13}\ s$. This is still short compared to the time the bubble spends close to the minimum. That means that translational temperature is established rather fast and that ions and electrons could be assumed to be at the same temperature.

It is important to note here that, by including the ionization and dissociation into the gas-dynamic equations, we covered only the most important non-radiative processes present in high temperature air. Chemical reactions between nitrogen and oxygen have not been incorporated into the treatment, as well as the possibility of the presence of water vapor, which might lead to a variety of chemical reactions. The quantities which are important for radiative processes are the degree of ionization and the temperature. Since our main goal is to explain the effect of SL, we tried to include the effects which are the most important in this regard.

3.5.4 Radiation

Understanding the physical mechanism which leads to radiation is very important because, first, it is responsible for the effect of SL, and second, it leads to a considerable difference in the results obtained for the values of the thermodynamic quantities. We are going to present two different approaches to the problem. The first one is based on the use of the radiative transfer equation for explaining the thermal radiation from an object characterized by a certain spatial and temporal temperature and density distribution. Let us emphasize that the resulting radiation is a priori not related to the black

body radiation. An object is going to radiate as a black body if it is optically thick ($d >> l_a$), where d is the typical dimension of the object and l_a is the radiation absorption length. It will radiate as a volume radiator if it is optically thin ($d << l_a$). We are going to refer to this approach as the "Thermal approach" in what follows.

Since the radiation transfer equation has not been used very much for "microscopic" problems like ours (where the typical dimension of the system is just a few times larger than the wavelength of the emitted radiation), we developed a model (bremsstrahlung (BRS) model) for comparison purposes. In this model we argue that the main part of the energy loss occurs inside the "ball of plasma" which develops close to the origin during the collapse of the shock waves (an approach similar to one in [30]). The main effect which leads to radiation in this region is bremsstrahlung. The simple bremsstrahlung radiation is to be corrected for the fact that the size of the radiation region is comparable to the wavelength of the emitted radiation and also for the absorption of radiation outside the plasma region.

Thermal Approach

Inclusion of radiation losses involves the coupling of the radiative transfer equation

$$\frac{1}{c}\frac{\partial I_\nu}{\partial t} + \hat{\Omega} \cdot \nabla I_\nu = \kappa'_\nu (I_{\nu p} - I_\nu) \tag{3.59}$$

with the gas-dynamic equations. In Eq. (3.59) I_ν is the radiative intensity of the body, $I_{\nu p}$ is the equilibrium Planck distribution given by $I_{\nu p} = 2h/c^2\ \nu^3 (e^{\frac{h\nu}{k_B T}} - 1)^{-1}$ and κ'_ν is the attenuation coefficient. All these quantities depend on the frequency, ν. Here c is the speed of light and T is the temperature. Equation (3.59) is based on the principle of detailed balance

and is written in a form applicable for spherically symmetric problems. The unit vector $\hat{\Omega}$ specifies the direction of photon propagation. In order to simplify the space integration, we assume the radiation propagating in the radial direction[13]. Further simplification is found by assuming equilibrium between the radiation and matter. It can easily be seen from Eq. (3.59) that the time t_p required for the equilibrium to be established is of the order of $1/(c\kappa'_\nu)$. Later we are going to show that the value of the attenuation coefficient is sufficiently high to make t_p short compared with the time the bubble spends close to the minimum. This occurs for frequencies at which most of the energy is emitted. This effectively says that Eq. (3.59) can be employed without the time derivative term. Solving this simplified Eq. (3.59) and calculating the energy flux $S_\nu(r,t)$ through the spherical surface of radius r from the radiative intensity[14], we finally obtain the energy loss per mass during the time Δt in the shell of width Δr:

$$\Lambda(r,t) = \frac{\Delta t}{m(\Delta r)} \int_0^\infty (S_\nu(r,t) - S_\nu(r-\Delta r,t))d\nu \qquad (3.60)$$

Here $m(\Delta r)$ is the mass in the shell and r is the distance from the bubble center.

The properties of matter enter Eqs. (3.59) and (3.60) through the attenuation coefficient κ'_ν. This quantity involves all processes which are responsible for absorption or emission of radiation. In general it is very difficult to calculate this in an exact manner, since there are many processes which are

[13]The full treatment of the radiative transfer equation is a complicated problem in itself. Since other quantities entering Eq. (3.59) (e.g., the attenuation coefficient) are not precisely known, our approximate treatment of Eq. (3.59) is satisfactory. A more exact treatment of radiative transfer for the conditions common in astrophysics can be found in [78].

[14]The energy flux per unit area is given by $\vec{S}_\nu(\vec{r},t) = \int I_\nu(\vec{r},\hat{\Omega},t)\ \hat{\Omega}\ d\hat{\Omega}$. Using the condition of thermodynamic equilibrium and spherical symmetry of our problem, the radial flux $S_\nu(r,t)$ was calculated [78].

involved. An overview of different processes which are important in getting approximate results for the attenuation coefficient under the extreme conditions in the bubble close to its minimum radius is given in Appendix E.4. Here we note that a crucial factor which has a strong influence on the results for the attenuation coefficient is multiple ionization, discussed in the previous part. Some representative values are given in Table 3.1. The strong temperature and frequency dependence of the absorption coefficient κ'_ν can be noted[15]. We see that, for high temperatures (more than 10^6 K), the values for the absorption coefficient are very high, giving very short radiation mean free paths. For lower temperatures the values of the absorption coefficient are smaller, giving radiation mean free paths which are comparable to the bubble size or larger. This says that the absorption of radiation in the bubble is going to be important, especially for the high temperatures in the bubble center. Finally, the energy loss given by Eq. (3.60) with I_ν calculated from the radiative transfer equation, Eq. (3.59), and the absorption coefficient κ_ν given by Eqs. (E.12 - E.16), was included in the loss term on the right hand side of Eq. (3.18).

Bremsstrahlung (BRS) Model

We may think of bremsstrahlung as radiation emitted due to the sudden changes of microscopic "dipole" moments associated with the collision process. Since the temperature close to the center of the bubble at the time of the

[15]For the typical values of temperature of $10^5 - 10^6$ K and frequencies which correspond to the maximum of the Planck spectrum (according to the Wien's law) of 10^{17} s^{-1}, the values of κ'_ν are $10^5 - 10^6$ cm^{-1}. This gives an absorption time t_p on the order of 10^{-15} s, which is very short compared to the time the bubble spends close to the minimum radius. After several absorption lengths one may assume thermal equilibrium between the radiation and matter, so the equilibrium time might be $\sim 10^{-14}$ s.

$T\ (K)$	$\omega\ (rad/s)$	$\overline{m}$	$\kappa'_\nu(1/cm)$
2.5×10^4	5.0×10^{15}	0.025	3.0×10^3
5.0×10^4	5.0×10^{15}	0.20	5.1×10^4
1.0×10^5	5.0×10^{15}	0.64	3.6×10^5
1.0×10^6	5.0×10^{15}	5.0	3.1×10^5
2.0×10^6	5.0×10^{15}	6.7	2.2×10^6
1.0×10^7	5.0×10^{15}	7.0	5.7×10^7
1.0×10^5	1.0×10^{15}	0.64	7.6×10^6
1.0×10^5	5.0×10^{15}	0.64	3.6×10^5
1.0×10^5	1.0×10^{16}	0.64	1.1×10^5
1.0×10^5	5.0×10^{16}	0.64	7.9×10^4
1.0×10^5	1.0×10^{17}	0.64	1.0×10^4
1.0×10^5	5.0×10^{17}	0.64	8.1×10^1
1.0×10^5	1.0×10^{18}	0.64	1.1×10^1
1.0×10^5	1.0×10^{19}	0.64	1.0×10^{-2}

Table 3.1: *Values of the absorption coefficient κ'_ν and average ionization $\overline{m}$ for a few temperatures T and angular frequencies of radiation, ω. These results are for a gas density of 0.7 g/cm^3.*

complete collapse of the shock waves reaches values of a few million degrees, one could expect the formation of plasma. That means that BRS happens in the "ball" of plasma and one has to include the corrections to individual scattering events due to the rest of the plasma. This correction is going to be important especially in the next chapter where we will be concerned with spectral properties of the radiation coming out of the bubble.

The radiation cross section $d\chi/d\omega$ for the BRS can be obtained using the Born approximation (Bethe-Heitler formula, see for example [79]). The result for the energy radiated per unit time/frequency/volume is (for details, see Appendix E.5)

$$\frac{dE}{d\omega\ dV\ dt} = < v\ \frac{d\chi}{d\omega} >\ n_e\ n_{ion} \tag{3.61}$$

where n_e and n_{ion} are the concentrations of electrons and ions, respectively, and $< v\ d\chi/d\omega >$ represents the thermal average of the product of the electron velocity v and the radiation cross section. It is assumed that the electron gas and ions are at the same temperature (the relaxation time is fairly short, viz. page 75), and that the velocity of the electrons obeys a Maxwell distribution[16]. The next step is to include corrections to individual scattering events which lead to radiation because of the presence of the rest of the plasma. This corrections can be included by noting that (in the dipole approximation) the electric dipole $\mu(\omega)$ in a "cavity" with dielectric constant $\epsilon(\omega)$ emits radiation as if it has an effective dipole moment $\vec{p}(\omega) = 3/[2 + \epsilon(\omega)]\,\vec{\mu}(\omega)$. (This results is independent of the location or orientation of the dipole.) Here $\epsilon(\omega)$ is the plasma dielectric constant given

[16]The relaxation time for establishing a Maxwell distribution is short compared to the time scale which is of interest to us.

by:

$$\epsilon(\omega) = 1 - \frac{\omega_p^2}{\omega\left(\omega + \frac{1}{\tau}\right)} \tag{3.62}$$

where ω_p is the plasma frequency and τ is the electron collision time. This collision time is assumed to result from Coulomb scattering of electrons and is given by $1/\tau = n_e v \sigma_c$ where n_e is the electron density, v is the electron velocity and σ_c is the Coulomb cross section. In this approximation, it is assumed that the "cavity" has well defined walls, i.e. that the electron density falls rapidly over a short distance. Finally, after inclusion of the above mentioned correction, one gets the following result for the emitted energy per unit volume per unit time (see Appendix E.5)

$$\frac{dE}{dt\ dV} = \frac{64\pi}{3}\frac{e^2 c}{m_e}\left(\frac{e^2}{m_e c^2}\right)^2\left(\frac{\beta m_e}{2\pi}\right)^{3/2}\frac{\omega_p}{\beta} n_e n_{ion} F(\beta\hbar\omega_p, \omega_p\tau) \tag{3.63}$$

where e and m_e are the electron charge and mass, respectively, c is the speed of light and $\beta = 1/(k_B T)$. The function F is given by:

$$F(\beta\hbar\omega_p, \omega_p\tau) = \frac{1}{\omega_p}\int_0^\infty d\omega \int_1^\infty dx \frac{e^{-\beta\hbar\omega x}}{\sqrt{x(x-1)}}\left|\frac{3}{2+\epsilon(\omega)}\right|^2 \tag{3.64}$$

The function F was calculated numerically and, finally, the energy loss given by Eq. (3.63) was included in the loss term on the right hand side of Eq. (3.18). The calculations were carried out by introducing a cutoff in order to define the size of the plasma region around the bubble center where bremsstrahlung is taking place. This cutoff was defined in terms of "critical" degree of ionization m_c. The plasma region was defined as one where the degree of ionization m is larger than m_c. The results for the energy loss are not very sensitive to the choice of m_c, which was taken to be 1.0 in the actual calculations.

3.6 Discussion of the Results

First, let us study the relative importance of the various mechanisms for energy loss. While the inclusion of vibrational degrees of freedom and dissociation has some effect, the primary corrections come from ionization and radiation. The profiles in space and time of the thermodynamic variables of the gas are similar to the uncorrected solution, as can be seen from Fig. 3.14[17]. The pressure is not very different from the results without corrections since there are two competing effects: increase of pressure due to increase in the number of particles (dissociation, ionization) and decrease because of the energy loss. The velocity is typically smaller, since a part of the energy is converted to potential energy. The most drastic changes occur in the temperature (cf. Fig. 3.15), especially close to the origin. The maximum temperature is about an order of magnitude smaller than the results without corrections. A very important point about the inclusion of losses (especially radiation losses) is that it provides a natural mechanism for cooling of the bubble. To illustrate this point we present in Fig. 3.16 the results for the temperature in the bubble at a time about 200 *ps* after it achieves its minimum radius. We can see that there is a big difference in the results, especially close to the origin (more than an order of magnitude).

Let us now discuss the influence of the change of some of the parameters on the results for the thermodynamic variables. The results for the pressure and temperature in the bubble after the first shock rebounds from the origin are shown in Figs. 3.17 and 3.18 for different acoustic pressure amplitudes. We see that a change of 10 percent in the driving pressure produces differences

[17]These are the results following from the Thermal approach. The results following from the BRS approach are similar.

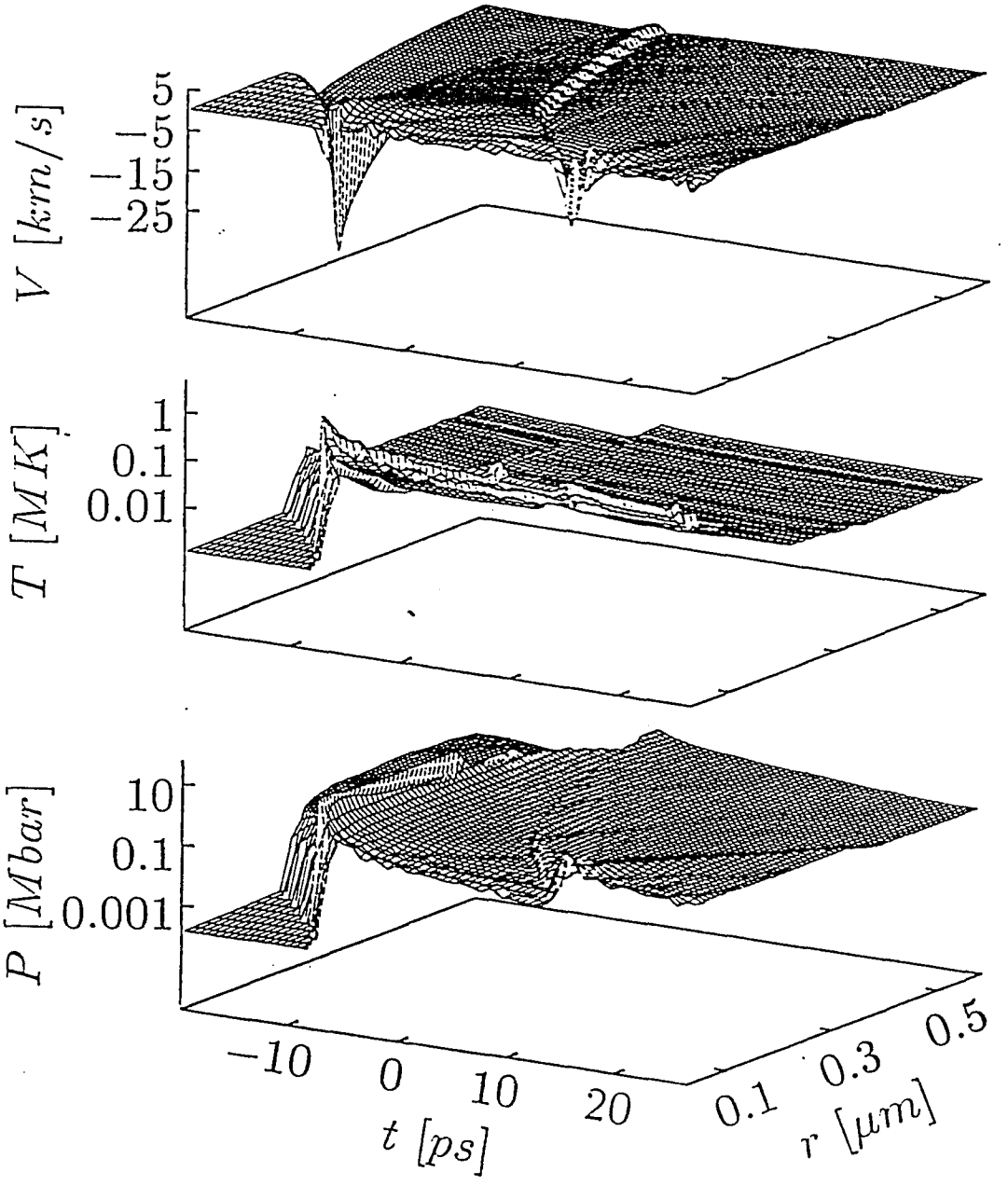

Figure 3.14: *Space-time profile of the dependence of the gas velocity, pressure and temperature following from the Thermal approach. All loss mechanisms mentioned in the text are included. The small oscillations result from the discrete procedure for including energy losses.*

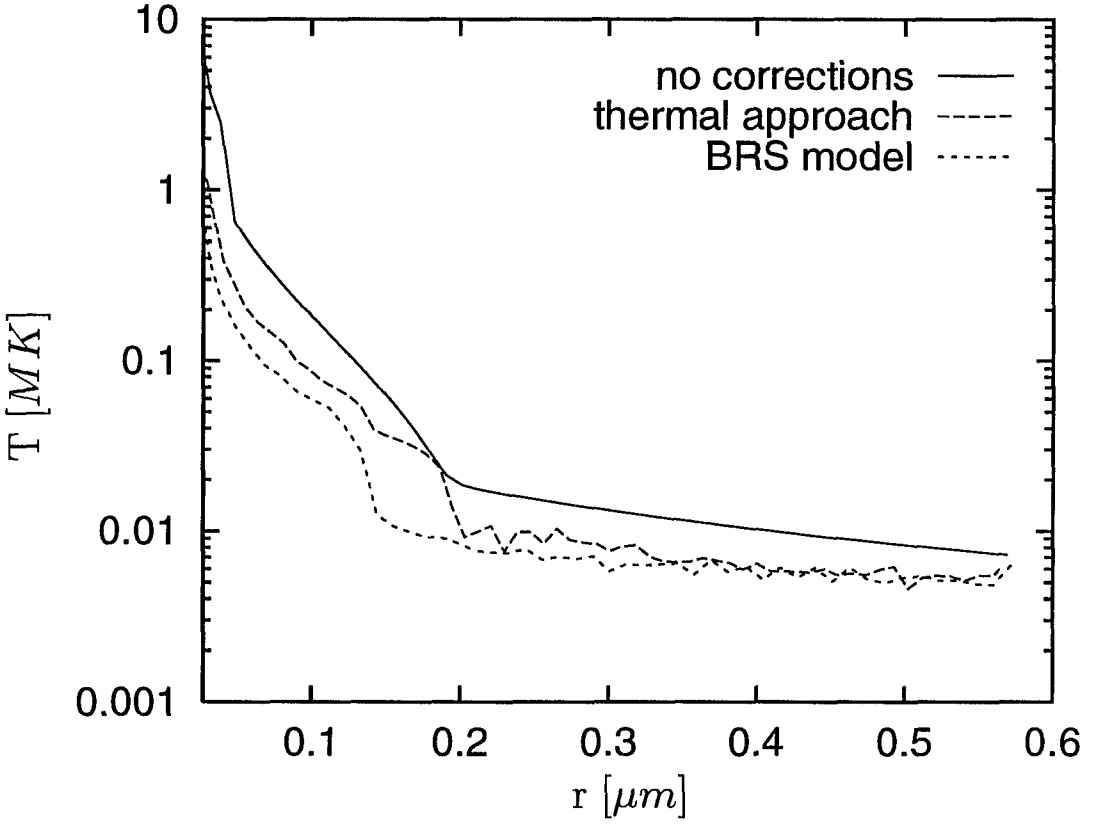

Figure 3.15: *Spatial profile of the gas temperature at the time immediately after the first shock rebounds from the origin for different methods of introducing energy losses. The acoustic pressure amplitude is* 1.325 *atm in this and the following figures, unless specified differently.*

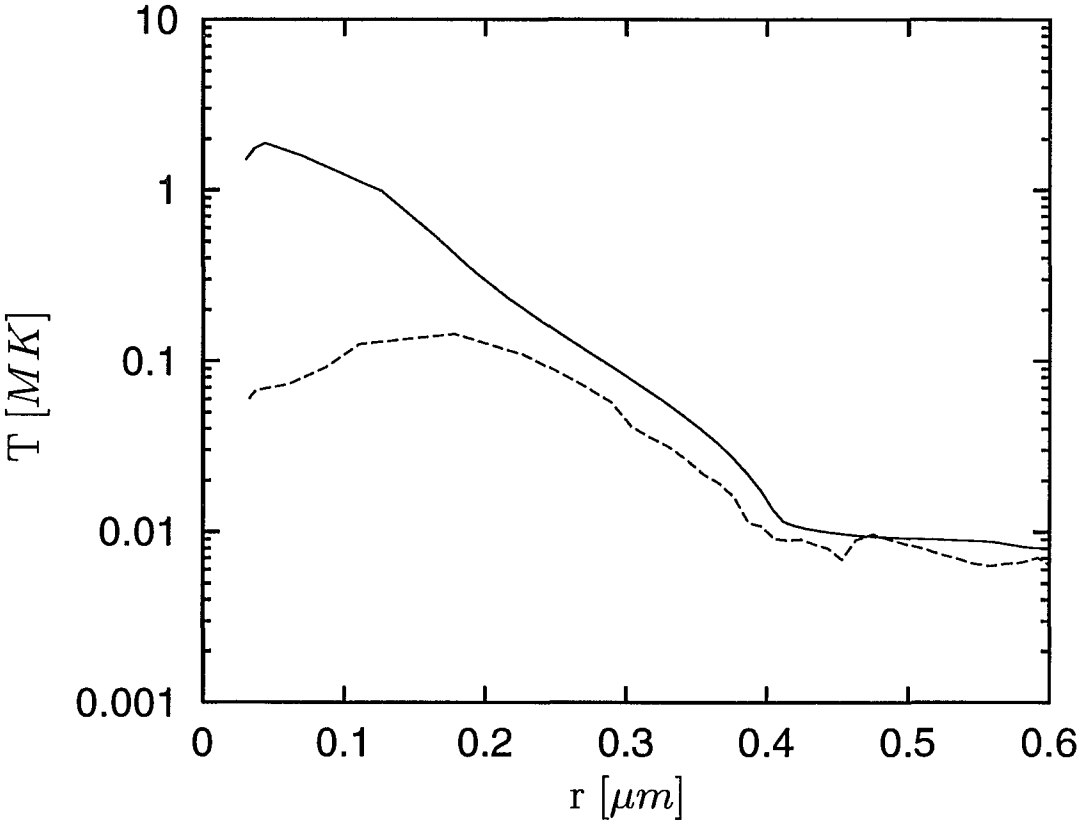

Figure 3.16: *Temperature in the bubble about 200 ps after the collapse of the first shock. The solid line represents the solution without the inclusion of loss terms. The broken line is the solution if all energy-loss mechanisms are included (the Thermal approach). The acoustic pressure amplitude is* $1.325\,atm$.

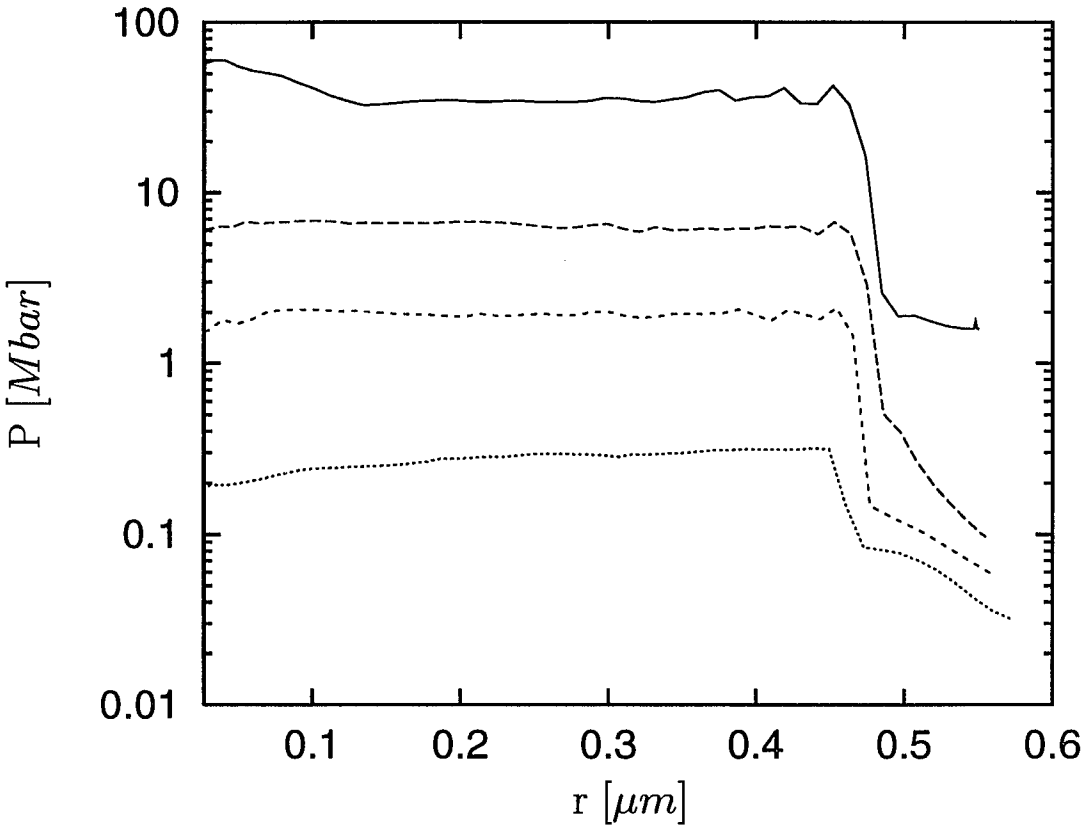

Figure 3.17: *Pressure in the bubble for different acoustic pressures, immediately after the first shock rebounds from the origin. The results are, from top to bottom, for acoustic pressures of* 1.375 *atm (solid line),* 1.325 *atm,* 1.275 *atm and* 1.225 *atm (dotted line).*

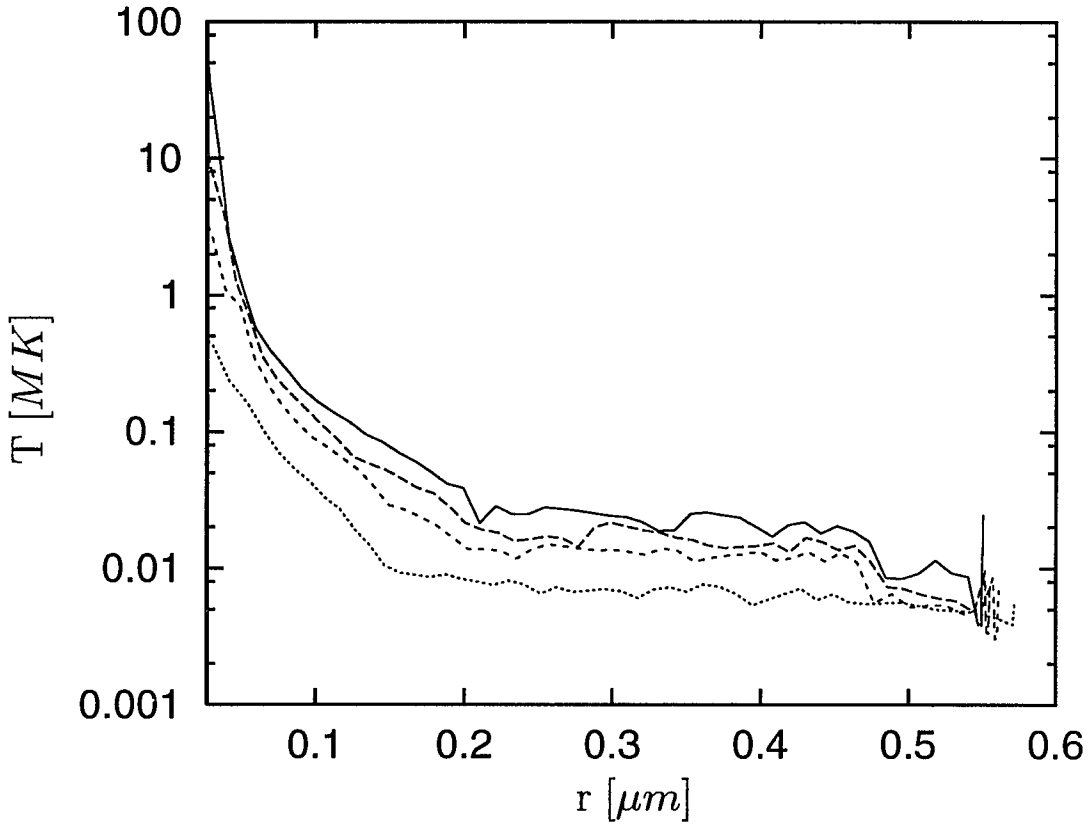

Figure 3.18: *Temperature in the bubble for different acoustic pressures, immediately after the first shock rebounds from the origin. The acoustic pressure amplitudes are the same as in the previous figure.*

of about two orders of magnitude for the temperature close to the origin and even more for the pressure. The explanation for these drastic changes can be found in Fig. 3.19 (see also Table 4.1 on page 100). From the Table 4.1 we see that for higher acoustic pressures the ratio R_m/R_0 is larger. This leads to a faster collapse of the bubble wall. It achieves supersonic speed with respect to the gas inside the bubble while the bubble is still relatively large (6.5 μm for an acoustic pressure of 1.425 atm). Thus, stronger shock waves are produced, and that leads to huge temperatures and pressures in the bubble. On the other hand, if the acoustic pressure is not high enough (cf. Fig 3.19d), the motion of the bubble wall never becomes supersonic. The conditions for formation of a shock wave are not fulfilled and conditions in the bubble are almost adiabatic. (And, of course, there is no SL radiation.) The influence of different acoustic pressure amplitudes on the motion of the bubble wall close to the minimum radius can be seen in Fig. 3.20. We see that for acoustic pressures above some threshold value (about 1.2 atm), the minimum bubble radius is almost independent of it (for the initial bubble radius of 4.5 μm this minimum radius is about 0.55 μm). Higher acoustic pressure results in a faster collapse of the bubble wall, as it was already noticed. But, if the acoustic pressure is not high enough (for example, $P_a = 1.175$ atm in Fig. 3.20), the minimum bubble radius is larger and the collapse is much slower. Later we are going to see that this threshold value of the acoustic pressure also represents the minimum pressure which still leads to the emission of a SL pulse.

Concerning the influence of a different initial bubble radius, the conclusion is not so simple. It seems that there are two competing effects taking place. On the one hand, from Table 4.1 we can see that a smaller bubble expands more (the R_m/R_0 ratio gets larger for smaller R_0), so the collapse of the

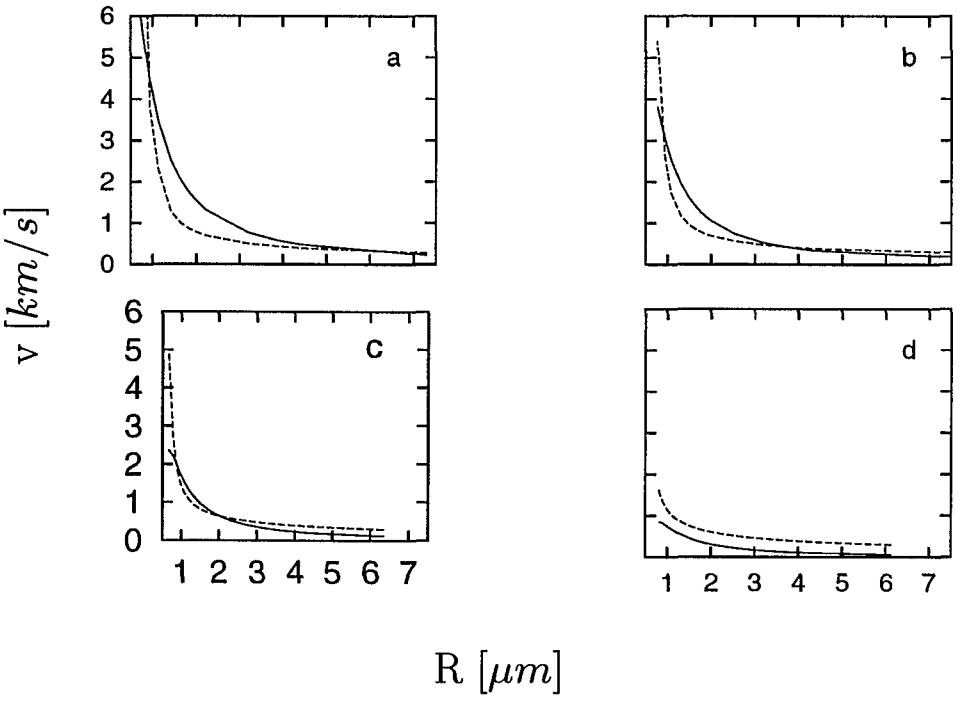

Figure 3.19: *Bubble wall speed (solid line) and speed of sound (broken line) close to the minimum radius. For certain acoustic pressure amplitudes, the motion of the bubble wall becomes supersonic with respect to the gas inside the bubble. The bubble radius where that occurs depends on the choice of the acoustic pressure. Here we present results for four different acoustic pressures: a:* 1.425 *atm; b:* 1.325 *atm, c:* 1.225 *atm, d:* 1.125 *atm. The wall motion does not become supersonic for the last case.*

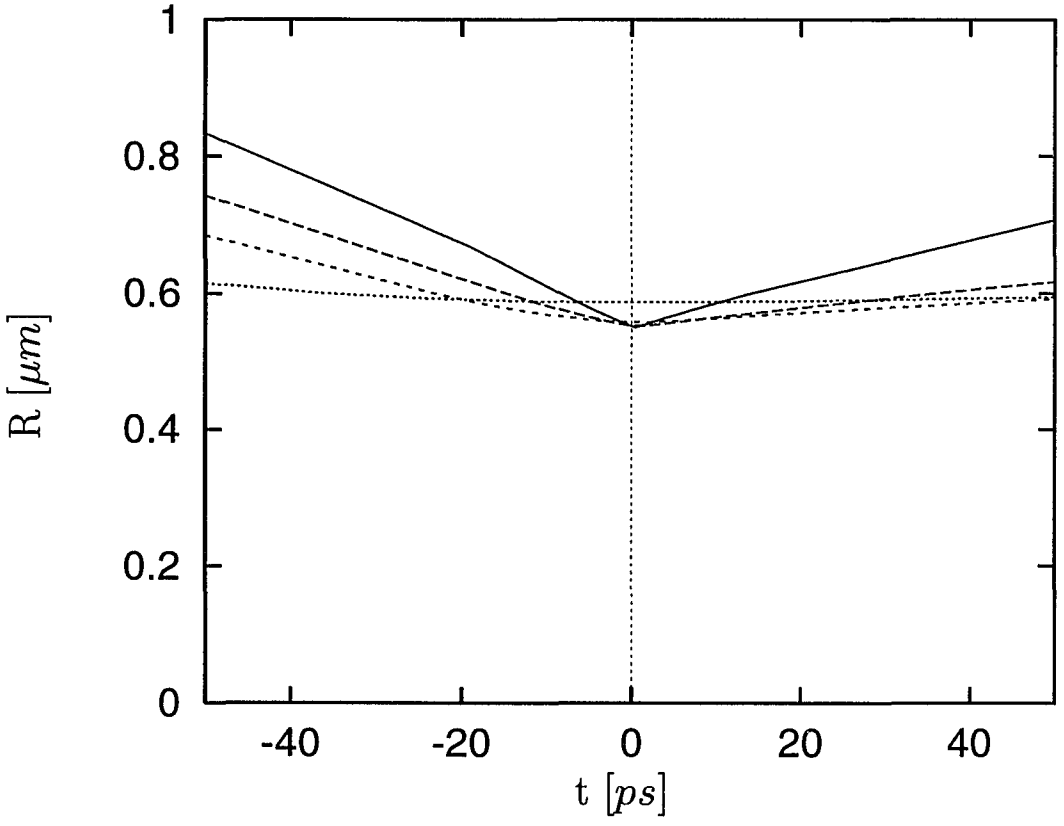

Figure 3.20: *Bubble radius close to its minimum for different acoustic pressures. Solid line is for* $P_a = 1.425$ *atm, first broken line is for* $P_a = 1.375$ *atm, second broken line is for* $P_a = 1.275$ *atm and dotted line is for* $P_a = 1.175$ *atm.*

smaller bubbles should be faster. This leads to an earlier production of the shock wave and a stronger shock collapse. On the other hand, in initially very small bubbles ($R_0 \sim 3.0\ \mu m$), the shock wave is produced rather close to the center, so it does not develop very high temperatures during the final stages of its collapse. For initially large bubbles ($R_0 \sim 10\ \mu m$), the situation is opposite. The bubble does not grow very much during the expansion part of the cycle, so the collapse is weaker. That leads to the production of a weaker primary shock wave and lower temperatures in the bubble center. We will see the influence of the initial bubble radius on the emission of SL pulses in the next section.

One of the interesting consequences of an initially small bubble radius is that the shock wave is produced relatively early, so the rebounding wave hits the bubble wall while it is moving inward rather fast. The result is an even stronger rebound. The rebounding wave hits the origin again, rebounds and reaches the bubble wall one more time. For the case of $R_0 = 3.0\ \mu m$ we were able to count at least five of these rebounds. As the rebounded waves become weaker, the temperature and pressure gradients are not as strong as for the first one.

Conclusion

In this chapter, which is the most important in this work, we gave a comprehensive explanation of the bubble dynamics for a strongly driven bubble in a acoustic field. The mechanical energy losses resulting from high temperatures and pressures in the bubble were coupled self-consistently with the gas-dynamic equations and the R.P. equation.

The treatment of radiation losses, which is discussed in this chapter, is

directly connected to the explanation of the effect of sonoluminescence. This will be the subject of the next chapter.

Chapter 4

Sonoluminescence

Introduction

In this chapter we explain the physical mechanism which leads to the emission of the sonoluminescent pulse. The discussion is based mainly on the results for the radiation mechanisms introduced in the previous chapter. The radiation in the optical region which is not absorbed in the bubble is going to escape and be observed in the form of a SL pulse.

The basic explanation of the mechanism which leads to the SL pulse is presented in section 4.1. The sensitivity of the SL pulse to input parameters is the subject of the following section 4.2. We mainly concentrate on the importance of the initial bubble radius and the applied acoustic pressure amplitude.

4.1 Explanation of the Emission of the Sonoluminescent Pulse

In the previous chapter we presented two approaches to the problem of radiation energy loss. The same mechanisms are going to be responsible for the

emission of a SL pulse. The main difference between these two approaches is in how to treat the small region where the temperature is very high. The Thermal approach does not make any corrections because the size of this region is smaller than the the typical wavelengths of optical photons. In order to check if this assumption is correct we formulated the BRS model which takes this into account through the inclusion of a frequency dependent dielectric constant. It is important to note that the effect of SL cannot be explained by pure BRS, since the spectral power of BRS radiation falls with increasing frequency instead rising as seen in experiment [29]. (The experimental spectral energy is presented in Fig. 4.4, on page 103). We would like to emphasize here that a very important factor in both approaches is the inclusion of an absorption coefficient into the calculation of the emitted spectrum. The absorption coefficient depends strongly on the temperature and density of the gas. These quantities are functions of initial conditions, particularly the acoustic pressure and the initial radius. These are not known precisely in the experiment [35]. The possibility of the presence of impurities, like water vapor, was not taken into account. While the approximations made in calculating the absorption coefficient are good enough to give an estimate for the energy losses, discrepancies between our results and the experimental data for the SL pulse could be attributed to the imprecise calculation of the absorption coefficient. In the rest of this section we are going to present the results based on the Thermal approach and BRS model.

4.1.1 The Thermal Model

In the Thermal approach the absorption coefficient determines if a body is going to radiate a black body spectrum (surface radiation) or whether it will be a volume radiator. In our case the results for the absorption coefficient

vary considerably for different temperatures and frequencies (see Table 3.1 on page 79). It could not be assumed that the bubble's contents behaves as any of these two limiting cases. In order to understand the spectral properties of the emitted radiation, let us separate the bubble into three regions. These regions are characterized as having quantitatively different temperatures and qualitatively different optical properties. The first one consists of the hot bubble center. In this region, as can be seen from Table 3.1, the absorption coefficient is large for the visible frequencies, so optical radiation which is produced in the bubble center is rapidly absorbed. The medium is opaque and this radiation never comes out of the bubble. The intermediate region (approximately for a radial distance of $0.1 - 0.2\ \mu m$ from the bubble center, cf. Fig. 3.18), is characterized by a sharp temperature gradient and an opacity which changes from being optically thick to optically thin across a distance which is comparable in size to the mean free path of optical radiation. The outer layer of the bubble (close to the bubble wall) is typically at temperatures of $10,000 - 15,000\ K$. At these temperatures the gas is optically thin (the mean free path for the optical radiation is larger than the characteristic size). So, the absorption coefficient is small, and this layer is not important in determining the absorption of radiation, It follows that the origin of SL stems from the intermediate zone where the brightness temperature is not very frequency dependent (the size of the region is comparable to the mean free path for the optical frequencies). Correspondingly, the SL radiation coming out of the bubble has spectral properties similar to black body radiation with a characteristic temperature corresponding to some average temperature in this intermediate zone. This could explain the fit of the observed SL pulse given in [29] to the Planck spectrum characterized by a temperature of $25,000\ K$. The actual calculations of emitted radiation

were carried through by using the results for the energy loss, Eq. (3.60). In this case the limits for the frequency integration had to be modified due to the absorption of radiation in water (the water window). The importance of the inclusion of radiation loss terms in the treatment of the gas-dynamic equations can be seen in Fig. 4.1. We see that there is not much difference in

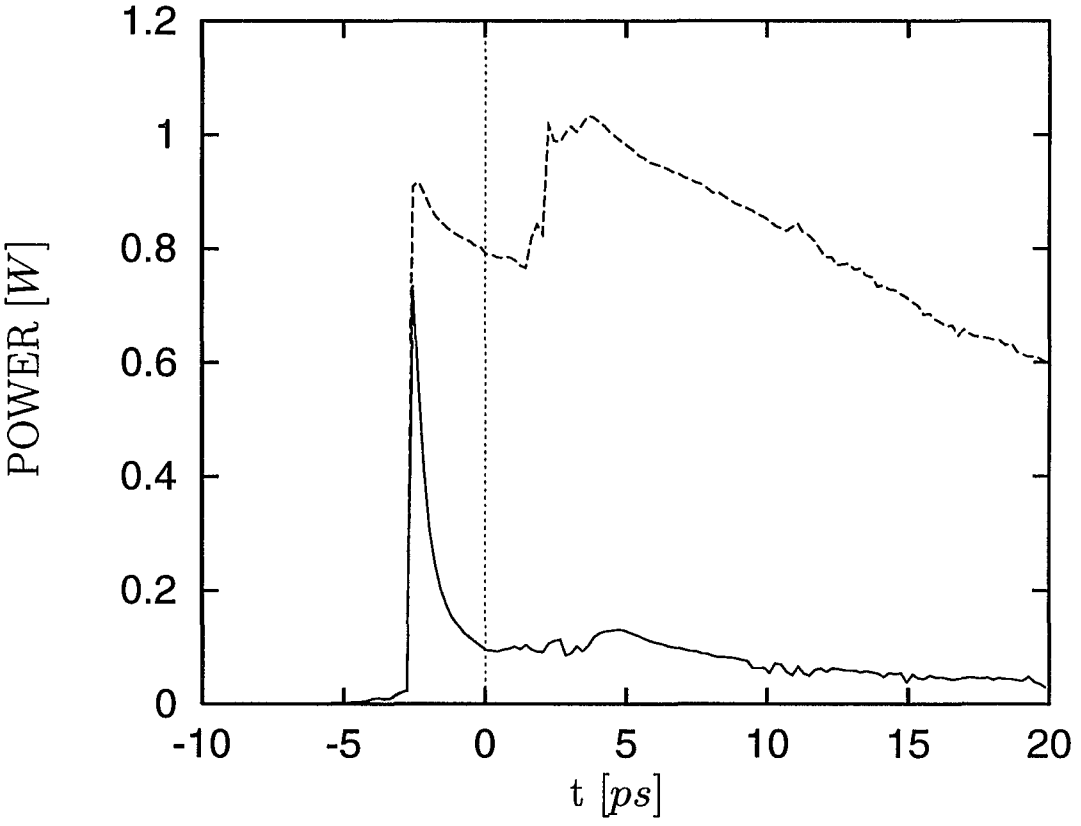

Figure 4.1: *Power versus time for the SL pulse. Results with inclusion of radiation losses (solid line) and without their inclusion (broken line) are presented (the Thermal approach). The acoustic pressure amplitude is* 1.325 *atm.*

the power emitted until the collapse of the first shock (at a time about 3 *ps*

before t_c, defined as the time when bubble wall velocity changes sign)[1]. At this point, however, a lot of energy is radiated and the temperature becomes much smaller than it did in the uncorrected solution. The second peak in the power spectrum of the uncorrected solution corresponds to the collapse of the second shock wave. We conclude that the inclusion of loss terms, especially radiation, is very important in order to explain the SL pulse. It also explains the short duration of the pulse. Our results imply that the duration of the pulse is actually even shorter than 50 ps, which is the current experimental upper bound [3]. The spectral properties of the optical radiation following from the Thermal approach are given in the following section (see also Fig. 4.2).

4.1.2 The Bremsstrahlung (BRS) Model

In the BRS model the absorption coefficient has a strong influence on the spectral energy and power output because of the absorption of radiation around the plasma region. The calculations were performed using Eq (3.63), where the limits of the frequency integrations were modified as explained before. The power output was corrected for the absorption in the region around the plasma.

The results for the power output versus time are similar to those resulting from the Thermal approach, with the pulse lasting longer than before. However, the problem which we meet with this approach is that the results strongly depend on the choice of the cutoff m_c, and show the common characteristic of becoming saturated at angular frequencies of about $5 \times 10^{15}\ s^{-1}$.

[1]The time of the collapse of the shocks relative to t_c is slightly different in Fig. 4.1 and the following figures compared to previously presented results (e.g. Fig. 3.5). The previous results were obtained with slightly different values for the acoustic pressure amplitude ($1.3\,atm$ compared with $1.325\,atm$ here.)

The results for the spectral energy of emitted radiation in the optical region, as well as the results from pure BRS, are shown in Fig. 4.2 (the results from the Thermal approach are also shown for comparison). We see that the correction due to the plasma which were introduced in our model, as well as the frequency dependent absorption, significantly modify the pure BRS spectrum, but still do not correspond to the experimental observation [35].

4.2 Sensitivity of SL Radiation to Experimental Parameters

4.2.1 Acoustic Pressure Amplitude

From now on we concentrate on the Thermal approach. The results for some important quantities which determine the radiation coming out of the bubble are summarized in Table 4.1. Clearly, a higher acoustic pressure amplitude leads to higher bubble wall speeds, so the shock wave is produced sooner and its collapse is stronger. This leads to higher temperatures in the bubble and more radiative energy output. This is also illustrated in Fig. 4.3. The sharp rise and slower decay of the pulse, which were observed experimentally [3], can be noticed as well. The other interesting result of our theory follows from the observation that the temperatures in the center of the bubble get to be very high if the bubble is driven with a high acoustic pressure (cf. Fig. 3.18 on page 87). We can see in Table 3.1 on page 79 that for high frequencies (10^{18} rad/s or more), the absorption coefficient is very small, implying that in this frequency region the bubble is optically thin. That means that emission of X-rays could be expected if the temperatures in the center of the bubble really reach values of the order of 10^8 K. Since the

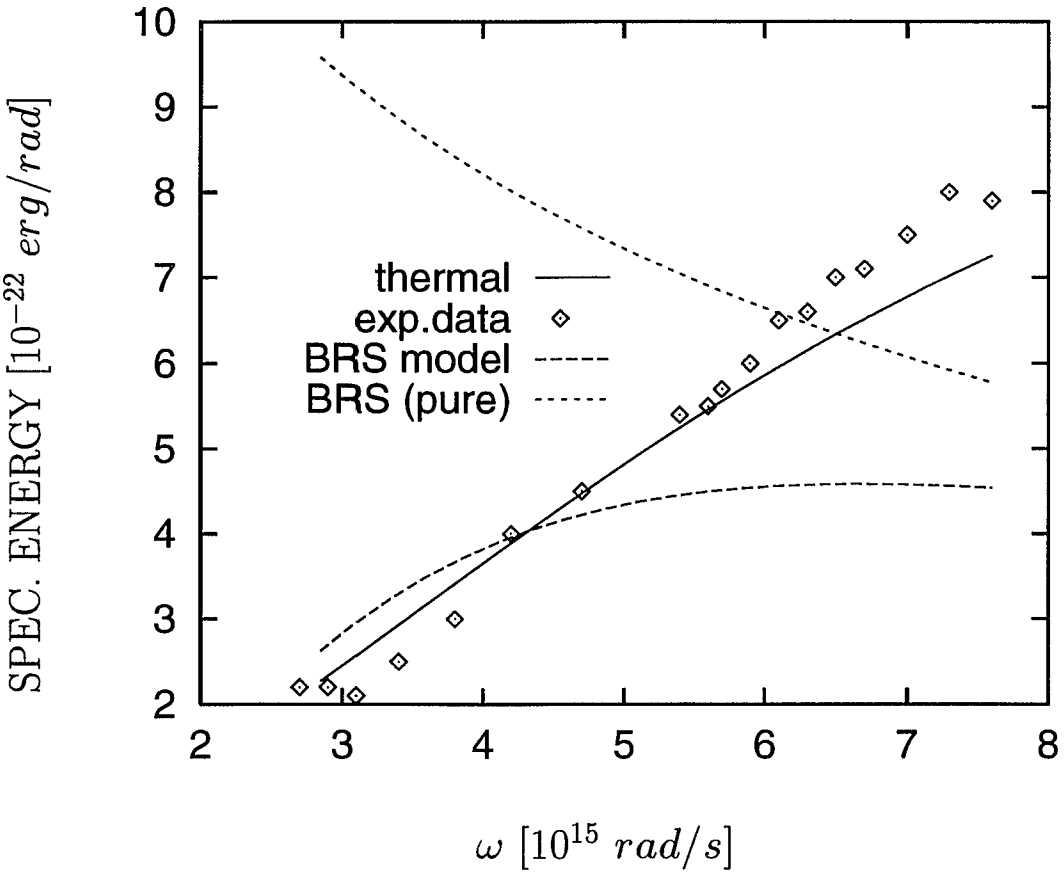

Figure 4.2: *Spectrum of emitted SL radiation resulting from the Thermal and BRS approach. The "pure" BRS results are obtained without corrections due to the presence of a plasma and absorption. The acoustic pressure amplitude is* $1.325\,atm$*, both for the theoretical and experimental results. The attenuation of radiation in the water and the container walls (see [33]), was not taken into account. The theoretical results were scaled down to the experimental ones.*

$P_a(atm)$	$R_0(\mu m)$	R_m/R_0	$v_m(km/s)$	R^{us}/R_0	N_p	$\overline{P}(mW)$
1.425	4.50	12.8	6.0	1.44	8.2×10^6	5.5×10^2
1.375	4.50	11.7	5.3	1.11	3.0×10^6	3.0×10^2
1.325	4.50	10.6	3.9	0.80	2.2×10^6	1.4×10^2
1.275	4.50	9.4	3.1	0.62	6.7×10^5	4.2×10^1
1.225	4.50	7.9	2.2	0.41	1.1×10^5	6.6
1.175	4.50	7.1	1.6	n/a	very small	very small
1.125	4.50	5.8	0.9	n/a	n/a	n/a
1.325	10.0	5.8	2.13	0.25	2.4×10^6	1.6×10^2
1.325	6.00	8.4	3.51	0.55	5.2×10^6	3.4×10^2
1.325	4.50	10.6	3.94	0.76	3.0×10^6	3.0×10^2
1.325	3.75	12.4	4.24	0.80	1.4×10^6	9.0×10^1
1.325	3.00	14.9	4.34	1.00	5.2×10^4	3.1×10^{-1}

Table 4.1: *The expansion ratio R_m/R_0, maximum velocity of the bubble wall v_m, radius at which bubble wall becomes supersonic R^{us}, number of photons N_p emitted in SL pulse, and average power $\overline{P}_a$ emitted during 10 ps around the maximum of the power output, are presented for different acoustic pressures P_a and equilibrium radii R_0.*

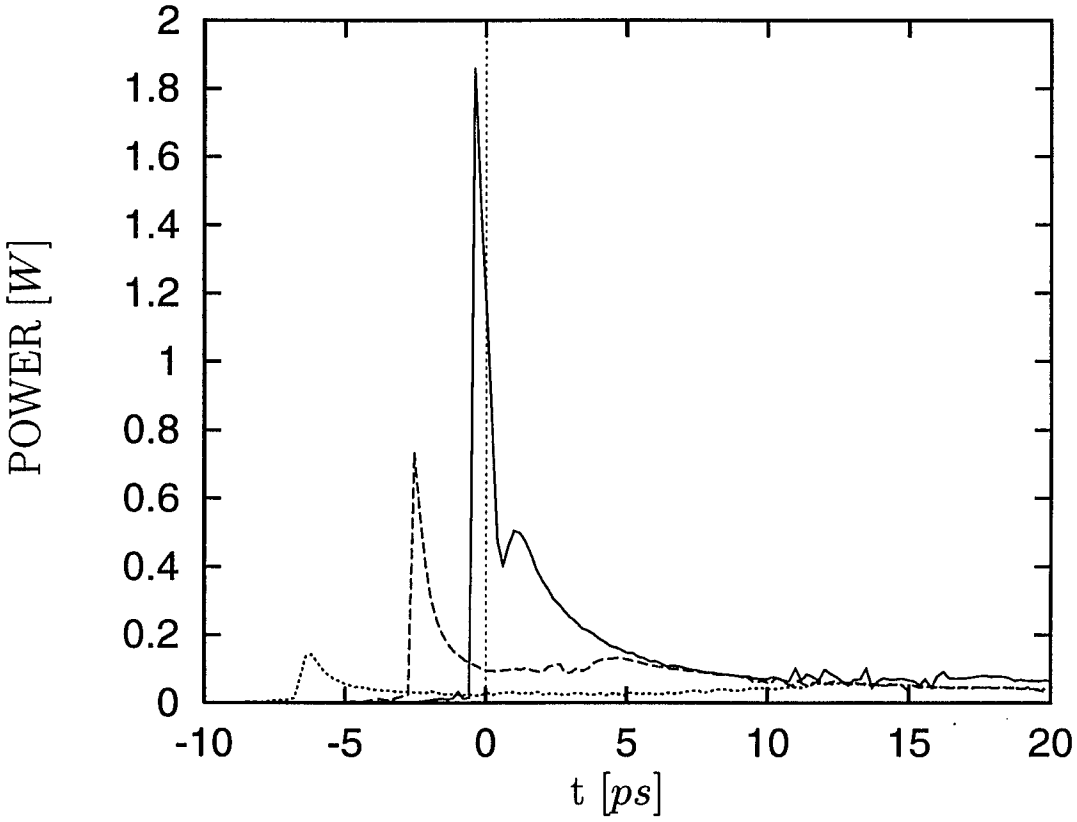

Figure 4.3: *SL emission for different acoustic pressures. The full line corresponds to* 1.375 *atm, the broken one to* 1.325 *atm and the dotted one to* 1.275 *atm. The results for lower acoustic pressure amplitudes are out of scale. These results follow from the Thermal approach.*

absorption length of X-rays is fairly long in the water as well, this effect should be observable. It could also give us the answer about how hot the bubble center really is. We shall emphasize that, as the result of our theory, this effect should be expected only for very strongly driven bubbles, with acoustic pressure amplitudes of at least $1.4 - 1.5\ atm$.

The spectrum of the emitted radiation is presented in Fig. 4.4. We show the experimental data and our results for a few acoustic pressure amplitudes. Note that higher acoustic pressure amplitudes lead not only to more power output, but they also change the frequency dependence of the spectral power. If one wants to fit the emitted spectrum to a black-body spectrum, the conclusion would be that the radiation from the bubble exposed to a higher "black body" temperature.

4.2.2 Equilibrium Bubble Radius

Concerning the influence of the initial bubble radius on the SL radiation, we have already seen in the previous section that there are two competing effects taking place. The net result is that the sonoluminescent emission is largest for some intermediate values of the equilibrium bubble radius. The SL power outputs for different initial bubble radii are presented in Fig. 4.5.

4.2.3 Water Temperature

Finally, we would like to comment on one of the most intriguing facts about SL radiation, i.e. the strong dependence of SL intensity on water temperature. The SL radiation increases more than ten times if the liquid is cooled down to the freezing point [29][2]. Our approach treats the bubble-liquid in-

[2]This effect was also observed in multiple bubble SL (MBSL), but there it was assumed that it results from the larger number of cavitation sites (see the discussion on page 9.)

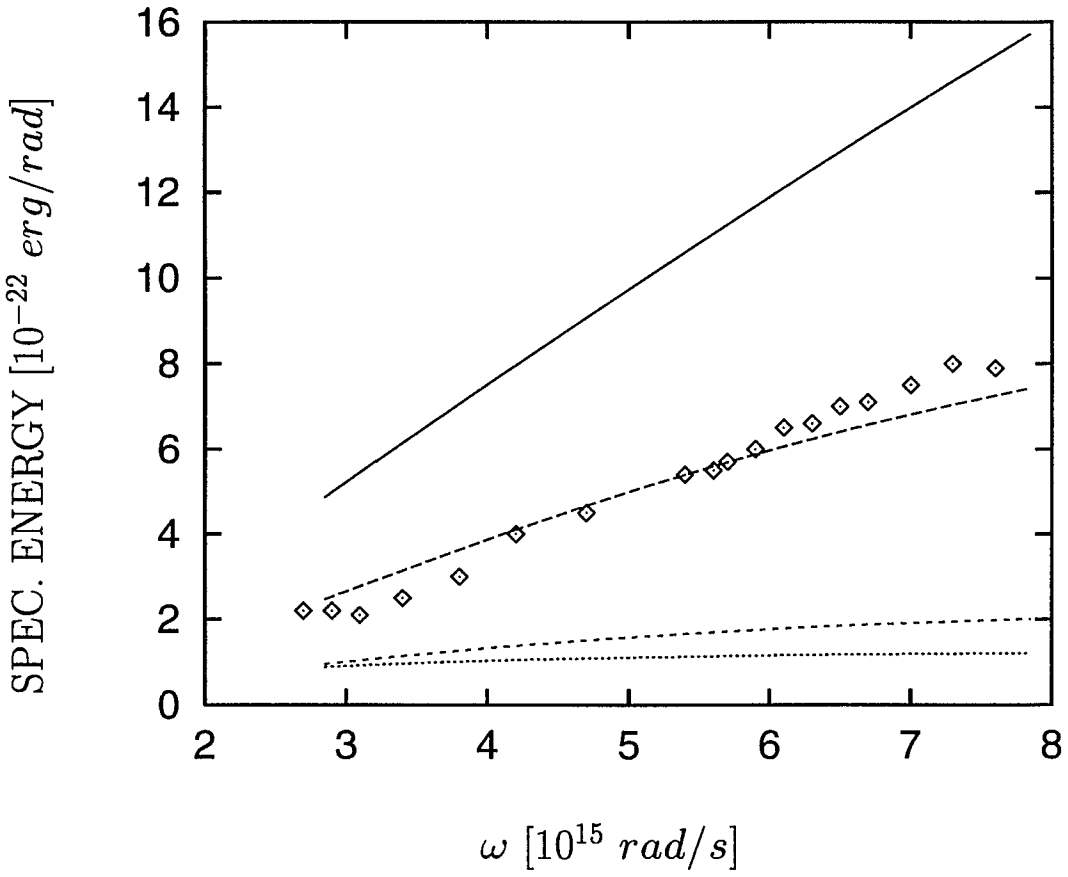

Figure 4.4: *Spectrum of emitted SL radiation. Squares are experimental data, lines correspond (from top to bottom) to acoustic pressures of* 1.375 *atm (solid line),* 1.325 *atm,* 1.275 *atm and* 1.225 *atm (dotted line). The experimental results were obtained with an acoustic pressure amplitude of* 1.325 *atm. The theoretical results are scaled down to the experimental values. The attenuation of the radiation in the water and in the container walls was not taken into account in the theoretical results.*

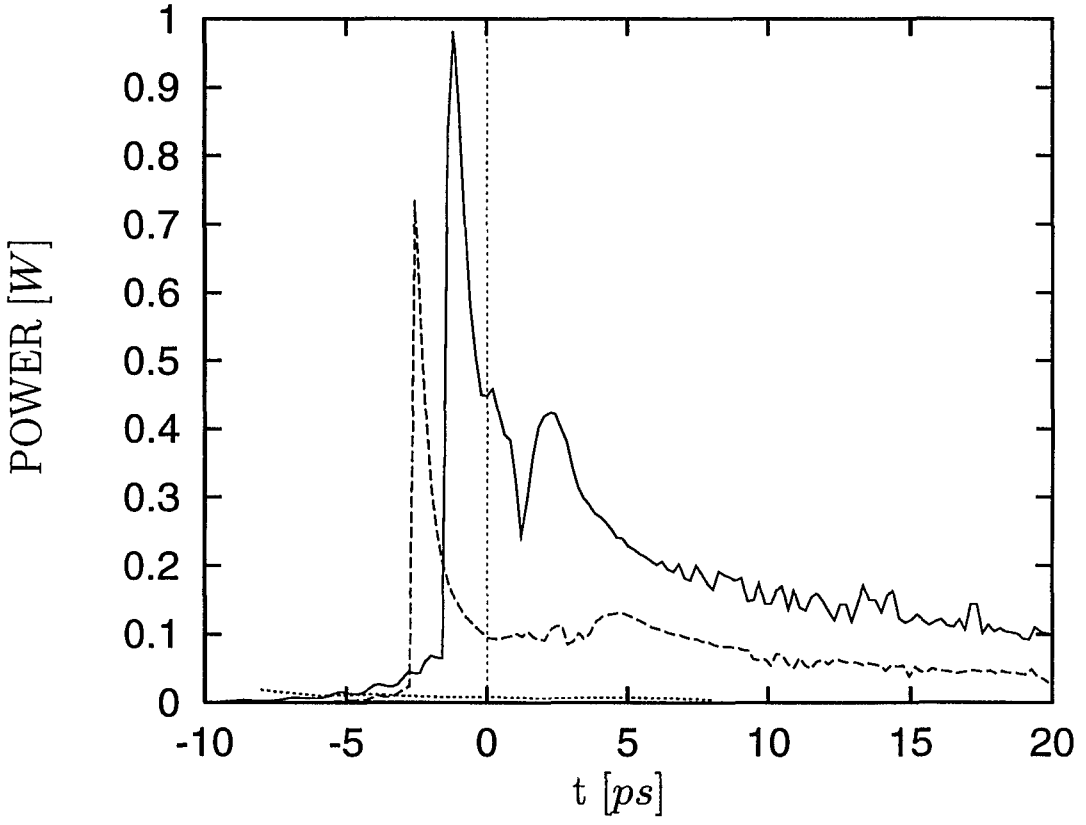

Figure 4.5: *SL emission for different initial bubble radii. The full line corresponds to* $R_0 = 6.0$ *μm, the broken one to* 4.5 *μm and the dotted one (barely visible) to* 3.75 *μm.*

teraction very approximately (through R.P. equation), but we hope that we can indirectly understand this striking observation. First, as noticed in [29], water dissolves about twice as much air at 0°C compared with at 20°C. The mass flow between the bubble and water is important in stabilizing the bubble oscillations through longer periods of time [35]. One would expect that more air from the water is going to evaporate into the bubble if the concentration of the dissolved air in the liquid next to the bubble is higher. (Following Henry's law, the partial pressure in the gas is proportional to the concentration in the liquid.) The conclusion is that one would expect more air in the bubble in a colder liquid, or, correspondingly, a larger bubble. If the bubble is initially small, (for example, 3 μm), this flow of air between the water and bubble might have a considerable influence. From Table 4.1 we can see that a 3.75 μm bubble produces more than an order of magnitude more radiation than a 3.0 μm bubble. Since mass diffusion is a slow process, the time delay for the emission of SL pulse, reported in [35], can be explained as well. On the other hand, it seems [35] that the experiments with water at lower temperatures were done with higher acoustic amplitudes. That would also increase the SL emission, as pointed out earlier. Also, the SL pulse from the cold liquid was fitted to a higher "black body" temperature [29]. That is equivalent to our observation that the SL spectrum corresponds to higher temperatures if the acoustic pressure is increased.

Conclusion

Our approach to the physics of a collapsing bubble in a liquid provides a satisfactory explanation for the production of sonoluminescent radiation. The inclusion of mechanical energy loss is necessary in order to fully understand

the phenomenon. The strong dependence of the SL pulse on parameters, which was reported experimentally [35], is explained from a theoretical point of view. The maximum temperature in the bubble is strongly dependent on the acoustic amplitude and might reach values of tens of millions of degrees.

Chapter 5

Conclusion

5.1 Summary

Single-bubble sonoluminescence was observed for a first time just a few years ago. In this work we presented a theory which possibly explains the effect. The main challenge for any theoretical approach is how to explain the very short duration of the light flashes ($50\,ps$) and high concentration of energy. The duration of the flashes was found to be sufficiently short to rule out conventional radiative relaxation processes (requiring times on the order of nanosecond or more). The energy spectrum was sufficiently broad to rule out superradiance, superfluorescence or laser type mechanisms, which rely on a high number of photons occupying a single optical mode. Furthermore, it seems that effects like charge separation in the bubble or the eventual charging of the liquid which surrounds the sonoluminescing bubble do not play a major role in producing the sonoluminescent pulse. Also, the possibility of light being trapped in the bubble because of a spatial variation of the optical properties of the gas was explored. We did not find enough evidence to conclude that this effect might be responsible for the emission of optical

radiation.

The key point in understanding SL was the discovery that the motion of the bubble wall becomes supersonic with respect to the local speed of sound. This supersonic motion results in the production of shock waves in the bubble. In order to fully explore the thermodynamic properties of the gas we solved the gas-dynamic equations for the gas, coupled with the equation which determines the dynamics of the bubble. We were able to confirm that the production of the shock waves really happens. Numerical solutions were obtained and found to be consistent with the self-similar solution for the collapse of strong shock waves. The consequence of the convergence of the shock waves to the bubble center are temperatures of millions of degrees and pressures at a megabar scale. These results imply that some very exotic processes, including nuclear fusion might occur in the bubble. However, these results also imply that mechanical energy losses might be considerable. Accordingly, various effects which might be important during the short time the bubble spends close to its minimum radius were included in our treatment of the gas dynamics of the gas. We found that the dissociation and ionization of the gas have some importance, but the main correction comes from the inclusion of radiative energy losses. Two models were developed in order to self-consistently account for the radiative processes in the gas. One (BRS model) is based on the bremsstrahlung from the hot bubble center, corrected for the presence of the plasma which forms because of the high temperatures in the bubble. The other (Thermal model) is based on the use of a radiative transport equation which properly takes into account the possibility of emission and reabsorption of the radiation in the hot bubble interior. The important point in these calculations was to realize that the absorption coefficient for the gas in the bubble is very high. One of the

consequences is that the absorption of radiation plays an important role in transferring energy from the hot bubble center to colder regions closer to the bubble wall. This leads to an effective cooling of the bubble center, bringing down the maximum temperature an order of magnitude, compared with the results where the radiation losses were not included.

The above mentioned mechanisms for the radiative processes in the gas also gave an explanation of sonoluminescence. The comparison of the spectral distribution of the emitted radiation with experimental results favors our Thermal model. It was found that the bubble behaves (in an optical sense) like a miniature sun. The inner parts of the bubble which are at very high temperatures (million or more degrees) are optically thick, so the radiation which is emitted from the bubble center is almost immediately absorbed. The observed radiation stems from the intermediate regions whose temperature is of the order of few tens of thousands of degrees. This explains the spectrum of SL, which is black-body like and corresponds to a temperature of $25,000 - 30,000\,K$. The cooling of the bubble center following the self-consistent inclusion of mechanical energy loss also allowed us to understand the short duration of the SL pulses. Our results for the duration of the pulse are even shorter than the experimental upper limit, which was put on $50\,ps$. The maximum power emitted as a result of our theory is larger than experimentally observed (experimental lower limit is about $30\,mW$). However, the absorption of radiation in water and the container walls was not taken into account.

Finally, in order to test our results against experiment, we explored the influence of varying some of the experimental parameters. It was experimentally observed that the intensity and the spectrum of SL are very sensitive to changes of the acoustic pressure amplitude and the equilibrium bubble size.

We find that our results are in very good agreement with experimental ones. For example, increasing of the acoustic pressure amplitude by a few percent leads to a 10-fold increase in the intensity of the emitted radiation. Furthermore, the spectrum of emitted radiation is steeper for a more strongly driven bubble (corresponding to a higher black-body temperature), in full agreement with experimental results.

Let us summarize here. It has been proposed that SL is associated with the production of shock waves in the air inside the bubble [29]. Theoretical calculations, based on the gas dynamic equations coupled to the bubble wall dynamics, have found shock waves [30]. The predicted high temperatures, coupled with a bremsstrahlung mechanism, were used to explain SL. In this work we found that important modifications of this theory occur if these equations are solved self-consistently with the radiative transport equation. In particular the shock core temperature is lowered by an order of magnitude. This is the first important contribution of this work. We also focused on the spectral properties of the emitted radiation and found that pure bremsstrahlung alone cannot account for the observed spectrum [30]. We proposed a new mechanism (Thermal approach) which explains, in qualitative manner, the spectral properties of the SL radiation. This is the second important contribution.

We conclude that our theory provides the basic mechanism which explains the most important points about sonoluminescent radiation. However, since the physical problem is very complicated, we are aware that there is much more research to be done in this exciting field. Some of the ideas about possible improvements of our theory, and some still unresolved questions about SL are summarized in the following section.

5.2 Directions for Future Research

Let us summarize the most important improvements which could be done based on our theory for the bubble dynamics and emission of the SL pulse. Further work in these directions should lead to a possible solution to still unresolved questions about SL, which are mentioned as well.

- *Bubble-Liquid Interaction;* In this work we assumed that this interaction follows from the Rayleigh-Plesset equation. The heat conduction, as well as mass transfer across the bubble wall were not taken into account. Unfortunately, the problem is extremely complicated and has not been solved until now. The proper understanding of the physical mechanism which governs this interaction would lead to a more precise explanation of the strong dependence of the SL intensity on the liquid temperature.

- *Radiation Mechanism;* The inclusion of the radiative transfer theory was significantly simplified, in order to allow us to couple the radiation problem efficiently with the gas dynamics. A more precise treatment of the radiative transfer equation would also require a more precise calculation of the absorption properties of the gas. Since this is very computing-intensive problem, a significantly improved treatment of the radiation-matter interaction would definitely require the use of high-speed computers.

- *Gas Dynamics and Strong Shock Implosion;* Further research in this direction might be very rewarding. We presented a rather simple (first order) numerical scheme which allowed us to solve the problem of the strong shock implosion. However, second order effects, like gas viscosity

and heat conduction should be explored. This is important research independent of the sonoluminescence problem. Also, the question of the stability of the shock implosion during its final stages of convergence is an important one in order to understand what the limits are on the gas temperature which can be achieved. On the other hand, new experimental results on the large influence of rare gases on sonoluminescent radiation [33, 80] require an explanation as well. It is our understanding that the answer to this question might require the solution of the gas-dynamic equations in the supersonic regime for a mixure of different gases. This would be a very demanding project, but an understanding of this problem could lead to even more important results, which would go even beyond sonoluminescence. It would be an important contribution if one could predict a particular liquid-gas combination which would lead to an even higher energy concentration.

Appendix A

The Collective Effects

The essential ingredient for any collective effect is a highly organized system. How can we expect to have these conditions satisfied in a gaseous cavity under the extreme conditions of high pressures and temperatures? The interaction taken into account in [81]-[83] is between the atoms and the electric field. In our model we assume that there is also an interaction among the atoms in our sample, which could get to be fairly strong. We want to see if we can expect to have some kind of "locking" [84] among the atoms, which can produce a collective state which satisfies the conditions for collective emission.

A.1 Model Hamiltonian

We consider a collection of N atoms (molecules) in thermal equilibrium and model the individual atoms as two-level systems with ground state energy e_0 and excited state energy e_1. We assume the atoms to be close to each other, i.e. that the internuclear separations are small compared with the wavelength of the emitted radiation. Next we add the interaction with the radiation field and the possibility of near field (dipole-dipole) interaction.

The interaction part of the total Hamiltonian we model in a way to cor-

respond to a given atom getting deexcited and resonantly transferring its energy to another atom:

$$H_2 = \sum_{i,j,i\neq j} \Lambda_{ij}\sigma_i^-\sigma_j^+ \tag{A.1}$$

where Λ_{ij} is the coupling and σ_i^+, σ_i^- are atomic excitation and deexcitation operators, respectively. The total Hamiltonian is

$$H = H_0 + H_{int} + H_2 \tag{A.2}$$

where

$$H_0 = \sum_{\vec{k}s} \hbar\omega_{\vec{k}s}\left(\hat{a}_{\vec{k}s}^+\,\hat{a}_{\vec{k}s} + \frac{1}{2}\right) + \sum_{n=0}^{N}\left(\frac{e_0+e_1}{2}I_n - \frac{\hbar\omega_0}{2}\sigma_n^z\right) \tag{A.3}$$

and

$$H_{int} = \sum_{\vec{k}si} \gamma_{\vec{k}s}\vec{\mu}\cdot\hat{\epsilon}_{\vec{k}s}\left(\hat{a}_{\vec{k}s}^+\sigma_i^- + \hat{a}_{\vec{k}s}\sigma_i^+\right) \tag{A.4}$$

Here $\hat{a}_{\vec{k}s}^+$, $\hat{a}_{\vec{k}s}$ are the creation and the destruction operators for the photon field, $\hat{\epsilon}_{\vec{k}s}$ is the polarization vector, $\{\sigma\}$ are Pauli matrices, $\gamma_{\vec{k}s}$ is given by $\sqrt{2\pi\hbar\omega_{\vec{k}s}/V}$, where V is the quantization volume, ω_0 is defined as $(e_1 - e_0)/\hbar$ and $\vec{\mu}$ is a transition dipole matrix element. This is the Hamiltonian in the dipole and rotating wave approximation. We follow by making some additional approximation in order to see what we can expect from this approach.

A.2 Atom - Atom Interaction

For the time being, we assume that Λ_{ij} is a constant (the equal coupling approximation) and drop the radiation coupling. The argument for the last approximation is that we want to explore the effect of coupling among atoms

through the "near field". The radiation coupling will be considered later. So, the Hamiltonian becomes

$$H = -\frac{\hbar\omega_0}{2}\,\sigma^z \;+\Lambda\,\sigma^-\sigma^+ \tag{A.5}$$

where the σ operators are defined as

$$\vec{\sigma} = \sum_{n=1}^{N} \vec{\sigma}^i \tag{A.6}$$

We calculate the spectral distribution of the emitted radiation using

$$I(\omega) = \int_{-\infty}^{\infty} e^{-\imath\omega t}\; Tr[\rho\;\sigma^+(t)\;\sigma^-(0)]\;dt \tag{A.7}$$

where ρ is the density matrix, given by

$$\rho = \frac{e^{-\beta H}}{Tre^{-\beta H}} \tag{A.8}$$

We use the fact that the system of N atoms can be represented as a system having a quasi-angular momentum $N/2$ [81]-[86]. Using the Dicke notation we represent our basis states with two quantum numbers j, m (j is so called "cooperation number"), satisfying the condition $|m| \leq j \leq N/2$.

The final result for the radiation intensity is

$$I(\omega) = 2\pi \frac{\sum_{m=-N/2}^{N/2} \delta(\omega_0 - \omega + \frac{2m\Lambda}{\hbar})\, e^{\beta\hbar\omega_0 m - \beta\Lambda m(1-m)}\; \mathcal{F}(N,m)}{\sum_{m=-N/2}^{N/2} e^{\beta\hbar\omega_0 m - \beta\Lambda m(1-m)} \sum_{j=|m|}^{N/2} g_j\, e^{-\beta\Lambda j(j+1)}} \tag{A.9}$$

where

$$\mathcal{F}(N,m) = \sum_{j=|m|}^{N/2} g_j\, e^{-\beta\Lambda j(j+1)} j(j+1) - m(m+1) \sum_{j=|m|}^{N/2} e^{-\beta\Lambda j(j+1)} \tag{A.10}$$

and g_j is the degeneracy of a state with a given j

$$g_j = \frac{N!\,(2j+1)}{(\frac{N}{2}+j+1)!\,(\frac{N}{2}-j)!} \tag{A.11}$$

By examination of the results for the intensity versus number m, or frequency radiated, for different numbers of atoms, we notice that the width Γ (full width at half maximum) grows sublinearly with the number of atoms (time scale for the pulse emitted is $\Delta t \propto 1/\Gamma$). In order to check the dependence of the total emitted radiation (if we do not resolve individual lines) on the number of atoms, we calculate the total intensity as $I = \int I(\omega) d\omega$ and the results also show sublinear growth. Thus, it turns out that with these approximations of our model, we do not get evidence that a cooperative effect takes place.

A.3 Atom - Field Interaction

In the previous section, the interaction of the atoms with the radiation field was neglected. In what follows, we will try to explore the possibility of obtaining a population inversion through this interaction.

We consider a simplified Hamiltonian, corresponding to $H_0 + H_{int}$, given by Eqs. (A.3, A.4)

$$H = \frac{\hbar\omega_0}{2}\sigma^z \; + \; \alpha(t)\,\sigma^-\hat{a}^+ \; + \; \alpha^*(t)\,\sigma^+\hat{a}^- \tag{A.12}$$

The time dependence in α, α^* comes from the exponential factor in the electric field and also from the time dependence of the temperature and other parameters which depend of the bubble radius $R(t)$. Furthermore, we generalize this Hamiltonian by adding phenomenological relaxation times T_1 and T_2. Using the density matrix formalism and expressing the density matrix in terms of a Bloch vector $\vec{P}$

$$\rho = \frac{1}{2}[I + \vec{P}\cdot\vec{\sigma}] \tag{A.13}$$

we obtain the following expression for the components of $\vec{P}$

$$\dot{P}_z = -\frac{2\imath}{\hbar}[\alpha P_+ - \alpha^* P_-] \; - \; \frac{1}{T_1}[P_z - P_z^0] \tag{A.14}$$

$$\dot{P}_- = -\imath\omega_0 P_- \; - \; \frac{P_-}{T_2} \; + \; \frac{4\imath\alpha^*}{\hbar} P_z \tag{A.15}$$

$$\dot{P}_+ = \; \imath\omega_0 P_+ \; - \; \frac{P_+}{T_2} \; - \; \frac{4\imath\alpha^*}{\hbar} P_z \tag{A.16}$$

Here P_z^0 is the initial condition, following from

$$\rho^0 = \frac{1}{Z}\begin{pmatrix} e^{-\beta e_1} & 0 \\ 0 & e^{-\beta e_0} \end{pmatrix} \tag{A.17}$$

where Z is the partition function. The above equations were obtained using the Heisenberg equations of motion for the components of the density matrix. Here e_1 and e_0 are defined as before. The initial value P_z^0 is always less than 0 [1]. Now, solving the equation for $\dot{P}_z$ in the limit where T_2 is short, we see that the evolution of the system is constrained by the condition $P_z(t) < 0$ for every t. That means that, as the result of our simplified approach, we cannot expect a population inversion to be created.

Conclusion

Our approximate approach does not provide evidence that collective effects are important for the process of sonoluminescence. Of course, only by solving the complete problem, with the Hamiltonian given by Eqs. (A.1-A.4), would we obtain a rigorous theoretical answer to this question. The new experimental results [29, 33, 34], however, show that the spectral distribution of emitted radiation is sufficiently broad to rule out these mechanisms, so we have to explore other physical models in order to understand sonoluminescence.

[1] From the definition of P_z we see that $P_z > 0$ means negative temperatures.

Appendix B

Trapping of Light

The extreme conditions which exist in a collapsing gaseous bubble in a liquid might lead to high values of dielectric constant, and even to the possibility that the dielectric constant of the gas ϵ_1 will be larger than the dielectric constant of water ϵ_2, which is 1.77 at high frequencies. In Fig. B.1 we see that, if really $\epsilon_1 > \epsilon_2$, there is a possibility of total internal reflection. The critical angle of incidence for this phenomenon to occur is given by $\phi_c = \sin^{-1}(\sqrt{\epsilon_2/\epsilon_1})$. Assuming a uniform distribution of radiators, simple geometric arguments give that the trapped part of the total radiation emitted is given by

$$f = \Theta(\epsilon_1 - \epsilon_2) \left(\frac{\epsilon_1 - \epsilon_2}{\epsilon_2}\right)^{\frac{3}{2}} \tag{B.1}$$

The question is, of course, could the possibility of this high dielectric constant of the gas be expected. The Clausius-Mossotti equation gives the following result for the dielectric constant

$$\epsilon(\omega) = \frac{1 + \frac{8\pi n}{3}\alpha(\omega)}{1 - \frac{4\pi n}{3}\alpha(\omega)} \tag{B.2}$$

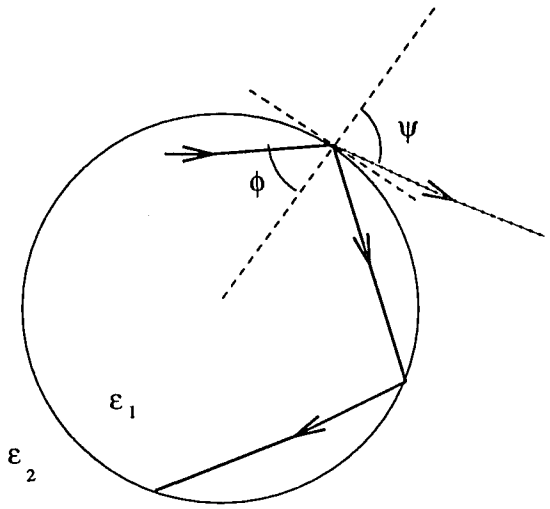

Figure B.1: *The possibility of total internal reflection for the radiation produced in the bubble. Total internal reflection happens if the angle of incidence ϕ is larger than the critical angle ϕ_c, which is defined in text.*

where n is the gas density and $\alpha(\omega)$ is molecular (atomic) polarizability, given as a Lorentz oscillator

$$\alpha(\omega) = \frac{q^2}{M} \frac{1}{\omega_0^2 - \omega^2} \tag{B.3}$$

where q is the electron charge, M is the molecular mass, and ω_0 is the natural electronic frequency. We see from Eq. (B.1) that ϵ depends not only on the frequency, but also on the density of the gas. What is encouraging about this approach is that it favors blue light (as reported in the experiment [3]) over other frequencies (following from Eq. (B.3)). The light could be eventually liberated by the expansion of the bubble.

The idea itself is simple, but the calculation of ϵ_1, is not. The initial expression for the dielectric constant could be questioned, because the necessary compression ratio[1] is larger than 10 (in order for the dielectric constant

[1]Defined as equilibrium over minimum radius.

of the gas to be larger than for the liquid), and at this ratio the densities involved are already those of liquidified or even solidified gases. The index of refraction of these substances is smaller than that of water. On the other hand, effects like the production of free electrons, or the eventual alignment of the gaseous molecules can produce a large change in dielectric constant.

The other physical situation which could leads to the trapping of light in the bubble would be the existence of a spatial gradient of the thermodynamic quantities of the gas in the bubble (temperature, pressure, density) and a corresponding gradient in the dielectric constant, So, let us explore what the space dependence of the dielectric constant should be to produce light trapping inside the bubble (assuming a spatial nonuniformity of the gas in the bubble). For this purpose we employ geometrical optics. Using the Eikonal equation [87]

$$\nabla n = \frac{d}{ds}\left(n\frac{d\vec{r}}{ds}\right) \tag{B.4}$$

(following from the Fermat principle), we get following expression

$$\frac{dr}{d\theta} = \pm r\sqrt{\left(\frac{nr}{A}\right)^2 - 1} \tag{B.5}$$

where A is a constant, $n = n(r)$ is the index of refraction of the gas and r, θ are spherical polar coordinates. We see that, in order to have, for example, circular orbits ($dr/d\theta = 0$), n should be proportional to r^{-1}. That gives a r^{-2} dependence of dielectric constant.

It is hard to see why a spatial profile of this sort would exist in the bubble. Since the new experimental results [29, 34, 35] imply that the production of shock waves might be expected in the bubble, we tried to analyze this idea and how it can lead to the emission of short pulses of light. The evolution of the shock wave in bubble is presented in Fig. B.2. Before shock production,

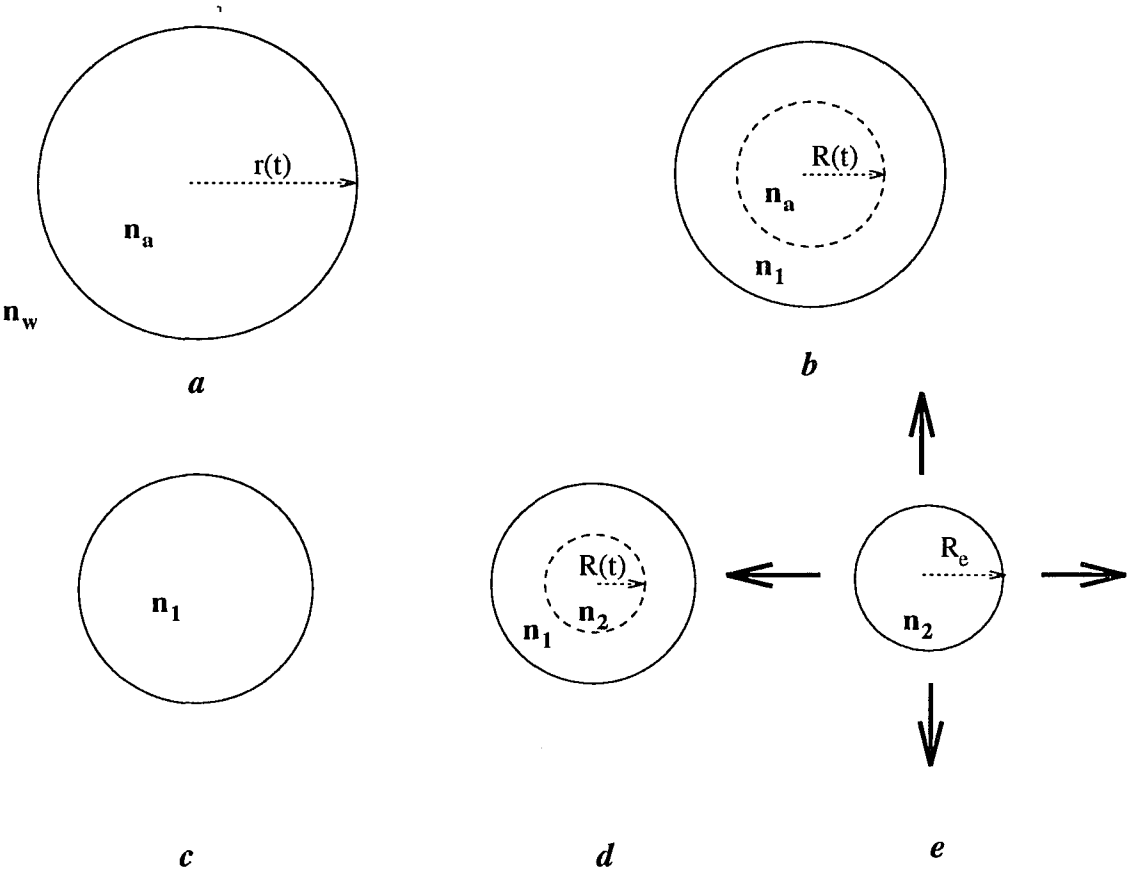

Figure B.2: *Different stages of bubble collapse and shock propagation. The bubble collapse just before it reaches the minimum radius is shown. A converging shock $R(t)$ is shown in part b. In part c, the shock converged completely. In part d, the rebounding shock wave propagates outwards. In part e the shock wave reaches the bubble wall, and at that point the trapped radiation may be emitted.*

the index of refraction in the bubble n_a is smaller than that of water n_w, so no trapping is possible. As the shock propagates in the bubble the density of air behind the shock front will be greater than the density in front of the shock front. Correspondingly, we will expect that $n_a < n_1 < n_w$, so again no optical trapping is possible. After the shock front collapse to radius zero, it starts expanding outward, and it is known (self-similar approach, cf. [75]) that the density behind the shock front is considerably larger than the density in front of the shock front (by about a factor of 23). We therefore now have the inequality $n_1 < n_2$. Light trapping is possible behind the expanding shock front. This situation lasts until we arrive at case "e" in Fig. B.2, where the expanding shock collides with the bubble surface. The trapped light is now free to escape into the surrounding liquid and will come out as a sudden burst of light.

The problem with this approach is that the shock radius at the point where the temperature is high is very small - smaller or of comparable size to the wavelength of the radiation which is eventually trapped, so the use of the geometric optics equations is very questionable. In addition there is the penetration of the electrical field into the region in front of the shock. The phenomenon of frustrated total internal reflection would occur and this would spread out the duration of the light pulse.

Conclusion

The mechanisms which we considered in this section do not give a precise answer about the duration of the SL pulse or about the shape of the spectrum of the emitted radiation. Still, many effects were not taken into account in our simplified approach. Let us mention some of them:

- The size of the region of interest is comparable to the wavelength of the emitted radiation. Correspondingly, physical optics should be used rather than geometrical optics;

- Physical and chemical processes in the gas in the bubble are not clearly understood [88]-[92]. Some of them could strongly influence the results for the dielectric constant of the gas in the bubble;

- There is the question if it is correct to consider the liquid layer around the bubble as structurless; some of our preliminary results show that if high pressures and temperatures are developed, there can be some ice-like structure in this layer [92, 93];

- There is a possibility (we will not go into the details in this work) that some charge could be expected to be transferred to the bubble from the liquid. The charging of the bubble would involve large changes in the dielectric constant and even calls to question the correctness of the macroscopic dielectric theory that we are using here (cf. [94]-[96]).

Appendix C

"Electrical" Models

Introduction

We have already seen that the temperature in a bubble can reach very high values even for the case of an adiabatic compression. Assuming that the temperature in the liquid just next to the bubble is high as well, we would have a high percentage of dissociated water molecules (dissociation energy is $0.5 - 0.6\ eV$ [97]). The natural question to ask is can we expect that this, or some electrical phenomena, play an important role in producing the light signal. Actually, it has been shown in the literature [18, 98] that the production of a surface charge on the bubble-liquid boundary will occur even for a stationary bubble. This is a result of the Poisson - Boltzmann equation.

We consider here a few possible mechanisms for the formation of free charge in (or on) the bubble and explore the possibility that these effects lead to the sonoluminescent radiation. In this Appendix we show that some of the electrical effects might be expected to take place, but it seems that they do not give an explanation for sonoluminescence.

C.1 Electrification of the Liquid

Here we would like to calculate the electric field in the liquid just outside the bubble and also the amount of charge in the bubble. We do not expect H^+ ions to deposit themselves in the bubble; the energy needed for that is about $16\,eV$ [93], but the energy for evaporation of OH^- is just about $4\,eV$. The other mechanism for the transfer of negative charges to the bubble is by collisions of positive gaseous (or water vapor) ions M^+ with the bubble wall, by a process like $M^+ + H_2O \leftrightarrow M + H_2O^+$.

The electric current of the positive charges in the liquid consists of conduction, diffusion and convection term and is given by

$$\vec{J}_+ = \frac{\sigma_+}{e}\vec{E} - D_+\nabla n_+ + n_+\vec{u} \tag{C.1}$$

with a similar expression for the negative charges. Here $\vec{u}$ is the velocity of a particle in the liquid, the conductivity is given by $\sigma_+ = n_+e^2\tau_+/M_+$ and the diffusion constant can be expressed by the Einstein relation $D_+ = \tau_+ k_B T/M_+$, where n_+ is the concentration of + charges, τ_+ is their mean collision time and e, M_+ are the charge and the mass of the proton, respectively. Here the Soret effect was neglected.

These currents (J_+, J_-) satisfy the continuity equations and the electric field follows from Gauss law. The charge concentrations n_+ and n_- result from the process $H_2O \leftrightarrow H^+ + OH^-$ with production rates k', k for the backward and forward directions. These constants were calculated from the vibrational frequencies of the water molecule [93]. The fact that some of the OH^- charges evaporate into the bubble should be included as well. The probability of evaporation of OH^- radicals strongly depends on the temperature and solvation energy. The solvation energy can be found using the Born

solvation scheme to be $U_s = -e^2/2a \cdot (1 - 1/\epsilon)$, where a is the size of the solvation shell. This energy is small if ϵ is taken to be the dielectric constant of the gas, following from the Clausius-Mossotti equation. This is correct even at high densities which we expect in the bubble. In the course of the research it was found, interestingly enough, that this energy is much larger if OH^- is solvated at the wall (within a solvation hemisphere). The value of the solvation energy is close to the value for solvation in water (about $0.5\,eV$).

The temperature in the liquid next to the wall is to be found[1] from the heat conservation equation

$$\nabla \cdot \vec{J}_q + \frac{\partial q}{\partial t} = 0 \tag{C.2}$$

with

$$\vec{J}_q = -K\nabla T + q\vec{u} \tag{C.3}$$

and

$$\nabla q = C\ \nabla t \tag{C.4}$$

where we assume that K (thermal conductivity) and C (heat capacity) are temperature independent (Peltier effect was neglected). This equation was solved using the POST-package [72]. The result for the temperature gradient in the liquid, just next to the bubble wall, is of the order of $10^7\,K/cm$. The electric field resulting from this gradient (thermopower of water) is of the order of $10^4\ V/cm$, which, as we will see later, is not a very important contribution.

[1]This is true if we assume that the temperature just next to the bubble wall in the liquid is the same as in the bubble. The constant evaporation of water vapor from the liquid surface probably lowers this temperature.

Finally, with the solved temperature and bubble equations, we are left with the following system of equations. The continuity equation for positive charges is

$$\frac{\partial n_+}{\partial t} - D_+ \nabla^2 n_+ + \vec{u}\,\nabla n_+ = -\beta e D_+ \left[\vec{E}\,\nabla n_+ + \frac{4\pi e}{\epsilon}(n_+ - n_-)\,n_+\right] \quad \text{(C.5)}$$

The equation for the negative charges has the same form

$$\frac{\partial n_-}{\partial t} - D_- \nabla^2 n_- + \vec{u}\,\nabla n_- = \beta e D_- \left[\vec{E}\,\nabla n_- + \frac{4\pi e}{\epsilon}(n_+ - n_-)\,n_-\right] \quad \text{(C.6)}$$

The equation for electric field $\vec{E}$ follows from Gauss's law

$$\nabla \cdot \vec{E} = \frac{4\pi e}{\epsilon}(n_+ - n_-) \quad \text{(C.7)}$$

In order to specify the boundary conditions, we have to estimate the charge transfer between the bubble and the liquid. If we label the fraction of the collisions of the positive ions with the bubble wall, leading to ionization, as σ, the effective transfer of charge due to collisions is given by $\Gamma = \sigma\, n_{M^+} < v > /4$. Here $< v >$ is the average ionic thermal velocity. Finally, the current density satisfies

$$\hat{r} \cdot \vec{J}_+(R_-(t), t) = \Gamma(t) \quad \text{(C.8)}$$

and

$$\hat{r} \cdot \vec{J}_-(R_-(t), t) = 0 \quad \text{(C.9)}$$

The adsorption of electrons from the bubble is neglected. The boundary condition for the electric field is given by

$$\left[\hat{r} \cdot \vec{E}\,\right]_{r=R_+(t)} = -\frac{4\pi e}{\epsilon} N_- \quad \text{(C.10)}$$

following from the continuity equation for the radial component of the electric field. Here N_- is the number of negative charges in the bubble. The

additional boundary conditions are that the ion density should return to its equilibrium value ($pH = 7$) far from the bubble and the electric field should approach zero there.

The system of the equations, Eqs. (C.5-C.7) is fairly complicated, especially taking into account the fact that the boundary conditions are time dependent because of the motion of the bubble wall. Anyway, by estimating the relative size of the different terms in these equations, we conclude that the diffusion term is probably the most important. So, by neglecting convection and conduction terms in Eq. (C.5), and also by eliminating the nonlinear terms on the right hand side of this equation, we get the decoupled equation for the concentration of positive charges in the liquid, just next to the bubble wall. After change of variables $\xi \equiv r^3 - R(t)^3$, $\tau \equiv t$, this equation becomes

$$\frac{\partial n_+}{\partial \tau} = 9D_+ \frac{\partial}{\partial \xi}\left(\xi^3 - R(\tau)^3\right)^{4/3} \frac{\partial n_+}{\partial \xi} \tag{C.11}$$

with the boundary conditions

$$\left[-3D_+ R(\tau)^2 \frac{\partial n_+}{\partial \xi}\right]_{\xi=0} = \Gamma(\tau) \tag{C.12}$$

$$[n_+]_{\xi\to\infty} \longrightarrow 0 \tag{C.13}$$

A further change of variables

$$s(\tau) \equiv 9D_+ \int_0^\tau R(\tau')^4 \, d\tau' \tag{C.14}$$

allows expressing the solution in the following form

$$n_+(\xi, s) = \frac{3R_{min}^2 \Gamma_0}{\sqrt{\pi}} \sum_{n=0}^{\infty} \frac{\Theta(s - ns_a)}{\sqrt{s - ns_a}} \exp\left(-\frac{\xi^2}{4\,|s - ns_a|}\right) \tag{C.15}$$

where $s_a = s(\tau = \tau_a)$ and τ_a is the acoustic period. Here R_{min} is the minimum bubble radius and the ionization rate $\Gamma(\tau)$ is modeled as $\Gamma(\tau) = \Gamma_0 \sum_{n=0}^{\infty} \delta(\tau - n\tau_a)$.

From the result for the concentration of the positive charges, Eq. (C.15), we are able to estimate the electric field in the liquid and the total electromagnetic energy contained in the system consisting of the negatively charged bubble and the liquid layer around the bubble. The rough estimate gives that this field might be strong enough to lead to the emission of the high energy photons observed in SL experiments. However, the short duration of the pulse does not follow from this model. The other possibility would be that the emission of radiation happens as a result of a recombination process during the expansion part of bubble cycle (immediately after the bubble reaches its minimum radius). But, it is observed experimentally that the SL pulse is emitted shortly *before* the bubble reaches its minimum radius, in contradiction to this idea.

C.2 Polarization Model

One of the assumptions of the previous model was that there is a considerable number of free electrons in the bubble close to its final stages of collapse. This result follows from the Saha equation, which predicts that there are $10^5 - 10^6$ free electrons in the bubble[2]. Some flow of negative charge from the surrounding liquid might be expected as well. Let us analyze the interaction of the electrons in the bubble with each other and with the liquid. The ion distribution, being spherically symmetric, sets up a constant potential inside the bubble. Suppose for the moment that all the electrons are on the surface of a sphere of radius r' and allow r' to vary. We start with the usual power series for a potential which is finite (except at point charges) and goes to

[2]This estimate is strongly dependent on thermodynamic parameters in the bubble, especially temperature. The high temperatures which develop if a shock wave is produced would lead to an even larger number of electrons.

zero for infinite r. After including the boundary conditions of continuity for the potential and the radial component of the $\vec{D}$ field at $r = R(t)$, we get following expression for the total electrostatic energy of the system

$$U = \frac{q^2}{2r'} \sum_{ij, i \neq j} \frac{1}{|\hat{r}_i - \hat{r}_j|} - \frac{q^2}{2R} \sum_l \frac{(\epsilon - 1)(l+1)}{l + \epsilon(l+1)} \left(\frac{r'}{R}\right)^{2l} \sum_{ij, i \neq j} P_l(\hat{r}_i \cdot \hat{r}_j) \quad \text{(C.16)}$$

for $r' < R$. The analogous solution for $r' > R$ is

$$U = \frac{q^2}{2}(1-\epsilon) \sum_l \frac{l}{l + \epsilon(l+1)} \frac{R^{2l+1}}{(r')^{2l+2}} \sum_{ij, i \neq j} P_l(\hat{r}_i \cdot \hat{r}_j) + \frac{q^2}{2\epsilon r'} \sum_{ij, i \neq j} \frac{1}{|\vec{r}_i - \vec{r}_j|} \quad \text{(C.17)}$$

The dielectric constant for the surrounding liquid is ϵ, where $\epsilon >> 1$. The terms with $i = j$ give rise to the image interaction with the wall of the cavity. The other terms describe the direct and indirect Coulomb interaction of the charges with each other. These formulae were programmed and the output is in agreement with what we get from a continuum limit (which is more than justified if we have $10^5 - 10^6$ electrons in the bubble). The result from the continuum approximation is

$$U = \begin{cases} \frac{q^2 N^2}{2(r'-R)} - \frac{q^2 N}{2R} \frac{1}{1-(\frac{r'}{R})^2} + O(\frac{1}{\epsilon}) & if\ r' < R \\ \frac{q^2 N^2}{2\epsilon r'} \left(1 - \frac{1}{\sqrt{N}}\right) + \frac{q^2 N}{2\epsilon R} \left[\frac{R^2}{r'-R^2} + \ln\left(1 - \frac{R^2}{r'^2}\right)\right] + O(\frac{1}{\epsilon^2}) & if\ r' > R \end{cases} \quad \text{(C.18)}$$

where only leading terms in $1/\epsilon$ are kept. Examination of these formulae shows that the total electrostatic energy is positive for small r', becomes negative and approaches $-\infty$ as r' approaches R from below, falls from $+\infty$ above R and eventually falls to zero. Of course, the presence of the positive ions, which were neglected here, would cause the energy to get smaller as r' gets larger.

We conclude that for negative energy the system is likely to find itself with the electrons inside the bubble near $r' = R$. For positive energy, however,

the system is unstable and the r' would like to expand to infinity. The image potential poses a barrier to this expansion and a tunneling event or a thermal excursion must happen in order for this to occur.

For the moment, we approximate our potential energy for $r' > R$ to be infinite, so it does not allow for tunneling. Furthermore, we assume a two-dimensional electron gas trapped on the wall and use the variational method to get the energy of the electrons. Without going into details, we get what is expected: for a large number of electrons, the Fermi energy is positive. This critical number is of order 10^6. To the Fermi energy we have to add the Coulomb energy of repulsion of the electrons. This energy again depends on the number of electrons in the layer.

The conclusion is that for a high number of electrons, at the final stages of collapse, the total energy of the electrons can be positive and fairly large. These electrons are trapped inside the bubble next to the bubble wall. On the other hand, as a results of section C.1 we know that there is a certain concentration of positive ions in the liquid next to the bubble wall. Here we explore the possibility that this configuration could produce radiation.

Since the energy of the electrons becomes elevated as the bubble contracts (Coulomb repulsion), one would expect that the bubble discharges at some point. The question is why should this discharging occur on so short time scale? A hypothetical answer to this question could be that discharging at one point of the bubble produces a big change of the electric field at some other points on the bubble wall. If this were true then we can expect that one of two things happen: either this change of the electric field is large enough to considerably increase the probability for tunnelling, or this additional field is strong enough to produce an electrical breakdown.

In order to get some qualitative results, we formulated a model in which

we assumed a polarization layer formed on the bubble. We assumed that polarization is given by

$$\vec{P}(\hat{r},\omega) = \hat{r}P(\hat{r},\omega)\,\delta(r-a) \tag{C.19}$$

As a result of this polarization, the power radiated is

$$P = 2\pi ck^2R^2 \sum_{lm} l(l+1)|P_{lm}(\omega)|^2 j_l^2(kR) \tag{C.20}$$

where P_{lm} is lm coefficient in the expansion of the polarization in a series of spherical harmonics and $R(t)$ is the radius of the bubble. We see, as expected, that no radiation is emitted for the $l = 0$ spherically symmetric mode.

By solving the field equation for this model, we get a simple and interesting result:

$$\hat{r}\cdot\vec{E}(\vec{r},t) = \frac{1}{a}\,\mathcal{L}^2 \int \frac{P\left(\hat{r}', t-\frac{a}{c}|\hat{r}-\hat{r}'|\right)}{|\hat{r}-\hat{r}'|}\,d\hat{r}' \tag{C.21}$$

where $\vec{\mathcal{L}} = -\imath\,\hat{r}\times\nabla$ is proportional to the angular part of Laplacian.

So, the electric field at a time t depends on the polarization at previous times t'. Efforts have been made to solve this equation self-consistently (the polarization itself depends on the electric field), but at this moment we have to use a more intuitive argument which tells us that we will have large electric field at some points. First we establish an equivalence between our result for the electric field of a polarized layer and the result for the dipole field given, for example, in [79]

$$\vec{E}(\omega) = k^2[\hat{n}\times\vec{\mu}(\omega)]\times\hat{n}\frac{e^{\imath k\vec{r}}}{r} + [3\hat{n}\hat{n}\cdot\vec{\mu}(\omega)-\vec{\mu}(\omega)]\left[\frac{1}{r^3}-\frac{\imath k}{r^2}\right]e^{\imath k\vec{r}} \tag{C.22}$$

in the continuum approximation. In "near field limit", we see that the switching of one of the dipoles will produce a weaker field for others, but this is

not true in general; at some points the field will be larger. We checked this point by doing explicit calculations for a system of two dipoles, four dipoles at the vertices of a tetrahedron and for eight dipoles at the corners of a cube. The conclusion was that if one dipole decays fast enough, it can produce a switching of other dipoles (the condition is that $\beta > Ka/c$, where β is a decay constant for the exponential decay of a dipole and K is a number of order one). Our next step is to assume that, first, this additional electric field is large enough to produce tunnelling or breakdown and, second, that the decay happens immediately (tunneling is a very fast process).

We developed a few models for "decay" of the polarization layer which models our physical system. The result is that neither of these models was able to reproduce the observed SL pulse, especially the observed spectrum, which is black-body like. We conclude that there is not enough evidence that the sudden decay of the polarization layer is responsible for the emission of radiation which is observed in the form of sonoluminescence. (It is worth comparing the approach here (based on classical electrodynamics) with the quantum approach developed in Appendix A.)

Appendix D

Plasma Radiation

In Appendix E.3 we will see that multiple ionization happens at temperatures of a few tens of thousands of degrees, leading to a large number of free electrons. These thermally energized electrons randomly scatter off the ions, eventually leading to radiation.

In order to explore this possibility in a more precise manner, we assume that our system consists of N fluctuating dipoles

$$\vec{\mu}_i(t) = -e\left(\vec{r}_i(t) - \vec{R}_i\right) \tag{D.1}$$

where $\vec{r}_i$ gives the position of i^{th} electron, and $\vec{R}_i$ is the position of i^{th} ion. The thermal motion of electrons is much faster than that of ions, which are assumed to be stationary. Correspondingly, the time rate of change of a dipole is given by

$$\dot{\vec{\mu}}_i = -e\vec{v}_i(t) \tag{D.2}$$

where $\vec{v}_i(t)$ is the velocity of i^{th} electron. The power radiated by such a dipole can be calculated using the Larmour formula

$$P_i(t) = \frac{2}{3}\frac{\left|\ddot{\vec{\mu}}_i\right|^2}{c^3} \tag{D.3}$$

Assuming no interaction between the electrons we postulate an exponential model for the velocity autocorrelation

$$< \vec{v}_i(t) \cdot \vec{v}_j(t') >=< v^2 > \delta_{ij} \exp\left[-\frac{|t-t'|}{\tau}\right] \tag{D.4}$$

Here the average is over an ensemble and τ is the autocorrelation time, assumed to be identical to the inverse of the collision rate of the electrons with the ions.

In calculating the radiated energy, it is useful to realize that there are two time scales in the problem: A fast scale, characterized by the electron motion and a slow scale, characterized by the ion motion or the time the bubble spends close to its minimum radius. So, if we calculate the energy radiated during one "frame" of slow motion, we can assume that the ions are stationary, and that the conditions (i.e. temperature) in the bubble do not change significantly. Correspondingly, the energy radiated during the time characterized by the slow time scale t_s is given by

$$W_i = \int_0^{t_s} P_i(t)\, dt = \frac{2}{3c^3} \int_0^{t_s} \left|\ddot{\vec{\mu}}_i\right|^2 \tag{D.5}$$

and Eq. (D.2) can be employed. The calculations were done in frequency space and the result for the spectral power radiated is

$$P_i(\omega) = \frac{4e^2}{3\pi c^3} \frac{< v_i^2 >}{\tau} \frac{\omega^2}{\omega^2 + \frac{1}{\tau^2}} \tag{D.6}$$

We get the average electron velocity from the electron thermal energy (assuming thermal equilibrium). Furthermore, the result for the spectral power radiated should be corrected because of the presence of the rest of the plasma. This correction factor is explained in more detail in Appendix E.5. The final result for the spectral power radiated from N electrons is

$$P(\omega) = \frac{4e^2}{\pi mc^3} \frac{N k_B T}{\tau} \frac{\omega^2}{\omega^2 + \frac{1}{\tau^2}} \left|\frac{3}{2 + \epsilon(\omega)}\right|^2 \tag{D.7}$$

where $\epsilon(\omega)$ is the frequency dependent plasma dielectric constant given by Eq. (3.62). The total number of electrons N was calculated using the Saha equation. Finally, the electron collision time was assumed to follow from $1/\tau = n_e v \sigma_c$, where n_e is the electron density, and σ_c is the Coulomb cross section. The typical result for the collision time is $\tau \sim 10^{-14} s$.

Since our final goal is to compare the results with experiment, we want to check what radiation spectrum results from this approach. By fitting the result of our approach to the experimental spectrum (viz. Fig. 4.2), and using τ as a fitting parameter, we get a fairly good correspondence with experiment for a value of the electron collision time of $\tau = 1.3 \times 10^{-16}\, s$.

One cannot understand why the collision time should be so short. We tried to improve our model, by including more sophisticated effects, like screening, which lowers the ionization energy. Still, we are not able to reproduce so short a collision time. Also, the result for the duration of the SL pulse turned out to be much longer than experimentally observed ($50\, ps$)[1]. These results indicated that the mechanism for SL radiation should be given on the basis of some other model for the hot gas in the SL bubble.

[1]This results from our model because it does not provide a mechanism for the self-consistent calculation of the gas temperature. In chapter 3 we see that the radiated energy is not negligible compared to the thermal energy and that it has to be included in the calculation of the gas temperature.

Appendix E

Mathematical Appendices

E.1 Heat Conduction between the Bubble and the Liquid

We want to estimate the importance of heat conduction between the gas in the bubble and the liquid during the final stages of bubble collapse. What is presented here is an estimate of the upper limit for the amount of the energy which can be transferred.

The heat transferred per time is given by

$$\dot{Q} = N_c C_v \Delta T \frac{1}{N_a} \tag{E.1}$$

where N_c is number of collisions of gas molecules with the bubble wall, C_v is the molar heat capacity, ΔT is the temperature difference between the gas and liquid and N_a is Avogadro number. Expression, Eq. (E.1), overestimates the heat transfer since it assumes that all available energy is transferred in the collisions. The number of collisions follows from an estimate of the total momentum transferred to the wall during the time Δt due to collisions $\Delta P/\Delta t \sim 2m\overline{v}/3\, N_c$ where m is molecular mass and $\overline{v}$ the average thermal velocity of the molecules. By equating the total momentum transferred in the

time interval Δt with the average force, which in turn equals to the pressure exerted on the bubble wall multiplied by the area, we get a final estimate for the heat transferred per unit time

$$\dot{Q} \sim \frac{15}{4}\left(\frac{k_B N_a}{3MT}\right)^{1/2} AP\Delta T \tag{E.2}$$

Here P is the pressure in the bubble, A is the area of the bubble, M is the molar mass of the gas in the bubble and k_B is Boltzmann's constant. Typical values of the variables entering Eq. (E.2) for the bubble close to the minimum radius are[1] $P \sim 10^{11}\ dyn/cm^2$, $A \sim 4.5 \cdot 10^{-8}\ cm^2$ and $\Delta T \sim 10^4\ K$. This gives $\dot{Q}\Delta t \sim 7 \cdot 10^8 \Delta t\ erg/s$. This value should be compared with a typical value of the total energy in the bubble E_T given by Eq. (3.22) multiplied by the bubble mass. For $\rho \sim 0.5\ g/cm^3$ and a bubble mass of approximately $5.5 \cdot 10^{-12}\ g$ we get $E_T \sim 1\ erg$. For the time interval $\Delta t \sim 100\ ps$, the upper limit on heat transferred between the bubble and liquid is about $0.07\,erg$. We conclude that at most a few percent of the energy of the gas could be expected to be transferred to the liquid, so the effect of heat transfer between the bubble and the liquid is not important, at least not for the short time which the bubble spends close to its minimum radius.

E.2 Heat Conduction in the Gas

One of the assumptions that we made in our research on shock propagation is that heat conduction in the gas can be neglected. Let us check what the importance of this effect is for the time scale at which shock wave(s) actually exist - about $50 - 100\ ps$. The flow of heat is given by the heat conduction

[1] We assume that the liquid is at room temperature. This assumption again overestimates the transfer of heat since the liquid next to the bubble wall is heated as well.

equation

$$\frac{\partial T}{\partial t} = \chi \nabla^2 T \tag{E.3}$$

where the coefficient of thermal diffusion is given by $\chi = l_a \overline{v}/3$. Here l_a is the molecular mean free path and $\overline{v}$ is the average thermal speed of the molecules. For standard values of temperature T and number density n_s the value of χ is about 0.2 cm^2/s [75]. Noting that l_a is inversely proportional to the density of gas n, and $\overline{v}$ is proportional to $T^{1/2}$, for the case where the shock is close to complete collapse ($n \sim 500\ n_s$ and $T \sim 10^5\ K$), we get a value for $\chi \sim 6 \cdot 10^{-3}\ cm^2/s$. From Eq. (E.3) we see that the time Δt required to equalize the temperature across distance a Δx is approximately given by

$$\Delta t \sim \frac{(\Delta x)^2}{\chi} \tag{E.4}$$

So, for a typical distance of $10^{-5}\ cm$, the time required is a few ns. This is very long compared to the typical lifetime of the shock waves, so we conclude that the effect of heat conduction in the gas is not important in our problem.

E.3 Saha Equation for Multiple Ionization

The Saha equation, which allows for multiple ionization, is given by [75]

$$\frac{n_{m+1}\ n_e}{n_m} = 2\frac{u_{m+1}}{u_m} A T^{3/2} \exp\left(\frac{I_{m+1}}{k_B T}\right) \tag{E.5}$$

where constant A is defined on page 73, n_e is the density of electrons, n_m is the density of m-ions ($m = 0, 1, 2...$), I_m is the ionization potential for removing the m^{th} electron, u_i are electron partition functions, k_B is Boltzmann constant and T is the temperature. For the conditions where multiple ionization is important (as in our problem), the system of algebraic nonlinear equations, Eq. (E.5), should be solved for each pair of temperature and

density values. This would increase the computational time considerably, so we chose to use a "continuous" method explained in [75]. The essence of the method is as follows. First we assume that the ion number density n_m and the ionization potentials I_m could be considered to be continuous functions of ionic charge m, obtained by connecting the discrete values of n_m and I_{m+1} by continuous curves. Next, we replace the finite differences entering Eq. (E.5) by differentials

$$n(m+1) = n(m) + \frac{dn}{dm}, \qquad \Delta m = 1 \tag{E.6}$$

The ratio of the ion electronic partition functions u_{m+1}/u_m entering Eq. (E.5) varies in an irregular manner when the charge m changes its value for a given element, and also varies for different elements (statistical weights of electronic states are entering here), but it is always of the order of unity. So, by assuming this ratio is equal to unity, we can replace the system of Saha equations by the differential equation

$$\left(1 + \frac{d\ln n}{dm}\right) n_e = AT^{3/2} \exp\left[-\frac{I(m+1)}{k_B T}\right] \tag{E.7}$$

Next we can write the particle and charge conservation conditions in the form

$$\int n(m)dm = n, \qquad \int mn(m)dm = n_e \tag{E.8}$$

Let us note that the distribution function $n(m)$ has a narrow peak about some value m_{max}. We approximate the average number of free electrons per original atom by

$$\overline{m} = \frac{\int mn(m)dm}{\int n(m)dm} = \frac{n_e}{n} \tag{E.9}$$

and $\overline{m}$ is exactly equal to m_{max}. We denote by $\overline{I}$ the ionization potential of ions with average charge $\overline{m}$ and use the fact that $dn/dm = 0$ at the peak.

With these conventions, Eq. (E.7) can be written in the simple form

$$\overline{m} = \frac{AT^{3/2}}{n} \exp\left(-\frac{\overline{I}}{k_B T}\right) \tag{E.10}$$

The comparison of the results of the approximate and exact calculations shows that the best agreement for a variety of gases under different conditions is obtained by assuming that $\overline{I} = \overline{I}(\overline{m}+1/2)$ in the last equation. That finally allows to rewrite this equation in the form

$$I(\overline{m} + \frac{1}{2}) = k_B T \ln \frac{AT^{3/2}}{\overline{m}n} \tag{E.11}$$

and this is the result which we used in 3.5.3. This equation can be easily solved by the iteration method.

E.4 Calculation of the Absorption Coefficient

Electronic transitions which are connected with emission or absorption of light can be divided into three types:

- Free-free transitions (bremsstrahlung emission and absorption);
- Bound-free transitions (photoelectric absorption);
- Bound-bound (discrete) transitions.

From an energy point of view, continuous transitions (free-free or bound-free) are of primary interest. At the temperatures which are of interest to us (5×10^4 K or more) it can be assumed that air molecules are mostly dissociated and atoms are multiply ionized. Thus, in what follows we are going to limit our treatment to these conditions and neglect additional complications

(such as molecular transitions). The attenuation coefficient κ_ν, in principle, consists of an absorption part $\kappa_{\nu a}$ and a scattering part $\kappa_{\nu s}$. Scattering (mainly photon scattering from electrons, known as Thomson scattering) is usually important only in a very rarefied gas. The reason for this is that the cross section for scattering is much smaller than the cross section for absorption. Only at low densities and high temperatures does scattering become important. Under these conditions full ionization takes place, so the bound-free transitions are absent and the free-free transitions are small. The latter are proportional to the square of the gas density. The absorption coefficient $\kappa_{\nu a}$ (we are going to drop subscript a in what follows) should be corrected for induced emission and leads to the following expression for the effective absorption coefficient:

$$\kappa'_\nu = \kappa_\nu (1 - e^{-\frac{h\nu}{k_B T}}) \tag{E.12}$$

This is what appears in Eqs. (3.59) and (3.60). The calculation of the absorption coefficient itself is extremely involved and requires a detailed knowledge of the structure of gas. The best one can hope for is to get good approximate results for this quantity. The result, which includes bound-free and free-free transitions in the hydrogen-like approximation for atoms (Kramers-Unsöld formula) used for the conditions of multiple ionization, is [75]

$$\kappa_\nu = \sum_m \kappa_{\nu m} \tag{E.13}$$

$$\kappa_{\nu m} = \frac{a N_m (m+1)^2}{T^2} e^{-x_{1m}} F_m(x) \tag{E.14}$$

where

$$a = \frac{16\pi^2}{3\sqrt{3}} \frac{e^6}{hck_B^2}, \qquad x = \frac{h\nu}{k_B T}, \qquad x_{1m} = \frac{I_{m+1}}{k_B T} \tag{E.15}$$

and the frequency dependence of function $F_m(x)$ is given by:

$$F_m(x) = \begin{cases} e^x/x^3 & \text{if } x < x_{1m} \\ 2x_{1m}e^{x_{1m}}/x^3 & \text{if } x > x_{1m} \end{cases} \quad \text{(E.16)}$$

where N_m is the number of ions per unit volume with charge m and I_m is the ionization potential for removing $m-1$ electrons. The m sum can be omitted by going to the continuum limit, as discussed before. The contribution of bound-free (photoelectric effect) and free-free (bremsstrahlung absorption) transitions to the total absorption coefficient are in the ratio $(e^x-1)/1$. Thus for low energy photons ($x << 1$), the main contribution comes from free-free transitions, and for the high energy photons ($x >> 1$), the main contribution comes from bound-free transitions. In our problem, in which there is a wide range of frequencies and temperatures, both kinds of transitions are going to be important in the absorption process.

E.5 Derivation of Bremsstrahlung Results

The result for the radiation cross section for bremsstrahlung radiation emitted during a "collision" of an electron and a singly ionized ion in the nonrelativistic approximation is [79] (without corrections for the rest of plasma)

$$\frac{d\chi}{d\omega} = \frac{16}{3}\frac{e^2}{c}\left(\frac{e^2}{m_e c^2}\right)\left(\frac{c}{v}\right)^2 \ln\left[\lambda' \frac{(\sqrt{E}+\sqrt{E-\hbar\omega})^2}{\hbar\omega}\right]\Theta(E-\hbar\omega) \quad \text{(E.17)}$$

In the Born approximation the factor λ' is equal to one. In Eq. (E.17) E, v and m_e are electron energy, velocity and mass, respectively. The Θ function enters because the electron energy has to be larger than the energy of the emitted photon. The product $v\ d\chi/d\omega$ was thermally averaged over the electron velocity assuming a Maxwell distribution. The result is

$$< v\ \frac{d\chi}{d\omega} >= \frac{64\pi}{3}\frac{e^2}{c}\left(\frac{e^2}{m_e c^2}\right)\left(\frac{\beta m_e}{2\pi}\right)^{3/2} I(\beta,\omega) \quad \text{(E.18)}$$

where $\beta = 1/(k_B T)$ and the integral I is given by

$$I(\beta,\omega) = \int_{\hbar\omega}^{\infty} e^{-\beta E} \ln\left[\frac{\left(\sqrt{E}+\sqrt{E-\hbar\omega}\right)^2}{\hbar\omega}\right] dE \qquad \text{(E.19)}$$

By partial integration, this integral can be written in the form

$$I(\beta,\omega) = \frac{1}{\beta}\int_1^{\infty} \frac{e^{-\beta\omega\hbar x}}{\sqrt{x(x-1)}}\, dx \qquad \text{(E.20)}$$

where $x \equiv E/(\hbar\omega)$.

The next step is to include corrections to individual scattering events which lead to radiation due to the presence of the rest of plasma. As discussed on page 80, a correction term $|3/[2+\epsilon(\omega)]|^2$ should be included in the integrand of the $I(\beta,\omega)$. In order to calculate the total power emitted per volume, the thermal average given by Eq. (E.18) should be integrated over all frequencies

$$\int < v\frac{d\chi}{d\omega} > \, d\omega = \frac{64\pi}{3}\frac{e^2 c}{m_e}\left(\frac{e^2}{m_e c^2}\right)^2\left(\frac{\beta m_e}{2\pi}\right)^{3/2}\frac{\omega_p}{\beta}F(\beta\hbar\omega_p,\omega_p\tau) \qquad \text{(E.21)}$$

with

$$F(\beta\hbar\omega_p,\omega_p\tau) = \frac{1}{\omega_p}\int_0^{\infty} d\omega \int_1^{\infty} dx \frac{e^{-\beta\hbar\omega x}}{\sqrt{x(x-1)}}\left|\frac{3}{2+\epsilon(\omega)}\right|^2 \qquad \text{(E.22)}$$

Expression, Eq. (E.21), after being multiplied by the density of electrons and ions gives Eq. (3.63).

Bibliography

[1] L.A. Chambers, J. Chem. Phys. **5**, 290, 1937.

[2] D.F. Gaitan, L.A. Crum,C.C. Church,R.A. Roy, J. Acoust. Soc. Am., **91**, 3166, 1992.

[3] B.P. Barber, S.J. Putterman, Nature, **352**, 318, 1991.

[4] K.S. Suslick, Science **247**, 1439, 1990.

[5] A.J. Walton , G.T. Reynolds, Adv. in Phys. **33**, 595, 1984.

[6] "Handbook for Chemistry and Physics", M.I.T. Press, Cambridge, 72^{nd} edition, 1991-1992.

[7] E.N. Harvey, J. Am. Chem. Soc., **61**, 2392, 1939.

[8] E.N. Harvey at al., J. Cell. Comp. Physiol., **15**, 495, 1944.

[9] B.E. Noltingk, E.A. Neppiras, Proc. Phys. Soc. (London), **B63**, 679, 1950.

[10] C. Seghal, R.G. Sutherland, R.E. Verall, J.Phys.Chem. **84**, 227, 1980.

[11] C. Seghal, R.G. Sutherland, R.E. Verall, J.Phys.Chem. **84**, 388, 1980.

[12] C. Seghal, R.G. Sutherland, R.E. Verall, J.Phys.Chem. **84**, 525, 1980.

[13] C. Seghal, R.G. Sutherland, R.E. Verall, J.Phys.Chem. **84**, 529, 1980.

[14] C. Seghal, R.G. Sutherland, R.E. Verall, J.Phys.Chem. **85**, 315, 1981; Ultrasonics **37**, jan.1982.

[15] P.K. Chendke, H.S. Folger, J.Phys.Chem. **87**, 1362, 1983.

[16] P.K. Chendke, H.S. Folger, J.Phys.Chem. **87**, 1362, 1983.

[17] M. Degrois, P. Baldo, Ultrasonics, **25**, Jan.1974.

[18] M.A. Margulis, Russian J.Phys.Chem. **59**, 882, 1985.

[19] M.A. Margulis at al., Russian J.Phys.Chem. **60**, 731, 1986.

[20] M.A. Margulis, Russian J.Phys.Chem. **60**, 734, 1986.

[21] M.A. Margulis, Ultrasonics **30** , 152, 1992.

[22] F.R. Young, J.Acoust.Soc.Am. **60**, 100, 1976.

[23] T.K. Saksena, W.L. Nyborg, J.Chem.Phys. **53**, 722, 1970.

[24] K.S. Suslick at all., J. Phys. Chem. **97**, 3098, 1993.

[25] P.D. Jarman, J.Acoust.Soc.Am. **32**, 1459, 1960.

[26] L.A.Crum, J.Acoust.Soc.Am. **95**, 559, 1994.

[27] J. Schwinger, Proc. Natl. Acad. Sci. USA **89**, 1118, 1992.

[28] L. Frommhold, A.A. Atchley, Phys. Rev. Lett. **73**, 2883, 1994.

[29] R. Hiller, S.J. Putterman, B.P. Barber, Phys. Rev. Letters **69**, 1182, 1992.

[30] C.C. Wu, P.H. Roberts, Phys. Rev. Lett.**70**, 3424, 1992.

[31] B.P. Barber, R. Hiller, K. Arisaka, H. Fetterman and S.J. Putterman, J. Acoust. Soc. Am **91**, 3061, 1992.

[32] L.A. Crum, Physics Today, 22, September 1994.

[33] R. Hiller, K. Weninger, S.J. Putterman, B.P. Barber, Science **266**, 248, 1994.

[34] B.P. Barber, S.J. Putterman, Phys. Rev. Letters **69**, 3839, 1992.

[35] B.P. Barber, C.C. Wu, R. Lofstedt, P.H. Roberts, S.J. Putterman, Phys. Rev. Lett. **72**, 1380, 1994.

[36] H.P. Greenspan, A. Nadim, Phys. Fluids A **5** , 3424, 1993.

[37] W.C. Moss, D.B. Clark, J.W. White, D.A. Young, Phys. Fluids **6**, 2979, 1994.

[38] A. Prospereti, J.Fluid.Mech. **222**, 587, 1991.

[39] V. Kammath, A. Prospereti, F.N. Egolfopoulos, J.Acoust.Soc.Am, **94**, 248, 1993.

[40] R.G. Holt, D.F Gaitan, A.A. Atchley, Phys. Rev. Lett. **72**, 1376, 1993.

[41] L. Kondic, J.I. Gersten, C. Yuan, (to be published).

[42] L. Kondic, J.I. Gersten, C. Yuan, (to be published).

[43] B.G. Levi, Phys. Today **44**, (11), 17, 1991.

[44] E.B. Flint, K.S. Suslick, Science **253**, 1397, 1991.

[45] I. Amato, Science **255**, 1511, 1992.

[46] A.C. Johnston, Nature, **354**, 361, 1991.

[47] M.W. Browne, New York Times, C1, December 20, 1994.

[48] Lord Rayleigh, Phil.Mag. **34**, 94, 1917.

[49] R. Apfel, J. Acoust. Soc. Amer., **26**, 1179, 1970.

[50] K.S. Suslick (editor), "Ultrasound", VCH Publishers, New York, 1988.

[51] L.D. Landau, E.M. Lifshitz, "Fluid Dynamics", Pergamon Press, New York, 1987.

[52] A. Prospereti, Ultrasonics, 69, March 1984.

[53] A. Prospereti, Ultrasonics, 115, May 1984.

[54] M.S. Plesset, D.Y. Hsieh, J.Appl.Phys. **23**, 95, 1951.

[55] M.S. Plesset, D.Y. Hsieh, Phys.of Fluids **3**, 882, 1960.

[56] E.A. Neppiras, Phys.Rep. **61**, 159, 1984.

[57] H. Poritsky, Proc. 1st U.S. National Conress in Applied Mechanics, (A.S.M.E.), 813, 1952.

[58] L. Trilling, J.Appl.Phys. **23**, 14, 1951.

[59] A. Eller, H.G. Flynn, J.Acoust.Soc.Am **37**, 493, 1964.

[60] W.P. Masson, "Physical Acoustics", Academic Press, New York, 1964.

[61] L.D. Rossenberg (editor), "High Intensity Ultrasonic fields", Plenum Press, New York, 1971.

[62] H.G. Flynn, J.Acoust.Soc.Am. **57**, 1379, 1975.

[63] W. Lauterborn, J.Acoust.Soc.Am. **59**, 283, 1976.

[64] J.E. Williams, Y.P. Guo, J.Fluid.Mech. **224**, 507, 1990.

[65] L.A. Crum, Ultrasonics, 215, September 1984.

[66] L.A. Crum, J.Acoust.Soc.Am. **73**, 116, 1983.

[67] L.A. Crum, J.Acoust.Soc.Am. **73**, 121, 1983.

[68] A. Prospereti, A. Lezi, J.Fluid.Mech. **168**, 457, 1986.

[69] A. Prospereti, L.A. Crum, K.W. Commander, J.Acoust.Soc.Am. **83**, 502, 1988.

[70] R.K. Pathria, "Statistical Mechanics", Pergamon Press, New York, 1972.

[71] R. Zallen, "The Physics of Amorphous Solids", John Willey & Sons, New York, 1983.

[72] N.L. Schryer, "Post - A Package for Solving Partial Differential Equations in One Space Variable", AT&T Bell Laboratories, 1984.

[73] S.K. Godunov, Mathematicheskii Sbornik **47**, 271, 1959.

[74] M. Holt, "Numerical Methods in Fluid Dynamics", Springer - Verlag, New York, 1977.

[75] Ya. B. Zeldovich, "Physics of Shock Waves and High Temperature Hydrodynamic Phenomena", Academic Press, New York, 1966.

[76] K.P. Stanyukovich, "Unsteady Motion of Continuous Media", Academic Press, New York, 1960.

[77] G. Guderley, Luftfahrtforschung **19**, 302, 1942.

[78] D. Mihalas, "Stellar Atmospheres", V.H.Freeman and Company, San Francisco, 1978.

[79] J.D. Jackson, "Classical Electrodynamics", John Wiley & Sons, New York, 1975.

[80] S.J. Putterman, Scientific American, 46, February 1995.

[81] R.H. Dicke, Phys.Rev. **93**, 99, 1954.

[82] R. Bonifacio, L.A. Lugiato, Phys.Rev.A **11**, 1507, 1975.

[83] W. Zakovicz, Phys.Rev.A **17**, 343, 1978.

[84] W.A. Lamb, M.O. Scully, M. Sargent, "Laser Physics", Addison-Wesley Pub. Comp., New York, 1974.

[85] R. Friedberg at al., Phys.Rep. **7**, 101, 1973.

[86] R. Friedberg, S.R. Hartman, Phys.Rev.A **10**, 1728, 1974.

[87] M. Born, E. Wolf, "Principles of Optics", Pergamon Press, New York, 1980.

[88] K.E. Weale, "Chemical reaktions at high pressures", Spon, London, 1969.

[89] N.E. Dorsey, "Properties of Ordinary Water Substance", Reinhold Publ. Comp., San Francisco, 1940.

[90] D. Eisenberg, W. Kauzman, "The Structure Properties of Water", Oxford Press, Oxford, 1969.

[91] A. Ben-Naim, "Water and aqueous solutions", Plenum Press, New York, 1974.

[92] F. Franks (editor), "Water", vol. 1-2, Plenum Press, New York, 1972.

[93] J.O. Hirschfelder, C.F. Curtis, R.B. Bird, "Molecular theory of gases and liquids", J.Willey & Sons, New York, 1954.

[94] J.I. Gersten, A. Nitzan, "Radiative properties of solvated molecules in dielectric clusters and small particles", preprint.

[95] A. Nitzan at al., Phys.Rev.Lett. **62**, 106, 1989.

[96] H. Fröhlich, "Theory of Dielectrics", Oxford Press, Oxford, 1958.

[97] G. Herzberg, "Electronic spectra of polyatomic molecules", D. van Nostrand Comp., Amsterdam, 1966.

[98] A.L. Loeb, J.G. Overbeek, P.H. Wiersema, "The Electrical Double Layer around a Spherical Colloid Particle", M.I.T. Press, Cambridge, 1960.